RISK ASSESSMENT DUE TO NATURALLY OCCURRING RADIOACTIVE MATERIALS IN KILIMAMBOGO, KENYA

NYAMBURA CATHERINE (M.Sc)
I84/ 32272/2015

THESIS SUBMITTED IN FULFILLMENT OF THE REQUIREMENTS FOR THE AWARD OF THE DEGREE OF DOCTOR OF PHILOSOPHY IN PHYSICS IN THE SCHOOL OF PURE AND APPLIED SCIENCES OF KENYATTA UNIVERSITY

DECEMBER 2023

DECLARATION

This thesis is my original work and has not been presented for a degree or other awards in any other University

Catherine Nyambura
Department of Physics
Kenyatta University
P.O Box 43844- 00100
Nairobi, Kenya

Signature .....

Date 06/11/2023

SUPERVISORS

We confirm that the work reported in this thesis was carried out by the candidate under our supervision

Dr. Nadir Hashim
Department of Physics
Kenyatta University
P.O Box 43844- 00100
Nairobi, Kenya

Signature .....

Date 06/11/2023

Dr. Margaret Chege
Department of Physics
Kenyatta University
Mombasa Campus
P.O Box 16778- 80100
Mombasa, Kenya

Signature .....

Date 06/11/2023

Prof. Shinji Tokonami
Graduate School of Health Sciences
Hirosaki University
66-1 Hon-Chuo
Hirosaki, Aomori 036-8564
Japan

Signature .....

Date 06/11/2023

DEDICATION

This thesis is dedicated to my late mother, Eunjeniah W. Benson, my sister, Sr. Esther and my sons Lewis, Benson, John and Charles.

ACKNOWLEDGEMENTS

I am sincerely grateful to my supervisors, Dr. N.O. Hashim, Dr. M.W. Chege and Prof. S. Tokonami for their immeasurable help and guidance throughout my research period. I also pass my sincere gratitude to the African Development Bank who offered me a scholarship through the ministry of Education to study at Kenyatta University. I wish to thank Prof. Tokonami and the entire management of Hirosaki University for providing radon, thoron, and thoron progeny monitors, facilitating their analysis and sponsoring my stay in the University as a visiting researcher. My sincere gratitude to Dr. Hosoda, Dr. Kudo and Mr. Suzuki, for taking me through the process of monitor preparation and RADUET analysis using the different state of the art equipment and machines. I also wish to thank all the members of Prof. Tokonami's radon research laboratory in the Institute of Radiation Emergency Medicine, Hirosaki University for their warm welcome and kind hospitality during my stay from 20th April to 14th May 2108 and 21st September to 3rd October 2018.

I am grateful to the Japan Society for promotion of Sciences (JSPS) for giving me a golden opportunity to participate in the 10th Hope Meeting with the Nobel Laureates held in Yokohama, Japan between 10th and 16th March 2018.My heartfelt gratitude to Kenya Education Network (KENET) for awarding me a travel grant to participate in the 9th International conference on High Level Environmental Radiation Areas held in Hirosaki University, Japan between 23rd and 27th September 2018.

My gratitude also goes to the Chairman, Departments of Chemistry and Food, Nutrition and Dietetics of Kenyatta University for allowing me to use their facilities for water analysis and to the laboratory technicians Ms. Catherine, Mr. Kariuki, and Mr. Maina for their assistance and guidance in the laboratory work. Special thanks to

the chairman, and the technical team, Mr. Fredrick Mudimba, Mr. Wataka, and Mr. Musyoka of the Physics Department, Kenyatta University for the assistance offered in facilitating the carrying out of the research activities. Many thanks to the village elders of the villages in Gatuanyaga and Kilimambogo regions for their assistance in installation and removal of the monitors and in sample collection used in this study. Special thanks to the villagers of Kilimambogo region for welcoming us to their residents, allowing us to install the monitors in their dwellings and for their assistance in collection of samples.

Immeasurable gratitude also goes to my family members, my late mum, my sister and my sons, for their patience, encouragement, and immeasurable support towards this study and during the time of the study.

Above all, I wish to thank the Almighty God for the opportunity to do my PhD study under a scholarship, for the grace He has given me in carrying out the research at all levels

TABLE OF CONTENTS

LIST OF TABLES

LIST OF FIGURES

LIST OF PLATES

ABBREVIATIONS AND ACRONYMS'

AAS	Atomic Absorption Spectrometry
ADC	Analog-to-digital converter
ADI	Accepted Daily Intake
AEDE	Annual Effective Dose Equivalent
ALARA	As Low As Reasonably Achievable
ANL	Argonne National Laboratory
ARS	Acute Radiation Syndrome
AT	Average Exposure
BD	Below Detection
Bq	Becquerel
BRF	Branch Factor
BW	Body Weight
CCD	Charge Coupled Device
CDI	Chronic Daily Intake
CEDE	Committed Effective Dose Equivalent
CF	Conversion Factors
CR-39	Columbia Resin -39
CSF	Cancer Slope Factors
CSF	Cancer Slope Factors
CT	Computed Tomography
DCF	Dose Conversion Factors
DNA	Deoxyribonucleic Acid
ED	Exposure Duration
EETC	Equilibrium Equivalent Thoron Concentration

EF	Exposure Frequency
ELCR	Excess Lifetime Cancer Risk
EPA	Environmental Protection Agency
ETF	Environmental Transport Factor
FA	Area Factor
FAAS	Flame Atomic Absorption Spectrometer
FCD	Depth and Cover Factor
Gy	Gray
HBRA	High Background Radiation Areas
H_{ex}	External hazard index
HI	Hazard Index
HPGe	High Purity Germanium Detector
HQ	Hazard Quotients
HV	High Voltage
IAEA	International Atomic Energy Agency
ICRP	International Commission on Radiological Protection
ILCR	Incremental Lifetime Cancer Risk
IR	Ingestion Rate (Average daily water Ingestion Rate)
ISO	International Organization for Standardization
LF	Leaching Factor,
LNT	Linear No-Threshold
MCA	Multi-Channel Analyzer
MDA	Minimum Detectable Activity Concentration
NaI (Tl)	Sodium Iodide Thallium Activated Detector
NORM	Naturally Occurring Radioactive Materials

PADC	Polyallyl Diglycol Carbonate
pH	Potential of Hydrogen
PMT	Photomultiplier Tube
PVC	PolyVinyl Chloride
RADUET	Radon–Thoron Discriminative Monitors
Ra_{eq}	Radium Equivalent Activity
RESRAD	RESidual RADioactivity
R_fD	Reference Doses
RNA	Ribonucleic Acid
ROI	Region of Interest
SF	Source Factor
SSND	Solid-State Nuclear Track Detectors
Sv	Sievert
TEDE	Total Effective Dose Equivalent
TENORM	Technologically Enhanced Naturally Occurring Radioactive Materials
UNSCEAR	United Nations Scientific Committee on Effects of Atomic Radiation
US EPA	United States Environmental Protection Agency
USNRC	United States Nuclear Regulatory Commission
WHO	World Health Organization

ABSTRACT

Man is continually exposed to ionizing radiation whose main origin is either natural or artificial. The primordial radionuclides found in building materials are important sources of radon and thoron in the indoor air. The main objective of this research was to assess exposure due to radioactive elements in indoor air, crops and building materials (soil and rocks), and determine the level of the risks. The concentration levels of radon, thoron, and thoron progeny were measured in mud-walled, iron sheet walled, and stone walled modern houses in Kilimambogo region, Kenya. Radon and thoron concentration levels were determined using passive radon–thoron discriminative monitors (RADUET), while thoron progeny levels were measured using thoron progeny monitors. The activity concentration of ^{226}Ra, ^{232}Th and ^{40}K present in the different environmental samples like rocks, soil, and cassava crop were determined using a Thallium- activated sodium-iodide scintillation (NaI (TI)) detector Model TS-2L. Elemental concentration in water samples was determined using an atomic absorption spectrophotometer (AAS). The mean external dose received indoors by the residents due to radionuclides present in rock and soil samples was measured to be 0.91 ± 0.26 mSv y^{-1} and 0.86 ± 0.19 mSv y^{-1} respectively. This is comparable to the total exposure dose limit of 1 mSv y^{-1} recommended by ICRP for members of the general public. This means that, soil and rocks in the region does not pose any radiological risk to the residents of Kilimambogo region. Consequently, they can be used for agriculture and construction of dwellings. The doses received due to intake of cassava tubers and leaves was 1.82 ± 0.60 mSv y^{-1} and 0.81± 0.30 mSv y^{-1} respectively, totaling to 2.63 ± 0.70 mSv y^{-1}. The ingestion dose contributes to 42.1% of the total dose received by the resident from measured sources. Residents should therefore reduce the intake of cassava. The annual effective dose received by the residents of Kilimambogo and Gatuanyaga regions due to inhalation of radon and thoron was determined for the three types of dwellings, from their respective progenies and found to be 1.3 ± 0.2 mSv y^{-1}, 1.1 ± 0.1 mSv y^{-1} and 1.4 ± 0.2 mSv y^{-1} for radon progeny and 2.4 ± 0.4 mSv y^{-1}, 0.5 ± 0.1 mSv y^{-1} and 1.5 ± 0.2 mSv y^{-1} for thoron progeny in mud-walled, iron sheet-walled and stone-walled houses respectively. It was observed that, residents living in iron sheet - walled houses with cemented floors received the lowest doses from inhalation of the radon isotopes hence such houses are safer than other types of dwellings. Residents living in mud houses and uncemented houses should consider improving the ventilation of their houses to reduce radiation exposure. The lifetime cancer risks for the residents due to intake of metal carcinogens, Cd, Ni and Pb in borehole and surface water was also estimated. The cumulative cancer risk in the borehole samples was 0.12 ± 0.06 and 0.19 ± 0.09 in the dry and wet seasons respectively. Those from surface water sources were 0.10 ± 0.07 and 0.21 ± 0.06 in the dry and wet seasons respectively. In both seasons, the cancer risks were much greater than the acceptable risks of 10^{-6} to 10^{-4} by a factor of 1000 and above. This indicates that about 10% of the residents are likely to die of cancer related ailments. RESRAD computer simulation code was used to estimate the doses received by the resident farmer and the quarry worker scenarios at time, t = 0 years. The doses received by the resident farmer and quarry worker scenarios were 0.22 mSv y^{-1} and 0.16 mSv y^{-1} respectively only for the external radiation pathway. This risk is low and does not pose any significant health risk to the residents. The data measured in this research will be used by future researchers as baseline study.

CHAPTER ONE: INTRODUCTION

1.1 Background of the study

Any environment that is either polluted or contaminated can pose detrimental impact on the inhabitants. Pollution is as a result of introduction of substances into the environment by man which would result to deleterious effects. However, contamination is as a result of presence of elevated concentration of substances in the environment above the natural background level. These can be foreign substances or naturally occurring substances. Heavy metals and radionuclides have received a paramount attention to different researchers and organizations since they are toxic in nature. Heavy metals are present in trace amounts in waters of which many of them are toxic even at very low levels, such as cobalt, mercury, nickel, lead, arsenic, cadmium, chromium, zinc and selenium. Increasing their levels in water resources is of greater concern since in most cases some industries discharge their metal containing industrial and sewage effluents into fresh waters without any adequate treatment.

Heavy metals in the environment could originate from agricultural discharges, illegal garbage disposal, discharge of domestic wastes and agricultural runoff, (Dilebo *et al.*, 2023; Mohammed *et al., 2023*). Others include electroplating, a process required in battery manufacturing industries as well as metal coatings, (Aziz *et al.*, 2023). Metals easily bioaccumulate in food chains due to their non-degradable and toxicity state. The heavy metals are also carcinogenic in nature hence making their presence in the environment a great threat to man and other organisms. Therefore, when these metals are ingested by man, they could cause harmful effects to organs like the brain, liver, skin, lungs, kidneys, and bones, (Zhou *et al.*, 2020; Dilebo *et al.*, 2023). Additionally,

their bioaccumulation nature makes them accumulate in bones and fatty tissues a condition that could lead to weakened immune systems as a result of nutritional deficiencies, (Aziz *et al.,* 2023). Radionuclides have been present in the environment since the creation of the earth. Primordial radionuclides include those materials that remain undisturbed due human activities and are called naturally occurring radioactive materials (NORM), while those that have been concentrated, exposed or disturbed due to human activities are referred to as technologically enhanced naturally occurring radioactive materials (TENORM).

Man has applied these radionuclides and radiation in various fields such as medicine, biology, agriculture, industries and electric power generation. These applications lead to radiation exposure. The risk from exposure to any particular radionuclide depends on the energy it emits, type of radiation, its activity, rate of metabolism and elimination upon ingestion or inhalation, organ where it concentrates and how long it stays and whether the exposure is internal or external. Environmental Protection Agency (EPA, 2017) bases its regulatory limits and non-regulatory guidelines for public exposure to low level ionizing radiation on the linear no-threshold (LNT) model. This model assumes that the risk of developing cancer due to a low-dose exposure is proportional to dose, with no threshold. Therefore, the assumption is that, the risk of exposure reduces as the dose reduces. Of great importance is the radon gas which is released when radium, a daughter product of Uranium-238 decays. Radon is present in soils and accumulates in homes and other buildings. It is the second leading cause of lung cancer in the United States where it is estimated to cause approximately 21,000 lung cancer deaths annually, (USEPA, 2011). Other radionuclides of concern are radium, thorium and uranium. If thorium is inhaled as dust, some may remain in

the lungs for long periods. If ingested, it leaves the body within several days but small amounts of thorium left in the body enter the bloodstream and are deposited in bones where it may remain for many years. Therefore, inhaling thorium dust may cause an increased risk of developing lung or bone cancer. Ingestion of high concentrations of uranium can cause harmful effects such as bone or liver cancer.

1.2 Background radiation

Radionuclides are elements with unstable atomic nuclei that spontaneously decay or disintegrate producing ionizing radiation in the form of alpha particles, beta particles, and gamma rays. Alpha particles are identical to the helium nucleus made up of two protons and two neutrons. They are heavy and move slowly relative to other forms of radiation like beta particles. They are highly ionizing and can cause multiple ionizations within a short distance and travel for a short range like a few centimetres in air, and are stopped by a piece of paper. Regarding external exposure. Alpha particles are not as dangerous because they do not penetrate the skin. Additionally, alpha particles have a large mass and this gives them a high ionizing power and greatest ability to damage tissue. Alpha emitters can be inhaled or ingested from the radioactive materials in the environment. If this happens, the alpha particles in the body could be very dangerous because they have a high ability to damage human cells. An element can undergo beta decay by releasing either beta particles or positrons. When the neutron to proton ratio of the element is too high, a neutron changes to a proton and an electron. When this happens, the electron is ejected from the nucleus in form of a beta particle. Therefore, beta particles are emitted from the nucleus as part of radioactive disintegration and are considered to be negatively charged electrons. Since they are light, they move fast and travel tens of centimetres in air and are

stopped by a thin sheet of aluminium. They are about 8,000 times smaller than the alpha particles hence they are able to penetrate through skin. External exposure to beta particles can cause burns and tissue damage. However, internal exposure would be more dangerous than the external exposure. On the other hand, for a low neutron to proton ratio, a proton changes into a neutron and a positron with the positron being ejected from the nucleus. Positrons have similar properties as electrons. However, when a positron comes into contact with a free electron, the two combine and are annihilated, producing two photons. Gamma radiations are highly energetic with high frequency electromagnetic radiation. They are similar to other types of electromagnetic radiation, for instance the visible light and the X-rays. They are the most dangerous form of ionizing radiation compared to alpha and beta particles. They are able to travel through most forms of matter due to the high amount of energy that they possess and due to the fact that they have no mass, and are not particles like the alpha and beta particles. The gamma rays therefore are highly penetrating radiations whose travel has no range in air. Gamma radiations mainly take place after a radioactive atom undergoes either an alpha or beta decay. External exposure to gamma radiations affects the entire human body since they pass through the skin and the bones as well. Gamma rays are stopped by a thick block of lead of about 1.3 feet or by 6.6 feet of concrete.

In the environment, radionuclides are responsible for the background ionizing radiation that human beings are continuously exposed to. The sources of the radionuclides can be of natural origin or of artificial origin. Natural sources include primordial terrestrial radionuclides which have half-lives comparable to the age of the earth and extra-terrestrial sources which include cosmic rays and originate from the

outer space. Terrestrial radionuclides ^{238}U, ^{232}Th, their decay products, (decay chains shown in appendices 1 and 3) and the singly occurring ^{40}K are the most important radionuclides with respect to radiation protection, (UNSCEAR, 2000; Garba *et al.*, 2023). This is due to the fact that, they contribute the largest fraction of natural radiation exposure. Exposure of the human body to radiation is primarily through alpha and beta particles as well as gamma rays which emanate from the radionuclides present in the environmental samples and in the human body. The primordial radionuclides, ^{238}U, ^{226}Rn, ^{232}Th and ^{40}K are virtually present in every rock, sand and soil profile, albeit in trace amounts. Consequently, they may be taken up by plants, enter underground water system and eventually end up in the human food chain. In addition, rock, sand and soil when used as building materials can be important sources of indoor ^{222}Rn (radon) and ^{220}Rn (thoron) which are radioactive gases in the ^{238}U and ^{232}Th decay chains respectively. Therefore, the measurement of their levels in the different matrices is important in trying to assess the threat they pose to the health of human beings, (Mehta *et al*., 2014).

Extraterrestrial radiation is the solar radiation that is incident outside the earth's atmosphere. It exists as high energy particles whose origin is the outer space in form of cosmic rays. Cosmic rays are made up of high energy protons and atomic nuclei from the sun or outside the solar system. Cosmic rays are made up of electrons, neutrons and atomic nuclei, which have been accelerated to very high speeds. Cosmic ray particles are mainly composed of protons (hydrogen nuclei) (87%), and some alpha particles (helium nuclei) (12%), and electrons (1%) with low amounts of carbon, oxygen and of heavier elements. They travel at a speed close to that of light and approach the Earth from all directions. Cosmic rays from outer space are called

primary cosmic rays. Along their path they collide with other particles in the upper atmosphere like nitrogen and oxygen molecules in air producing other particles in the atmosphere which in turn produce cascades of lighter particles, (Pions and kaons) called secondary cosmic rays. These secondary cosmic rays spread out and continue to hit other particles and air molecules creating muons which shower towards the earth. These atom fragments rain down on the Earth from outside of the solar system as illustrated in Figure 1.1. Some cosmic radiation gets absorbed by the earth's atmosphere and interacts with the upper layers of the atmosphere thereby producing secondary radiation of lower intensity. The interactions may also produce cosmogenic radionuclides such as ^{3}H, ^{7}Be, ^{14}C and ^{22}Na. Absorption of Cosmic radiation is higher in the lower altitude where the air is thick as compared to higher altitudes where the air is thinner. Exposure to radiation from this source therefore increases with altitude. Therefore, aircraft passengers and crew as well as persons living in higher altitudes are highly exposed to the cosmic rays at higher altitudes than at lower altitudes. The total exposure for instance on passengers on a flight therefore depends on the altitude, path taken and the duration of exposure. For example, a transatlantic flight may increase an average person's annual dose by about 2.5 per cent.

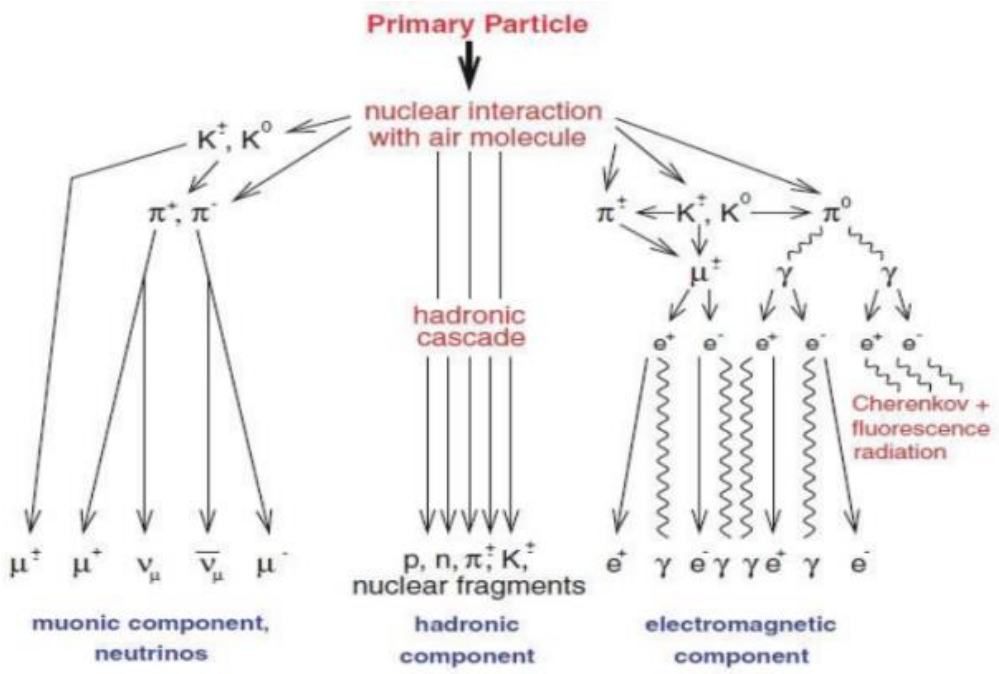

Figure 1.1: Atomic fragments of cosmic rays from the outer space
(Sources; Hakmana, 2007; Motari, 2018)

Artificial sources of radiation exposure are mainly as a result of anthropogenic activities. For instance, radionuclides released during nuclear weapon testing, nuclear installations such as power plants, research reactors and nuclear power plant accidents, like the Chernobyl accident that occurred in 1986 in Ukraine and, Fukushima Daiichi accident which occurred in Japan in 2011. Application of phosphate fertilizers to enhance food production also leads to radiation exposure since phosphates generally contain enhanced concentrations of elements in ^{238}U and ^{232}Th decay series. Application of these fertilizers for prolonged periods may lead to enhanced uptake of the radionuclides by plants and crops and consequently by man through the food chain. In cases where these fertilizers are applied to the crops by hand, there is also a likely exposure to man through dermal contact.

Additionally, exposure can occur during medical procedures such as in diagnostic radiology, image-guided procedures, radiation therapy and, nuclear medicine. Diagnostic radiology is the imaging procedures obtained using x-rays such as chest x-rays and images from devices that use computerized reconstruction techniques like the computed tomography (CT). Nuclear medicine involves the use of radioisotopes like tracers. These are usually administered to the patients by either inhalation, injection or in form of pills. The radioisotope circulates through the body or is taken up only by certain body tissues; furthermore, its distribution can be tracked depending on the radiation it gives off. The emitted radiation can be captured by various imaging techniques, which helps the physicians to examine blood flow to specific organs and assess organ function or bone growth. Notably, the Radioisotopes have short half-lives and usually decay before their emitted radioactivity can cause damage to the patient's body. They are also used in radiopharmaceuticals and radiotherapy.

In radiotherapy, the therapeutic applications of the radioisotopes are intended to destroy the targeted cells for instance in the treatment of cancer and other conditions involving abnormal tissue growth, like hyperthyroidism. In radiation therapy (radiotherapy), like in the case of cancer treatment, the patient's tumor is bombarded with ionizing radiation, in the form of beams of subatomic particles, such as protons, neutrons, alpha or beta particles. These particles directly disrupt the atomic or molecular structure of the targeted tissue where the ionizing radiation introduces breaks in the double-stranded Deoxyribonucleic acid (DNA) molecule, (Reddy *et al.*, 2022) causing the cancer cells to die and thereby preventing their replication. Therefore, radiation therapy refers to the application of ionizing radiations mainly from an external source in the treatment of diseases such as cancer, (UNSCEAR,

2008). Conversely, radiopharmaceutical is a medication used in nuclear medicine that has a combination of a radioisotope and a pharmaceutical part. The radioisotope part assists in imaging such as; Technetium-99, iodine-123, indium-111 and gallium-67. The pharmaceutical part may have a complex molecule that helps take the radioisotope to the body part being studied. Therefore, the pharmaceutical part determines where the radiopharmaceutical will go in the body and what organ system is being diagnosed, (Cain, 2017)

A summary of doses received by the general public from various radiation sources is illustrated in Figure 1.2;

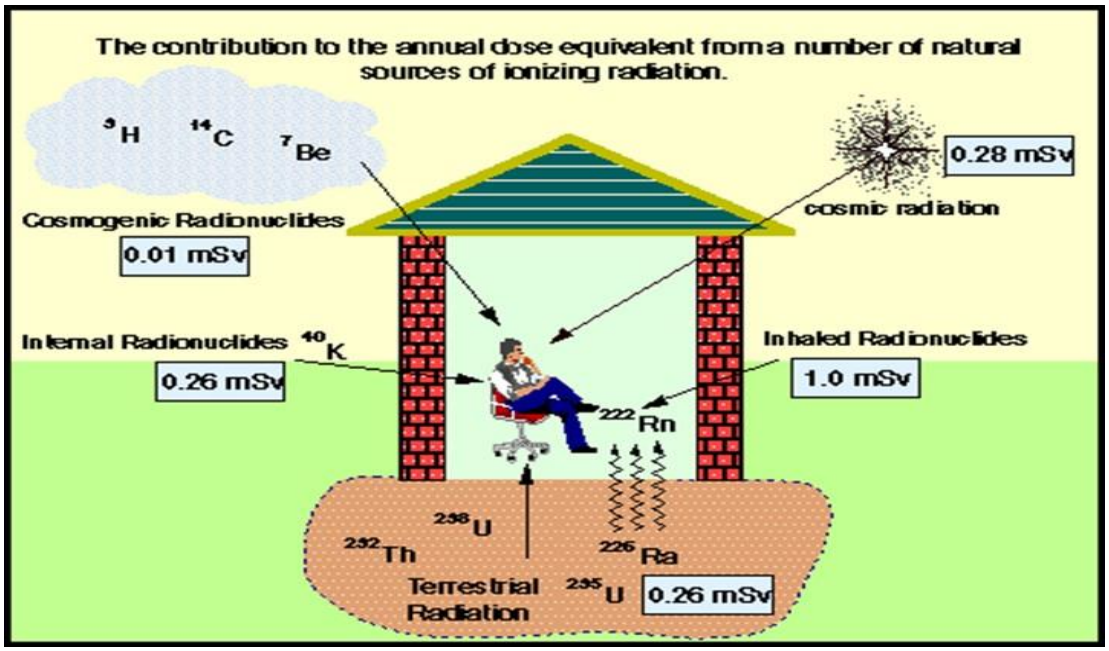

Figure 1.2: Chart on human exposure to sources of ionizing radiation
(Source; IAEA, 2003)

1.2.1 Radionuclides in environmental samples

Natural radioactive materials have been in the environment since the formation of the earth. Building materials obtained from soil and quarried rocks also contribute to

natural gamma radiation. Radioactive materials are also found in soil, water, and plants. Low levels of uranium, thorium, and their decay products are found everywhere. These radioactive materials are ingested with food and water, while others are inhaled like the radon isotopes. The doses received from terrestrial sources vary in different parts of the world. Locations with higher concentrations of uranium and thorium in their soil have higher dose levels. Small amounts of radioactive materials are found in foods, water and even in human bodies. Consequently, human beings are exposed to background radiation which originates from cosmic rays and primordial radionuclides present in soil, water, and air. The degree of damage to human health depends on the radionuclides exposed to that is the energy absorbed, time of exposure and body part exposed to, (Hassan, 2023).

Radionuclides in foods vary and depend on the type of food and geographic region where the food was produced. ^{226}Ra and ^{232}Th and their progenies and the singly occurring radionuclide ^{40}K, are found in food. Generally, ^{40}K is the most commonly occurring natural radioisotope especially in milk, meat, bananas, and other potassium rich products. In soil, it is reported to be the most abundant comprising of 2.59 % of ground soil, (Lee *et al.*, 2023). Large amounts of radioisotopes discharged into the environment get into the food crops either through surface deposition or through root uptake, (Njinga *et al*., 2013). Radioactivity in water may as well accumulate in rivers and seas, thereby depositing on fish and seafood. Radium and thorium can enter the blood stream and accumulate in bones for years, (USEPA 2011). ^{40}K contributes to both external and internal dose. Upon ingestion, it enters the blood stream and is quickly distributed to all body organs and tissues and behaves like the ordinary potassium, (Ziajahromi *et al.,* 2013). Exposure to ionizing radiation has as a result

been associated with cancers such as esophagus, lung cancer, stomach, thyroid among others, (Hassan, 2023). Exposure to elevated levels of radium over elongated periods could lead to death and other health problems like liver and bone cancers. Man-made sources of thorium that bring about environmental contamination which include application of phosphate fertilizers. This practice has been attributed to contribute to elevated levels of radiation in the environment in the study region.

In addition, the buildings in which human beings work and live have been constructed using materials containing radioactive elements such as uranium, thorium, and potassium. Knowledge of concentration levels in buildings and building materials is therefore important in assessment of population exposure since most individuals spend a good fraction of their time indoors. Moreover, building materials can cause significant gamma dose to dwellers due to the content of natural radionuclides therein. Though the buildings act as radiation attenuators from outdoor radiation, they also add up to the radiation dose to occupants if the construction materials contain significant levels of natural radionuclides.

1.2.2 Radon and thoron in the environment

Radon is a natural radioactive gas that is colourless, odourless, tasteless and chemically inert. It is the greatest source of exposure to ionizing radiation. It is formed when radium present in soils, rocks and building materials undergoes alpha decay, (Degu and Alemu 2021, Reddy *et al.,* 2022). Some of the atoms therefore escape to groundwater and air. It is present in the atmosphere and accumulates in poorly ventilated areas, like caves and basements of buildings, (Hashim *et al,* 2020). Radon atoms decay to give other radioactive atoms or progeny. The main radon isotopes are radon gas (radon-222), produced from the decay of radium, and thoron (radon-220)

from the decay of thorium which are present in rocks, soil and building materials. Therefore, the levels inside buildings can be higher particularly if there is poor ventilation enhancing trapping of the gases in the indoor air. Radon seeps into buildings from the ground through cracks and other openings in floors and walls. The accumulated radon isotopes in buildings can pose health hazard. Therefore, indoor flooring provides a shield against entry of radon and thoron. Since the progenies emit alpha particles upon decay, inhaling them can cause lung cancer since the alpha particles are deposited on the lung tissues. This is because the atoms of radon progeny stick to and irradiate the lung tissues, thereby exposing the lungs to internal dose, (Degu and Alemu 2021).

1.2.3 Heavy metals

A heavy metal is one that is considered to have a relatively high density. The main pollutants in drinking water are the heavy metals. Underground water is particularly susceptible to heavy metal enrichment. This is of concern as underground water serves as one of the main sources of drinking water especially in the rural Kenya, (Chege, 2014). Heavy metals being natural components of the earth's crust can find their way into human bodies predominantly through ingestion of water.

In the right amounts, some elements are essential and important for normal body functioning and growth of living organisms. Examples of essential elements include copper (Cu), iron (Fe), selenium (Se), zinc (Zn), manganese (Mn), cobalt (Co), and nickel (Ni). Nevertheless, concentrations of these elements higher than the recommended levels can cause risks to human body and the aquatic life or may lead to poisoning. Co for instance is required as a metal component of vitamin B_{12}. However, high levels could lead to over-production of red blood cells and abnormal

thyroid artery. High levels of Cu and Mn particularly in drinking water could result to mental diseases like Manganism and Alzheimer (brain disorder). Some heavy metals such as chromium (Cr), lead (Pb), cadmium (Cd), and mercury (Hg) are of no benefit, (Lenntech, 2016) with some like mercury, lead and cadmium being toxic, even in trace amounts. Pb poisoning for instance can lead to chronic health risks such as high blood pressure, headache, kidney damage, lung cancer, abdominal pain, nerve damages, and stomach cancer. High exposure of lead to children may cause severe health effects like memory deterioration, behavioral disturbances and reduced understanding ability. Besides, long-term Pb exposure can lead to anaemia. Similarly, high exposure to Cd also causes harmful health effects such as kidney damage, skeletal damage and itai-itai diseases, cancer, diarrhea, hair loss, dermatitis and depression, (Koki *et al*., 2015; Lenntech, 2016). These heavy metals increase cancer risks and exposure to such toxic metals over long periods could result in many types of cancers, (Mohammed *et al.*, 2019). Heavy metal contamination is a great threat to man since the levels tend to build up in the body to toxic levels. Water sources especially the rivers tend to be contaminated also as a result of industrial discharges, agricultural run offs, industrial and domestic waste discharges, (Mohammed *et al.*, 2023). Ground water abstraction in rural area not regulated and no testing done by regulatory authorities ran the risk of exposure hence the need to study the concentration levels of heavy metals in drinking water in the study region. Exposure to heavy metals is primarily through water and food ingestion as well as inhalation of dust particles. The level of toxicity increases with intake, (Mohammadi *et al.,* 2019).

1.3 Description of the study area

Kilimambogo gets its name from the nearby Mount Kilimambogo. *Kilimambogo* is a S*wahili* word meaning "mountain of buffaloes". It is also referred to as "*Ol-Donyo Sabuk"* by the Maasai pastoralists, meaning a "big mountain". The mountain is located in Kyanzavi Division, Matungulu District of Machakos County, near the border with Kiambu County, as well as home to the Ol-Donyo Sabuk National Park. It is in the vicinity of Ol-Donyo Sabuk town situated near the busy Thika-Garissa highway. Ol-Donyo Sabuk is located 18.5 km South East of Thika town and 85 km North East of Nairobi, the capital city of Kenya. Kilimambogo area is also home to the famous fourteen falls, one of the Kenya's most spectacular tourist attraction sites, Kilimambogo Teachers College, the Immaculate Heart of Mary mission hospital, and the Delmonte Kenya Estate, a commercial farm famed for large scale cultivation of pineapples. Several small-scale quarries run, are also very common in the region.

The main activities by the general public in the region include quarrying, small-scale farming of cassava, maize, beans, peas, and sugarcane. Some local residents work as farm hands in the Delmonte estates. A small percentage of the residents live in traditional mud-walled houses which are bare earthed while the rest live in houses constructed either with iron sheets or stone-modern houses made of building materials harvested from the local quarries. Soil generally offers easier mobility of radon and thoron as opposed to rocks. However, from the study results, it was observed that, radon accumulated more in the stone- walled houses as opposed to thoron and the thoron progeny which accumulated more in the mud-walled dwellings. Dwellings constructed using iron sheets recorded the lowest concentrations of the isotopes particularly those that had cemented flooring, (Nyambura *et al.*, 2019).

The main sources of water for the rural residents at the time this research was conducted were boreholes since the available rivers in the region are Athi river, Matathia stream and Thika River on the extreme end of the study region. Athi river which is generally polluted by effluents from Nairobi city and industries in Thika town is seldomly used for drinking. There exist some springs along the slopes of Mount Kilimambogo which almost dry up in the dry season. These are used by the residents to provide drinking water and water for other domestic uses.

1.4 Statement of the research problem

Radionuclides have been in existence since the formation of the earth. They are able to move to different parts of the ecosystem like the soil, underground water, indoor air, crops, and finally end up to the body of human beings either through inhalation or through ingestion. This increases total radiation received by the different organs in the body. Exposure to low doses of radiation over a considerable period of time could lead to cancers such as lung cancer, bone cancer, thyroid cancer, breast cancer, skin cancer or leukemia. Radon and thoron gases reported to emanate from soil are carcinogenic in nature and cause the largest fraction of cancer cases among non-smokers as reported by WHO (2011). Radon is considered to be the second most important cause of lung cancer after smoking, (Tokonami *et al.*, 2004; WHO, 2011, Reddy *et al.*, 2022). Exposure to intake of heavy metals in drinking water has been reported to cause gastric cancer, cervical, ovary, prostrate, lung cancers, skin allergies, lung fibroids, (Kumar and Trivedi., 2016), stomach cancers, hypertension and high blood pressure.

Studies on radioactivity, radon and elemental concentration levels have been done across the globe and in various parts of Kenya. However, such studies have not been

done in Kilimambogo region. Man has interacted with the environment in all aspects of his survival for instance air, water, soil for agriculture and rocks for construction of dwellings to live in. As a result, radiation exposure is paramount. The igneous and metamorphic rocks present in the study region have been associated with presence of radionuclides, (Al-Zahrani *et al.,* 2020; Ahmed *et al.,* 2006). Also, metamorphic rocks are rich in minerals such as Mg, Fe, Na, Co, Ca and K which upon weathering easily migrate into other environmental samples such as soil, borehole and surface water samples. This as a result could lead to elevated elemental concentration levels in water bodies in the region.

Many researchers therefore focus on establishing radioactivity and elemental concentration levels in the environment. Such baseline data assists in assessment of health risks, (Wanjala, 2021). Radiation emanating from radionuclides in the samples and elemental composition has been reported to contribute to cancer risks to man.

In Kenya, Globocan reported cancer to be the third cause of death, recording as high as 27,092 deaths and 42,116 new cases in 2020 alone as shown in Appendix 9, (Bray *et al* 2020). The cancer data report from Thika level 5 hospital, Kiambu county indicate that, 574 cancer cases were reported between January 2013 and December 2018, (Ruto *et al.,* 2020) as shown in Appendix 7. In the study, Kiambu residents contributed the highest number of cases, 43% and Machakos residents contributing only 4 %. Kamita *et al*. (2023) investigated the prevalence of cancer in Kiambu County between 2014 and 2020. 2,574 cancer cases were reported in the county (2014 - 2018) with 25% (820) of the patients residing in Kiambu and 5.22% (171) of the patients coming from Machakos county. This data is presented in Appendix 8. A similar study was carried out in Machakos County for cancer cases reported between

2015 and 2019, (Kamita *et al.*, 2020). Out of the 522 reported cases, 80% of the patients were Machakos residents with Matungulu recording the highest number of cases. These cases reported in Kiambu and Machakos counties might have been as a result of radiation exposure from the environment and elemental composition in water bodies.

1.5 Justification

Adequate data is important for regulatory and advisory purposes in an attempt to protect the general public from unnecessary exposure to ionizing radiation. While it is not possible to eliminate the radiation exposure in the environment completely, there is need to maintain it to as Low As Reasonably Achievable (ALARA principle), a fete only achieved if radiation levels in the ecosystem is available.

Exposure to radiation by members of the public has been reported to vary across the globe depending on the geology of a place. The geology of Kilimambogo region shows presence of volcanic, Igneous and metamorphic rocks associated with presence of radionuclides and important minerals. Man, and plants included require clean or safe water for survival. In addition, man requires soil and/ or rocks for construction of dwellings. If these materials are contaminated, then, potential risks associated with their exposure increases. The numerous minerals present in the metamorphic and igneous rocks present in the region becomes a significant source of heavy metals in the available water sources. These heavy metals such as Ni, Pb and Cd when present in drinking water even in small quantities pose adverse effects which are associated with cancers such as stomach, liver and kidney cancers, (Wanjala, 2021).

One of the eight themes for cancer control in Kenya as presented in Kenya Cancer Policy, 2019-2030, (MOH, 2019) is to promote cancer surveillance and research. This is in line with the constitution of Kenya, (2010) which endeavours to ensure all Kenyans have right to attain high standards of health. Data monitoring is therefore key for any country in order to evaluate presence of any pollutants that could hinder good health of its citizens. Many researchers have conducted research all over the world including Kenya. However, data on radioactivity concentration, radon, thoron and thoron progeny as well as elemental composition in water samples is not available for the Kilimambogo region. With the reported cancer prevalence in both Kiambu and Machakos counties, it was important to investigate environmental samples for any possible contribution to the cancer cases due to radiation or elemental composition in the region, (Kamita *et al.,* 2020; Ruto *et al.,* 2020; Kamita *et al.,* 2023;). Data presented in this research will inform future generations and policy makers on the country's cancer burden and consequently cancer control programs. In addition, the data will assist in categorizing the region in reference to NORM and heavy metals as well as providing baseline study on the same. Also, in an attempt to map radioactivity concentration levels in Kenya, this data will assist Kenya Nuclear Regulatory Authority to map NORM in the Kenyan map.

1.6 Objectives

1.6.1 General objective

Assessment of risks associated with radioactivity in building materials (soil and rocks), indoor air, crops (cassava) as well as heavy metals in water in Kilimambogo, Kenya.

1.6.2 Specific objectives

i. To compute effective dose due to the radionuclide concentration levels in the building materials and ingestion dose due to radionuclides in cassava.

ii. Determine the total inhalation dose due to indoor radon and thoron progeny inside mud - walled, metallic (iron-sheet) - walled and modern stone dwellings.

iii. Determination of cancer risk due to ingestion of elemental composition in underground and surface water samples in the region.

iv. Investigate the effective dose received by the resident farmer and quarry worker scenarios in the region using the RESRAD computer code.

It was therefore important to analyze different materials to ascertain the levels of naturally occurring radionuclides and their contribution to external and internal doses to the residents in the study region.

1.7 Scope

The target area for the current research was Kilimamogo region, which was within Ngoliba Ward in Kiambu County and Matungulu North ward in Machakos County, covering an area of about 25 square kilometres. The region is home to the famous fourteen falls, Delmonte pineapple farms, and the Oldonyo Sabuk National Park, located along the slopes of Kilimambogo Mountain. The research focused on determination of activity concentration levels of ^{226}Ra, ^{232}Th and ^{40}K in soil, rock and cassava samples, determination of radon, thoron and thoron progeny (EETC) concentration levels in modern stone houses, metal walled houses and mud houses as well as determination of the elemental concentration in surface and borehole water

samples. Also, the associated annual effective doses and lifetime cancer risk due to exposure to heavy metal intake in the region were also computed.

1.8 Limitations of the study

The limitations of the current study were mainly lack of previous research conducted on the radionuclide concentration in environmental samples as well as heavy metal concentration in water samples. The availability of geological data for the region was also limited. Some parts of the region particularly around the mountain have poor access roads and accessibility to sampling sites was also a challenge. Also, sample collection was done at a time when farmers had harvested their cassava produce making it a challenge to access adequate cassava samples for analysis. Installation of radon and thoron monitors in dwellings was received with suspicion by the locals. As a result, a good number of the residents were not willing to have the monitors installed in their dwellings.

CHAPTER TWO: LITERATURE REVIEW

2.1 Radiation exposure pathways

Radiation exposure to human beings can either be internal or external. Internal exposure is usually as a result of inhalation of radon, thoron, and their progenies, or ingestion of foods and/or drinks contaminated with the radionuclides. Ingestion mainly occurs when the radionuclides present in the environment enter the food chain. The contamination may also occur directly where the radionuclides are deposited on the above-ground parts of the plants. Also, indirect contamination takes place when the radionuclides are taken from the soil by the root system of plants through the sorption process (UNSCEAR, 2000). Animals that consume plants are regarded as secondary recipients. Plants together with the animal products all form the human diet. Animal pathways therefore include ingestion of animal products such as meat, milk, eggs, and fish. A schematic representation of the different pathways of radionuclides is highlighted in Figure 2.1.

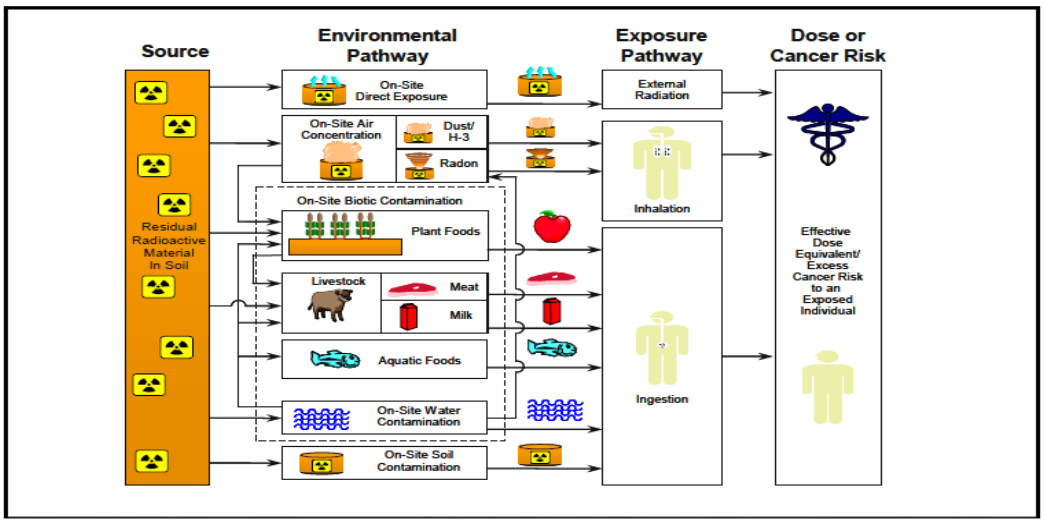

Figure 2.1: Schematic representation of radiation exposure pathways (Yu *et al*, 2001)

Land, plants and water contamination may occur from deposition of materials introduced into the atmosphere or from waste products which are discharged directly into the surface waters or placed in or on the ground where they are then carried off by ground water or erosion. This contamination in turn increases exposure of man to ionizing radiation (Merril, 1997). Grazing animals are regarded as important in transferring the radionuclides to man. This is because of the large surface area of pasture from which they feed. The transfer of the radionuclides to milk and meat occurs through root uptake or through deposition and subsequent grazing. These finally get to man via ingestion.

Food processing affects the amount of the radionuclides remaining in them. For instance, the concentration of the radionuclides increases in dried foods while it reduces in boiled food. Moreover, it reduces when vegetables are, cleaned, and/ or peeled.

Radon and thoron gases emanate from the soil in form of soil gas and can enter and attain high concentration levels in indoor air. The radon isotopes are carcinogenic and are responsible for the largest fraction of cancer cases among non-smokers, (WHO, 2011). Radon is considered as the second most important cause of lung cancer after smoking in many countries, (Tokonami *et al*., 2004; Chen *et al*., 2014; Kudo *et al*., 2015; Suman *et al.,* 2021) as declared by WHO, (2009). While most inhaled dose has previously been attributed to radon (^{222}Rn), more recent studies show that, thoron (^{220}Rn) is of concern particularly in dwellings where the main building material is soil. In China for instance, residential dwellings constructed using soil and earth-dug cave dwellings with elevated thoron concentration in some cases as high as 1,860 Bq m^{-3} have been reported, (Tokonami *et al*., 2004;). Radon concentration depends on the

type of building materials, humidity, place, and time, inflow of soil gas from the ground and ventilation of the house. Thoron on the other hand varies significantly due to its short half-life. The levels of the isotopes have also been reported to vary seasonally with highest levels being reported in winter, and lowest being reported in summer. In winter, doors and windows remain closed almost throughout the period resulting to poor ventilation. In summer however, the doors and windows remain open most of the time enhancing air exchange between the inside and the outside. Studies done in Garhwal Himalaya reported higher radon and thoron levels in mud houses as compared to wooden houses. Thoron progeny measured as equilibrium equivalent thoron concentration (EETC) levels in the same study were reported to be higher in mud-built houses and lowest in cemented houses (Singh *et al*., 2015; Ramola *et al.*, 2016; Suman *et al.,* 2021).

The isotopes *per se* are not responsible for the dose to the respiratory tract that is said to cause cancer but rather their progeny. Unlike the radon isotopes, the progenies, (^{210}Pb and ^{210}Po) are short-lived charged particles and may become attached to aerosol, dust, smoke and moisture particles. When inhaled in free or attached form, the progeny can lodge itself in the lungs. Consequently, upon decay, they deposit energetic alpha particles on the cells of the mucous membranes, bronchi and other pulmonary tissues which may damage the bronchial epithelial cells thereby increasing the risk of lung cancer, (Kudo *et al*., 2015). Information on radon and thoron concentration levels in Kenya is limited and research on simultaneous measurement of radon and thoron in Kenya for example has only been done in Mrima hill by Chege *et al* (2015). However, this is the first study in Kenya to measure EETC (thoron progeny) levels in dwellings.

Underground water is more prone to contamination by waste disposal than surface water. This is because it is in direct contact with the surrounding bedrock for a much longer period. With time, rocks undergo weathering and the elements contained in the rocks dissolve in water. Untreated underground water when used for drinking and/or cooking can therefore be an important source of internal exposure. In addition, underground water can be a source of radon, where it enters into the water from rocks that contain uranium and radium. When used for showering and washing, it releases about 50 percent of the radon present to the indoor air and nearly the whole amount when used for cooking. When the radon-rich water is used for drinking, people are exposed both through ingestion of the water and through inhalation. Therefore, exposure to radon in water or in indoor air over a long period of time, even in low concentration levels increases the risk of developing cancer, (Olise *et al*., 2016).

External exposure to ionizing radiation arises from radiation sources located outside the human body. The radiation can be in the form of gamma rays, alpha or beta particles. Of importance are the gamma rays which penetrate the body tissue most, unlike the alpha particles which rarely penetrate the outer dead skin layer of the body. Primordial radionuclides in the decay chains of ^{238}U and/or ^{226}Ra and ^{232}Th and the singly occurring ^{40}K present in soil, rock and crops are the major sources of external radiation exposure to human beings. The concentrations of the radionuclides are widely distributed and mostly depend on the local geology hence they vary from place to place. Their levels largely depend on the type of the rock from which the soils originated from. The igneous rocks such as granite have the highest concentration levels while sedimentary rocks have the lowest concentration levels. Other rocks such as shales and phosphate rocks are also known to have relatively high content of the

radionuclides, (Faanu *et al.,* 2016). Many radionuclides naturally occur in terrestrial soils and rocks which upon decay produce an external radiation field that we are all exposed to. The decay of these radionuclides in soil produces gamma radiation which cross the soil-air interface thereby producing radiation exposure to man.

Some human activities such as quarrying, processing of quarried rocks and application of phosphate fertilizers can enhance the natural background radiation levels leading to technologically enhanced naturally occurring radioactive materials, (Mwalongo *et al.,* 2023). Quarrying brings out large amounts of buried materials that contain naturally occurring radionuclides to the surface of the earth while processing further abets release of the radiation, (Okedeyi *et al*., 2012). Studies carried out in Egypt quarries (Ibrahim *et al*., 2014) reveal that quarry workers are generally exposed to higher doses of radiations than the general public.

Quarrying is a common activity in Kilimambogo region and the environs. It was therefore of paramount importance to establish the concentration levels of the radionuclides present in quarry rock samples and determine the exposure levels of the quarry worker as well as that of the general public.

2.2 Biological effects of ionizing radiation

Ionizing radiation is known to interact with atoms by the ionization process which may result to biological damaging effects. Radiation effects on human beings proceed from atoms which in turn affect molecules, cells, tissues, organs and consequently the whole body. Radiation ultimately affects body cells either directly or indirectly. Direct effects result when radiation interacts with the DNA molecules or other cellular parts important to the survival of the cells hence affecting the ability of the cells to

reproduce. Indirectly, radiation may interact with cell water by breaking their covalent bonds producing hydroxyl (OH) and hydrogen (H) ions. These ions may recombine, form compounds, like water (which is harmless), or toxic substances, like hydrogen peroxide (H_2O_2) (which is harmful to the cell). Some of the cells may completely repair themselves in case of any damage and function again normally while others may die if the damage is severe enough. In other instances, the damaged cells may reproduce but the daughter cells end up dying or getting mutated. The mutated cells reproduce thereby perpetuating the mutation which becomes the beginning of malignant tumor developments, (USNRC, 2011)

Biological long-term effects of radiation could be acute or chronic. Acute effects result when there is exposure to high doses within short time generating short term effects. Chronic effects result from exposure to low radiation doses for long time. High doses kill cells, while low doses damage or change the cell composition. High dose effects called acute radiation syndrome (ARS), may include; hemorrhage, diarrhoea, vomiting, death, skin burns, hair loss or epilation, sterility, cataracts or injury to gastrointestinal track or central nervous system. Acute radiation syndrome results when enough important tissues and/ or organs in the body are damaged as a result of the high radiation exposure, (WHO, 2016)

Exposure to low doses of radiation could also lead to genetic, somatic or in-utero effects. Genetic effects involve the mutation of sperm or egg cells consequently affecting the offspring of the exposed individuals. Somatic effects are suffered by the exposed individuals and sometimes called the carcinogenic effects given that cancer is the primary result. These may include; lung cancer, bone cancer, thyroid cancer, breast cancer, skin cancer or leukemia. In-utero effect is a special case of the somatic

effects where the embryo gets exposed to radiation. These effects can include; abnormalities in embryo development, retardation in growth, childhood cancers or intra-uterine death, (USNRC, 2011).

2.3 Radon and cancer

Exposure to radon isotopes and their progenies is one of the causes of lung cancer after cigarette smoking, (WHO, 2009). The leading cause of cancer worldwide is active smoking followed by passive smoking and then radon and the decay products. The EPA approximates that residential radon causes around 21,000 deaths from lung cancer in the United States annually, (Pawel and Puskin., 2004). Radon has also been linked to cause other types of malignancies though the conducted researches are insufficient and inconclusive. Research done in Spanish to establish correlation between residential radon and esophageal cancer revealed that radon contributes its cause to a great extent, (Ravina *et al.,* 2017; Reddy *et al*., 2022; Lorenzo *et al.*, 2017). This has been so because ionizing radiation has been reported to be a risk factor of esophageal cancer hence the significant correlation. These results are consistent to research conducted in Kenya and reported by the People Daily, (Kebaso, 2023) which confirmed that esophageal cancer is the leading cause of death in men and women, in Kenya, contributing to 15.6% of all mortalities. This again agreed to cancer cases reported in Kiambu where 24.4% and 6.5% of male and female cancer patients were diagnosed with esophageal cancer respectively, (Kamita *et al.*, 2020). Worldwide, esophagus is ranked eighth most common cancer, however, developing countries like Kenya contribute 80% of these cases. Reddy *et al* (2022) reported that ionizing radiation is a significant risk factor for esophageal cancer. Reddy *et al* (2022) also reported that radon isotopes could significantly cause skin cancer since the alpha

particles from the progeny ^{218}Po and ^{214}Po have the ability to penetrate into the epidermis, potentially reaching the skin basal layer in certain body parts. Also, when water containing soluble radon is ingested, it could remain in the stomach for a while and the risk significantly increases when water is consumed for relatively long periods. Such radon in water could trigger some cancers such as kidney and stomach cancers, (Lorenzo *et al*., 2017).

2.4 Radionuclides and heavy metals in the environment

The ecosystem has many radionuclides and heavy metals and their levels are of great concern to the health of the residents. Many researchers globally have embarked on rigorous research in trying to determine the concentration and risk levels of heavy metals and primordial radionuclides in different matrices in the environmental. The measured results have been compared to the safe concentration levels provided by UNSCEAR, (2019) to determine the level of exposure to human beings.

2.4.1 Radioactivity in rocks and soils

All rocks and soils contain some amounts of primordial radionuclides whose levels depend on the geology of the given area. Areas with extremely high concentration levels of the radionuclides are regarded to as high background radiation areas (HBRA). Some of the high background radiation areas in the world include Guarapari in Brazil, Ramsar in Iran, Paralana in Austria, Yangjiang in China and Karunagappally in India. Along the coast of four Brazilian States, Veiga *et al* (2006), reported significantly high concentration levels of naturally occurring radionuclides. ^{232}Th as high as 55,537 Bq kg^{-1} in Guarapari, Brazil which is 150 times the recommended limit and ^{226}Ra, as high as 4,043 Bq kg^{-1} were reported. The elevated levels were associated with sand eroded from Monazite; an ore of naturally radioactive thorium commonly

found in mountains. Background radiation as high as 175 mSv y^{-1} has been measured in the region. Ramsar, a city and county on the Southern Coast of the Caspian Sea in Iran has the highest levels of natural radiation reported on earth. Levels as high as 260 mSv y^{-1}, up to 80 times the world average from external terrestrial sources have been measured. This is attributed to high levels of ^{226}Ra (up to146 kBq kg^{-1}) and its decay products brought to the surface by water of the hot springs, (Ghiassi *et al.*, 2002). The water is heated by the geological activity under the earth's surface where it then travels through rocks containing radioactive substances. Annual external effective doses received by the residents range from 0.7 to 131 mSv. Residents living near the hot springs use limestone, sourced from the sea to make bricks for construction of dwellings. As a result, there are elevated levels of radon in homes which enhances the levels of radiation exposure to the residents, The internal doses due to ^{222}Rn range from about 2.5 to 72 mSv. Erosion of the local bedrock with high thorium content is associated with enhanced levels of the high radiation. Paralana hot springs are found inside the Arkaroola wilderness sanctuary in Australia where subterranean springs flow through uranium rich rocks bringing radioactive radon and uranium to the surface. The resulting radioactive decay raises the temperature of the water up to 62^{o}C.

In Yang Jiang China, located in the Southern Guangdong province, residents mainly build their dwellings using sand and clay. The sand in the region is believed to have eroded from the hills that contain monazite. Once this is incorporated in bricks, thorium in the monazite sand continues to decay into radioactive radium, radon, and actinium. The average annual effective dose is 6.4 mSv and an internal dose of 4.3 mSv, (Hendry *et al.*,2014). Kerunagappally, municipality in the Kollam district of Kerala, Southwest India is a monazite-bearing coastal region where monazite erodes

into the beaches. Radiation exposure in these areas is mainly due to the presence of thorium and its decay products in the surface soil. Residents receive annual external doses of about 4.5 mGy from gamma-rays and additional internal dose of about of 2.4 mSv from exposure to radon, (Nair *et al*., 2000).

Levels of ^{232}Th and ^{40}K, as high as 2,398 Bq kg^{-1} and 2,184 Bq kg^{-1} respectively were reported in mining areas and quarries of Eastern Uganda, (Mugaiga *et al.*, 2016). In gold mine Tailings of Gauteng Province in South Africa, very high concentration levels of uranium were measured, (as high as 2,669 Bq kg^{-1}) and a mean of 785 Bq kg^{-1} which was attributed to large volumes of uranium wastes found in the gold mines, (Kamunda *et al.,* 2016). This maximum value was more than thrice the maximum value reported in Eastern Uganda, of 698 Bq kg^{-1}.

Many researches have been done in Kenya. In Tabaka soapstone quarries of Kisii region, ^{226}Ra concentration as high as 1,780 Bq kg^{-1} was measured, (Kinyua *et al*. 2011). The high background radiation areas (HBRA) in Kenya have been identified in some areas such as Mrima hill, Lambwe East and Homa Mountain. Such regions are mainly characterized by carbonatite and monazite rocks (Odongo, *et al*., 2021) which are known to be rich in these primordial radionuclides. Soil samples collected around Mrima hill recorded ^{232}Th concentrations with a mean of 500 Bq kg^{-1}, and a maximum of 869 Bq kg^{-1}and ^{238}U recorded a mean concentration of 207 Bq kg^{-1} and a maximum of 354 Bq kg^{-1} (Kebwaro *et al.,* 2011). This was consistent to what was measured in Mrima hill, Chege, 2014 where ^{226}Ra recorded a mean concentration of 142 Bq kg^{-1} and a high of 250 Bq kg^{-1}. At the same time, ^{232}Th recorded a mean value of 457 Bq kg^{-1} and a maximum of 854 Bq kg^{-1}. Samples from Mt. Homa reported ^{232}Th concentration with a mean of 410 Bq kg^{-1}and a maximum of 1,447 Bq kg^{-1} while

the mean concentration of ^{226}Ra was 195 Bq kg^{-1} and a maximum of 1,568 Bq kg^{-1}, (Otwoma *et al.,* 2012). These values are more than forty times the world average values. Very high levels of ^{232}Th were also measured in Ruri, a hill which is also characterized by carbonate rocks, recording a mean of 1,397 Bq kg^{-1} and a maximum of 6,560 Bq kg^{-1}. This sample collected from the foot of North Spur of the hill was believed to have been deposited from the hill via erosion, (Opiyo, 2009). Similar study conducted by Odongo, *et al* (2021) measured ^{232}Th levels as high as 1094 ± 55 Bq kg^{-1}. Results that emanate from the current research would advise on the radiological risks posed to the residents of Kilimambogo region, and whether the soil and rocks harvested from the region could be safely used for agriculture and construction of dwellings or not.

^{40}K is associated with the presence of radioactive rich granite, phosphates, sandstones, and quartzites. Mean concentration of ^{40}K of 961 Bq kg^{-1} and a maximum of 2,179Bq kg^{-1} in Tongaren constituency, Bungoma has been reported and has been associated with granite and metamorphic rocks, (Musamali, 2016). Homa Mountain recorded ^{40}K concentration of as high as 3,018 Bq kg^{-1}, about 7 times higher than the world average, (Otwoma *et al.,* 2012) while Ruri hills recorded a maximum of 1,455 Bq kg^{-1}, (Opiyo, 2009). In Narok, a maximum and a mean of 1,725 Bq kg^{-1} and 1,384 Bq kg^{-1} respectively were reported, (Kiplangat, 2016). In Malindi and Mrima hill, a mean and maximum concentrations of ^{40}K of 519 Bq kg^{-1} and 899 Bq kg^{-1} were recorded, (Hashim, 2001; Hashim *et al.,* 2004), and 805 Bq kg^{-1} and 1,108 Bq kg^{-1}, (Kebwaro *et al.,* 2011) respectively.

2.4.2 Radioactivity in plants

Not much research has been done on the levels of radionuclides in plants across the globe and more so in Kenya. The levels of radionuclides in plants vary depending on the type of the crops and the soil in which they are grown. The consumption of food products by man is the most important cause of exposure to radionuclides through ingestion pathways since it results to internal radiation doses, (Jazzar and Thabayneh, 2014; Hassan, 2023). The absorption of the radionuclides by plants depends on their soil concentration and characteristics, the bioavailability in the soil, root structure and the shoot system, (Chandrashekara and Somashekarappa, 2015). Each radionuclide present in soil may be transported to plants in solution form or get bound to the soil particles. Migration of the radionuclides is also influenced by farming activities that disturb the soil profile and may in turn enhance the root uptake pathway.

The rate of absorption of the elements by the plants is determined by the concentration of exchangeable calcium present in the soil. Measurements of the radionuclides in food crops help determine the level of risks and harmful effects to the general public.

The transfer or uptake of radium, thorium and potassium by plants depends on biological, chemical and physical conditions of the soil as well as the chemical properties of the radionuclides, (Jazzar and Thabayneh, 2014). Thorium generally has a lower mobility from soil to plants compared to radium which is more soluble in water hence absorbed more easily through water uptake. Thorium on the other hand has a low solubility and its ions are more bound on the soil hence resulting to low transportation. Radium also portrays characteristics which are similar to calcium and magnesium. Potassium in plants provides an ionic environment for metabolic processes and acts as a regulator of various processes like growth, protein synthesis

and opening and closing of stomata, (Echessa, 2020). Application of fertilizers to the soil to enhance crop yield are the main anthropogenic sources of the radionuclides, (Kumar *et al.,* 2022; Njinga *et al.,* 2013) This is important especially for soils that do not have sufficient macronutrients for plant growth and development. It therefore assists in crop yield. Also, decaying plant materials replenish soils with a lot of potassium. It is easily absorbed by roots when the soil is not dry or soil is not alkaline. Extreme levels of potassium in soils however may cause damage to germinating seedlings, inhibit uptake of other important nutrients such as calcium, nitrogen and magnesium, and reduce quality of the crops. Long term potassium buildup can be minimized by advising farmers to consider using aged animal manure as a substitute for commercial fertilizers since the components of the manure break down more slowly, (Echessa, 2020).

The activity concentration of cassava crop was measured in Osun State, Nigeria. The levels of ^{226}Ra, ^{232}Th and ^{40}K reported were 2.0 ± 0.4 Bq kg^{-1}, 1.8 ± 0.1 Bq kg^{-1} and 40.1 ± 3.9 Bq kg^{-1} contributing an effective dose of 0.66 µSv y^{-1}, (Nwankpa, 2017). Levels reported in Onne Nigeria in Cassava flour for ^{238}U, ^{232}Th and ^{40}K were 19.3 ± 5.0 Bq kg^{-1}, 11.4 ± 3.3 Bq kg^{-1}, and 426.9 ± 33.8 Bq kg^{-1} respectively, (Avwiri and Agbalagba, 2015). ^{40}K measured in cassava in Mrima hill, Kenya recorded maximum concentration levels of 1,708 ± 552 Bq kg^{-1} in leaves. In the same study, maximum concentration of ^{226}Ra was reported to be 141.7 ± 74.6 Bq kg^{-1} and that of ^{232}Th reported to be below detection limit. According to studies done in Bitsichi, Jos Plateau in Nigeria, it was observed that the activity concentration in cereals was lower than that measured in tubers and vegetables. For instance, ^{226}Ra recorded a concentration of 34 Bq kg^{-1} and 86 Bq kg^{-1} in maize and yam respectively, while ^{40}K recorded 243

Bq kg^{-1} and 685 Bq kg^{-1} in the same crops. In the same study, higher concentration level of ^{226}Ra was measured in crops than the soil since it accumulates more easily in plants, (Jibiri *et al.,* 2007). Also, vegetables consumed by Malaysian people in Sungai Besar recorded ^{40}K concentration levels of as high as 1,223 Bq kg^{-1}, (Solehah *et al.,* 2016).

Mohammed *et al.* (2015) analyzed the distribution of ^{226}Ra, ^{232}Th and ^{40}K in different plant components of rice and found that about 47% of ^{226}Ra accumulated in the roots, 30% in straw, 14% in husk and 9% in grain. It was observed that ^{226}Ra is preferably retained in the roots compared to the other plant parts. Similarly, for ^{232}Th, 57%, 24%, 11% and 8% were concentrated in roots, straw, husk, and grain respectively. ^{40}K behaved differently, where its distribution reflected its mobility and transportation from the roots to the rest of the plant. 59%, 21%, 13% and 7% were found in the straw, husk, root, and grains respectively. This is because potassium being an essential mineral for plant growth is easily transported along with water from roots to the other parts of the plant.

The concentration of the radionuclides in cassava investigated in the current study and the corresponding doses will inform the public and the health organizations on the extent of the radiation ingestion dose received by the residents from the consumption of cassava.

2.4.3 Radioactivity in air

Radioactivity in indoor air is attributable to the radon isotopes. There are three radon isotopes; radon (^{222}Rn), thoron (^{220}Rn), and actinon (^{219}Rn) from ^{238}U, ^{232}Th, and ^{235}U decay series and having half-lives of 3.82 d, 56 s and 4 s respectively. Radon (^{222}Rn),

being one of the inert gases is also radioactive and readily found in the environment. It is regarded as the most important isotope among the radon isotopes since it has a relatively long half-life compared to the others. Of all the inert gases, radon is the most dense with an atomic mass of 86 and makes the highest contribution regarding internal radiation received by human beings. However, it is the radon progenies such as ^{218}Po,^{214}Pb, ^{214}Bi and ^{214}Po which are of a more radiological concern rather than radon itself since they deliver about 95% of the radon related effective dose from inhalation, (Bekelesi, 2015). Owing to its relatively long half-life, radon diffuses easily from the soil gas to the indoor air as compared to the other isotopes like thoron. A good percentage of thoron for instance decays before it gets into the indoor air as a result of its short half – life. High concentration of indoor radon is mostly found in modern houses due to its relatively long half-life while thoron decays before it is able to exhale out of the material. However, in dwellings constructed using raw soil (mud), which is more porous, thoron, is able to easily diffuse through the walls before it undergoes decay. It is therefore able to accumulate in indoor air of such houses sometimes to alarming levels, (Hashim *et al*, 2020; Suman *et al.*, 2021). Thoron decays forming thoron progenies which mainly contribute to the inhalation dose received by the occupants of the dwellings to a greater extent, (Nyambura *et al.*, 2019)

Several studies have been carried out across the world. Recently, researchers have developed great interest in thoron and the daughter products which have been ignored for a long time. In Kenya for instance, researchers started with measurement of only radon concentrations in different types of dwellings for instance in the Coast and Rift valley region. High radon levels in stone-built houses (199 Bq m^{-3}) in Soi region of Rift Valley, and lower levels in mud-built dwellings (67 Bq m^{-3}) in the same region

were reported. Higher radon levels were observed in mud-built dwellings of Taita (278 Bq m^{-3}) and Taveta (240 Bq m^{-3}) in the coast region as compared to relatively lower levels in wooden-built houses (60 Bq m^{-3}) in Olkaria, (Maina *et al*., 2002). Mustapha *et al*., (2002) reported different radon levels in indoor air in different floors in various parts of Kenya with basements recording the highest mean radon concentration levels (424 Bq m^{-3}), ground floor (155 Bq m^{-3}), first and higher floors recording the lowest (148 Bq m^{-3}) levels. Chege *et al*. (2009) measured radon concentration in model mud-walled traditional huts located in Kenyatta University, Kenya and levels up to 315 Bq m^{-3} was reported. In the same study, classrooms built using building blocks and basements recorded mean radon concentrations of 193 Bq m^{-3} and 202 Bq m^{-3} respectively. Chege *et al*. (2015) was the first researcher in Kenya to simultaneously measure radon and thoron concentration levels in dwellings. The average concentration levels of radon and thoron reported in Mrima hill, Kenya were up to 56 Bq m^{-3} and 1,295 Bq m^{-3} respectively.

Relatively lower radon levels of 39 Bq m^{-3} were reported by Hashim *et al* (2020) in Karbala, Iraq. In Garhwal Himalaya, the variation of the isotopes in cemented, mud-built, and wooden-built houses was investigated. Higher radon and thoron levels in mud houses were reported as compared to wooden-built houses. Thoron progeny levels were reported to be higher in mud-built houses and lowest in cemented houses, (Ramola *et al.*, 2016). In Canada, higher values of radon, 96 Bq m^{-3}, more than double the world average and lower values of thoron; 9 Bq m^{-3}were reported, (Chen *et al*., 2014). In Yang Jiang, China; a HBRA radon and thoron levels of up to 476 Bq m^{-3} and 3,957 Bq m^{-3} respectively were reported, (Kudo *et al.*, 2015). In Southwestern Cameroon, radon, and thoron concentrations of up to 937 Bq m^{-3} and 700 Bq m^{-3}

respectively were measured, (Saidou *et al*., 2015). Senthilkumar, (2014) however reported lower annual average values of 28 Bq m^{-3} and 17 Bq m^{-3} for radon and thoron concentrations respectively in dwellings of Shahjahanpur. He reported least concentration in summer and highest in winter and associated the possible cause for the radon and thoron variation to the fact that, in summer, the houses remain open for long time which contributed in increased air exchange rate in the rooms. On the contrary, in winter, the rooms remain closed for long hours thus decreasing air exchange in the rooms. Similar results were measured by Suman *et al* (2021) in dwellings of Buddonithanda village in India. He further observed that, higher radon and thoron levels were measured during the day when dwellings were closed and residents were out in the fields and at night when the ventilations in the dwellings were poor. Lower levels of the airborne radioactivity levels were however measured at dawn and dusk when there were more human activities, attributed to increased aeration of the dwellings. The levels were also noted to vary with construction materials of the dwelling. Nkoulou II *et al (*2023) reported radon and thoron concentration levels of 133 ± 39 Bq m^{-3} and 93 ± 96 Bq m^{-3} in Betare- Oya Gold mining areas of Eastern Cameroon which were within recommended reference levels.

The concentration of thoron progeny in dwellings by different researchers have been determined and expressed as equilibrium equivalent thoron concentration (EETC). Studies have been done in Shaanxi, China, (Tokonami *et al.*, 2004), Orisa, India, (Ramola *et al.*, 2010), Gansu, China, (Yamada *et al.*, 2006), Ireland, (Mc Laughlin *et al*., 2011), Canada, (Chen *et al*., 2014), Yang Jiang, China, (Kudo *et al.*, 2015) among other areas. The EETC levels in most of these studies reported up to 10 Bq $m^{-3,}$ except in Yang Jiang, China, where up to 36 Bq $m^{-3,}$ of EETC were measured. In a similar

study conducted in Betare- Oya Gold mining areas of Eastern Cameroon, lower levels of thoron progeny, 6 ± 4 Bq m^{-3} were measured, (Nkoulou II *et al.,* 2023).

In Kilimambogo region, there are diverse types of dwellings constructed by the residents. It was therefore necessary to investigate how the different types of construction materials contributed in the concentrations of radon and thoron in the dwellings and consequently the doses received by the residents. Also, the type of flooring varied from cemented or concrete to bare earth. The behaviour of the radioactive gases in the different types of floors was also investigated. As a result, it will be possible to advice the public on how to reduce radiation exposure based on the nature of dwellings.

2.4.4 Heavy metals in water

The concentration levels of the non-radioactive elements in water are also related to the geology of a region. In Manzala Lake, Egypt, Badry, (2016), reported average concentrations of heavy metals such as Cd, Pb, Zn, Ni, Co and Cu to be 0.4, 5.8, 0.9, 2.44, 2.8, and 1.45 μg L^{-1} respectively. In India, however, Maurya and Malik, (2016) measured the concentrations of Cd, Cr, Pb, Cu Mn and Zn in river water to be 0.009, 0.056, 0.056, 0.058, 0.049, 0.883, 0.36 mg L^{-1} respectively. Those that were measured in Mafikeng, South Africa by Mathuthu and Olobatoke, (2016) were up to 656, 655, 5, 1, 860, 3, 4, 7, 8 and 3μg L^{-1} for Na, Ca, Cr, Mn, Fe, Ni, Cu, Zn, As and Bi respectively. In North West, Nigeria, the mean concentrations computed for borehole water samples were 0.006, 0.04, 0.03, 3.419, 0.029, 0.399, 1.867 and 0.089 mg L^{-1} for Cd, Co, Cu, Fe, Pb, Mn, Hg and Ni respectively, (Abdullahi *et al*., 2016). Mn, Cd, Pb, Cu and Zn were measured in Mrima hill where the concentration levels were generally low with Cu recording up to 5.123 mg L^{-1} (Chege, 2014). Lower levels of Cu (0.017

ppm) and Cd (0.023 ppm) were reported in Chereti, along Borkena River in Ethiopia, (Mohammed *et al.,* 2023). Wanjala *et al.,* (2020) also reported lower levels of Pb (0.004 mg L^{-1}), Ni (0.037 mg L^{-1}), Cd (0.0002 mg L^{-1}) and Mn (0.0002 mg L^{-1}) indicating that the water sources were safe for human consumption. Determination of heavy metal concentration in water samples in Kilimambogo region was necessary in order to advise the public and the health organizations on the status of pollution and how this could possibly be reduced in order to improve water quality by reducing possible water pollution.

2.5 Doses using RESRAD computer code

Ziajahromi *et al* (2013) evaluated the activity concentrations of natural radionuclides in Khak-Sefid, Iran and evaluated the total effective dose equivalent (TEDE) from exposure to high level natural radiations. The evaluation was done on the farmer, construction worker and the resident scenarios using the RESRAD computer code. The mean activity concentrations were 23,118 $\pm$ 468, 26 $\pm$ 2 and 403 $\pm$ 17 Bq $m^{-3,}$ for ^{226}Ra, ^{232}Th and ^{40}K respectively. Mathuthu *et al* (2016) also used the code to determine the doses received by miners in gold mine Tailings in Wonder fonteinspruit catchment area, in South Africa. TEDE received by workers working in a thermal power plant in Egypt were 17.4 µSv y^{-1}, (Hassan, 2023). Relatively lower doses were reported by Kipng'eno (2022) for residents of Bureti, Kericho county, Kenya with ^{226}Ra, and ^{40}K contributing doses equivalent to 0.17 mSv y^{-1} each. The doses measured in this study were however comparable to doses reported in Ortum, West Pokot County, Kenya by Wanjala (2021) of 0.28 mSv y^{-1}.

CHAPTER THREE:THEORETICAL CONSIDERATIONS

3.1 Natural radioactivity and radiations

3.1.1 Radioactivity

Radioactivity is the spontaneous disintegration of unstable nuclei (called radionuclides). This results in the release of ionizing radiation in form of alpha (α) particles, beta (β) particles or gamma rays (γ). The alpha particles are in the form of Helium (He) nuclei while that of beta particles are in form of electrons. Gamma rays are highly energetic electromagnetic radiation released mostly after either an alpha or beta particle decay takes place in a radioactive element. The nucleons (protons and neutrons) in the nucleus are held together by the nuclear force regarded as the strongest force in the universe. If this force is not strong enough to hold the nucleons together, the nucleus disintegrates by releasing alpha or beta particles and/ or energy in form of gamma rays in a process referred to as radioactive decay (Pentreath, (2021).

Ionizing radiation originates from natural or man-made sources. Radon, an inert radioactive gas adds over 50% of radiation exposure to the public. Uranium and thorium and their radioactive decay products have been in existence since the formation of the earth. While radon, a decay product of uranium decay series is inhaled, some other radioactive materials and radioisotopes are ingested with food and water. For instance, Iodine-131 accumulates in thyroid and emits beta particles upon decay. Cesium-137 accumulates in muscle and soft tissues and emits gamma rays upon decay. Plutonium-239 is found in lung, liver, and bones and emits alpha particles upon decay. National Academies of Sciences, Engineering, and Medicine. (2005).

Human beings are therefore continuously exposed to radiation that emanates from radioactive materials deposited in their bodies. On average, radon isotopes alone contribute about 55% of all the radiations received by the public from both natural and artificial sources while 11% comes from other radioactive materials inside the body, (IAEA2003). Other than radon whose exposure upon inhalation mainly depends on the amount of uranium or radium present in soil, ^{40}K is the most important internal radioactive element. However, the amount of radiation from ^{40}K is relatively stable and constant amongst individuals.

3.1.2 Radioactive decay series

The decay of an unstable nucleus is its attempt to become stable which is not achieved in a single decay. When unstable nuclei undergo radioactive decay, most of the daughter nuclei produced are also radioactive consequently undergoing radioactive decay. This as a result produces a chain of radioactive decays. The decay of the unstable nucleus is done by emitting subatomic particles such as alpha or beta particles. The long-lived primordial radionuclides produce a series of radioactive daughters until a stable isotope of lead is obtained. This chain of radioactive decays is regarded as radioactive decay series. Gamma radiation is highly energetic electromagnetic radiation that originates from the nucleus of an atom. It is therefore a mechanism of releasing excess energy from some radionuclides. There are four radioactive decay series, named depending on the parent radionuclide. Thorium, Neptunium, Radium and Actinium series whose parent radionuclides are Thorium, Neptunium, Uranium-238, and Uranium-235 respectively. The uranium series starts with uranium-238 and ends with stable lead-206 as illustrated in appendix 1. The actinium series comprises of the decay series of ^{235}U and ends with the stable lead-

207 isotope as illustrated in appendix 2. The Thorium series starts with thorium-232 and ends with a stable lead-208 isotope as illustrated in appendix 3. The neptunium series starts with neptunium-237 and most members are produced artificially. This series is illustrated in appendix 4.

When the radioactive isotopes decay, they are transformed to daughter nuclides which if they are also radioactive, they also decay to produce other radioisotopes. It is known that the activity of a pure radionuclide material decreases exponentially with time. For a parent radionuclide A with N_A atoms and a decay constant of λ_A, then the rate of radioactive decay follows the decay law given by equation (3.1);

$$\frac{dN_A}{dt} = -\lambda_A N_A \qquad (3.1)$$

If the initial conditions are such that, at the time t =0, $N_A=N_{A,0}$, then upon solving, equation (3.1) becomes;

$$N_A = N_{A,O} e^{-\lambda_A t} \qquad (3.2)$$

If the parent nuclide, A, decays and transmutes to a daughter radionuclide, B, then, the production rate of the daughter nuclide is equal to the decay rate of the parent, that is, B $(\text{production rate}) = \lambda_A N_A$, B in turn decays, with the decay rate given by; $B(\text{Decay rate}) = -\lambda_B N_B$ Where λ_B is the decay constant of the daughter nuclide and N_B is the number of daughter atoms present. The net rate of change of B at an instant in time is then given as;

$$\frac{dN_B}{dt} = \lambda_A N_A - \lambda_B N_B \qquad (3.3)$$

To determine N_B, we substitute equation (3.2) into (3.3), to obtain;

$$\frac{dN_B}{dt} = \lambda_A N_{A,O} e^{-\lambda_A t} - \lambda_B N_B \quad (3.4)$$

Rearranging;

$$dN_B + \lambda_B N_B dt = \lambda_A N_{A,O} e^{-\lambda_A t} dt \quad (3.5)$$

Multiplying equation (3.5) by$e^{\lambda_B t}$;

$$e^{\lambda_B t}\, dN_B + \lambda_B N_B\, e^{\lambda_B t} dt = \lambda_A N_{A,O}\, e^{(\lambda_B - \lambda_A)t} dt \quad (3.6)$$

It is worth noting that,

$$d(N_B e^{\lambda_B t}) = e^{\lambda_B t} dN_B + \lambda_B N_B e^{\lambda_B t} dt \quad (3.7)$$

This is the left-hand side of equation (3.6).

Equation (3.5) therefore becomes;

$$d(N_B e^{\lambda_B t}) = \lambda_A N_{A,O} e^{(\lambda_B - \lambda_A)t} dt \quad (3.8)$$

Integrating both sides of equation (3.8);

$$e^{\lambda_B t} N_B(t) = \frac{\lambda_A N_{A,O} e^{(\lambda_B - \lambda_A)t}}{(\lambda_B - \lambda_A)} + C \quad (3.9)$$

Where C is the constant of integration.

To determine C, we assume N_B=0 at t=0. After solving, C becomes;

$$C = -\frac{\lambda_A N_{A,O}}{(\lambda_B - \lambda_A)} \quad (3.10$$

Substituting C in equation (3.9), leads to equation (3.11);

$$e^{\lambda_B t} N_B(t) = \frac{\lambda_A N_{A,O} e^{(\lambda_B - \lambda_A)t}}{(\lambda_B - \lambda_A)} - \frac{\lambda_A N_{A,O}}{(\lambda_B - \lambda_A)}$$

(3.11)

Dividing equation (3.11) by $e^{\lambda_B t}$ and rearranging leads to equation (3.12);

$$N_B = \frac{\lambda_A N_{A,O}}{(\lambda_B - \lambda_A)}(e^{-\lambda_A t} - e^{-\lambda_B t}) \quad (3.12)$$

This is the solution to equation (3.3), indicating the number of daughter atoms present in the mixture of radioactive parent and daughter nuclides.

3.1.3 Radioactive decay equilibrium

Radioactive equilibrium is a state attained in a parent-daughter mixture when both are radioactive and have different half-lives. A sample in which a radionuclide produces one or more radioactive offsprings in a chain can acquire any of the following radioactive equilibrium states;

3.1.3.1 Transient equilibrium

The equilibrium is reached when the daughter's half-life is shorter than that of the parent and differs by a small factor. Also, $\lambda_B = \frac{0.693}{T_B}$, where T_B is the half-life of the daughter nuclide. When the observation time is much longer than the half-life of the daughter or t>>T_B, $\frac{0.693}{T_B}$ $t \to \infty$ hence $e^{-\lambda_B t} = e^{-\infty} = 0$. Therefore, equation (3.12) reduces to;

$$N_B \approx \frac{\lambda_A}{\lambda_B - \lambda_A}\{N_{A,O} e^{-\lambda_A t}\} \quad (3.13)$$

The term in parenthesis reduces to equation (3.2), Consequently, equation (3.13) becomes;

$$N_B = \frac{\lambda_A N_A}{\lambda_B - \lambda_A} \tag{3.14}$$

Rearranging, equation (3.14) becomes;

$$\frac{N_B}{N_A} = \frac{\lambda_A}{\lambda_B - \lambda_A} = \text{Constant} \tag{3.15}$$

Equation (3.15) shows that after a time longer than the half-life of the daughter, the ratio of the number of daughter atoms to that of the parent atoms remains constant. When this happens, the parent and the daughter nuclides are said to be in transient equilibrium.

Figure 3.1 illustrates the variation of the activities of the daughter and the parent in a state of ttransient equilibrium.

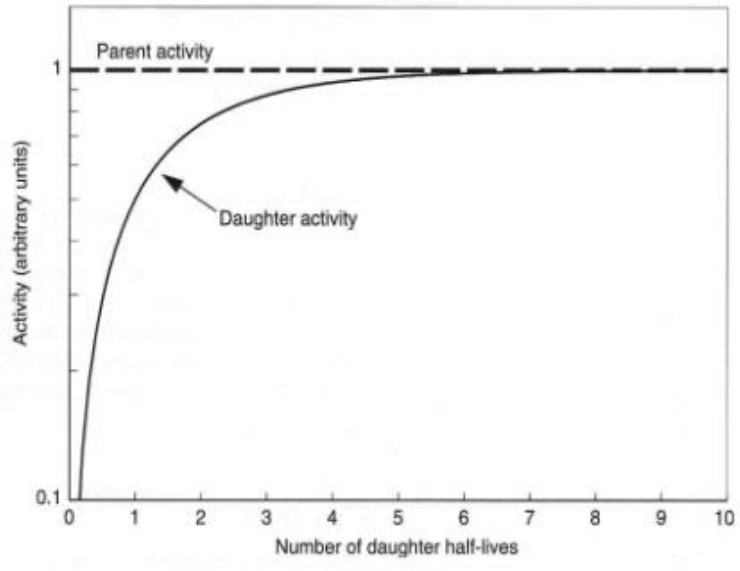

Figure 3.1: Illustration of transient equilibrium

(Miyaoka 2011).

3.1.3.2 Secular equilibrium

Secular equilibrium is a special case of transient equilibrium, where the parent's half-life is far much longer than that of the daughter nuclide by a factor of 10^4 or more. The decay constant of the daughter nuclide is therefore far much greater than the parent nuclide implying that; $\lambda_B - \lambda_A \approx \lambda_B$,. Equation (3.15) therefore reduces to;

$$\frac{\mathbf{N_B}}{\mathbf{N_A}} = \frac{\boldsymbol{\lambda_A}}{\boldsymbol{\lambda_B}} \text{ or } N_B\lambda_B = N_A\lambda_A. \quad (3.16)$$

Given that;$A = N\lambda$, then, the first term represents the activity of B whereas the second term the activity of A.

Therefore, the daughter activity becomes equal to that of the parent as illustrated in Figure 3.2. In such a case, the two nuclides are said to be in secular equilibrium. This case is assumed when the activity concentration of the primordial radionuclides in environmental samples is being determined. In this case, the samples are sealed and stored for a time that is equivalent to about seven half-lives in order for the parent to attain secular equilibrium with the daughter nuclides. At this time, the activity of the parent is assumed to be equal to the activity of the daughter nuclides. Therefore, the activity concentration of the progeny is determined and assumed to be equivalent to that of their long-lived parents.

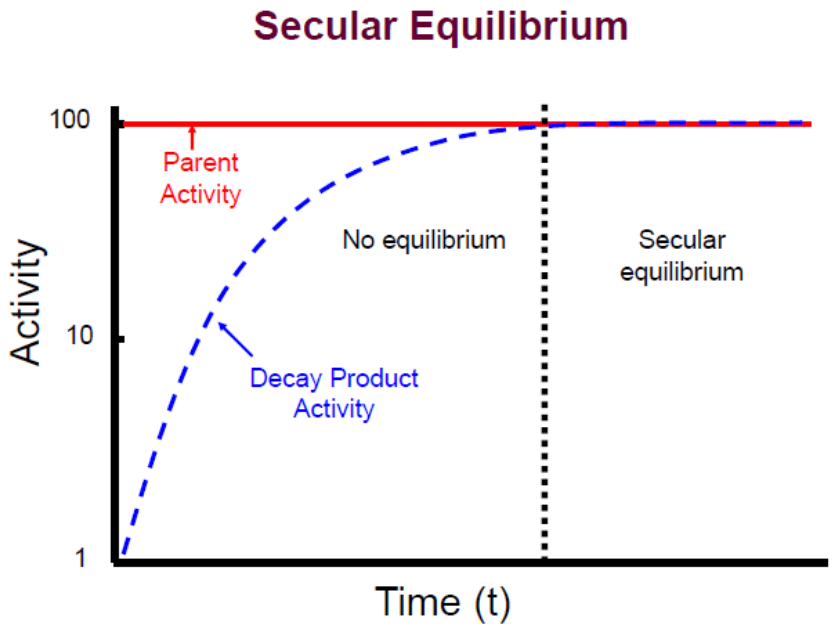

Figure 3.2: Schematic illustration of secular equilibrium
(USNRC, 2011)

3.1.4 Types of radiation

Radioactive materials decay by emitting alpha (α) particles, beta (β) particles, and /or gamma (γ) rays. These radiations interact with matter along their path. The most common interactions of α particles, β particles, and γ- radiation are by ionization where some electrons are ejected from neutral atoms leaving behind positively charged ions. Alpha radiation consists of a stream of positively charged alpha particles whose initial energy is in the order of MeV. They are composed of a Helium nucleus which is made up of two protons and two neutrons. They exhibit high ionization with low penetration range in matter. Beta radiation mainly comprises of a flux of electrons with a continuous energy spectrum and higher penetration range in matter. Gamma rays are electromagnetic waves with very short wavelengths, and with higher photon energies. They are produced from the nucleus as a result of deexcitation of the nucleus after it has undergone a radioactive decay. The gamma rays have no mass or charge,

travel at a speed of light, and have discrete energy and frequency. Gamma photons produce ionization indirectly unlike alpha and beta radiation which produce their ionization directly.

3.1.5 Interaction of gamma radiation with matter

When gamma rays interact with matter, they may either be completely absorbed or scattered by an electron or nucleus depending on the photon energy. A gamma photon can interact with an atom in matter in any of the following ways; photoelectric effect, Compton scattering or by pair production.

3.1.5.1 Photo-electric effect

Photo-electric effect is a phenomenon where electrons are emitted from a metal surface when a gamma photon falls on it. The gamma photon transfers all of its energy to the electron, and ejects it from the atom as illustrated in Figure 3.3. An incident photon of frequency *f* having energy equal to h*f* where h is the Planck's constant, strikes the electron transferring all of its energy to the electron. The energy of the photon is partly used to eject the electron and the rest used as the kinetic energy of the ejected electron.

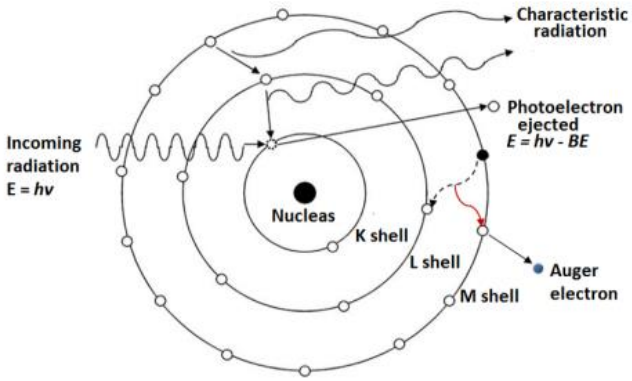

Figure 3.3: Illustration of photoelectric effect
(Mahuvana, 2016)

Therefore, the kinetic energy (E) of the resulting photo-electron is equal to the energy of the incident gamma photon (hf) less the binding energy (E_b,) of the electron, given by equation (3.17);

$$E = hf - E_b \tag{3.17}$$

The process does not take place with free electrons but rather with the electrons in the most tightly bound shell (K or L shell) of the atom. There exists a minimum frequency of the photon, (called threshold frequency), below which no photoelectric emission can take place, no matter the intensity of the radiation. This is because, in such a case, the photoelectron does not acquire enough energy to be ejected from the atom. Increasing the intensity of the photon increases the number of photoelectrons emitted while increasing the photon frequency increases the kinetic energy of the photoelectrons. Photoelectric effect occurs mostly with substances that have a high atomic number.

The probability of photoelectric absorption per atom (τ) over all ranges of energy and atomic numbers Z, is given by equation (3.18) where the exponent *n* depends or varies with the atomic number of the atoms and varies between 3 (for Z > 53) and 4 (for Z< 53). On the other hand, the probability varies inversely proportional to the cube of the photon energy hence photo- electric effect predominates in the low energy region, (IAEA, 2003).

$$\tau \propto \frac{Z^n}{(hf)^3} \tag{3.18}$$

Activity concentration of primordial radionuclides in environmental samples is measured using gamma ray detectors, for instance the Sodium Iodide Thallium Activated Detector. The high atomic number, of iodine added in the crystal helps increase the gamma ray detection giving the detector a good efficiency. The added Thallium activates the crystal, enhancing the emission of visible photons.

3.1.5.2 Compton scattering

Scattering is a physical process whereby a beam of radiation deviates from a straight path in the medium through which it travels. In Compton scattering, a photon transfers only a fraction of its energy to an electron which is at rest. The ejected electron, called Compton or recoil electron moves with a velocity depending on the energy it receives from the incoming photon. The rest of the photon proceeds as a new photon (called scattered photon), but in a different direction. The scattered photon moves at a scattering angle Θ with respect to the original path of the photon while the recoil electron moves at an angle, ϕ as illustrated in Figure 3.4.

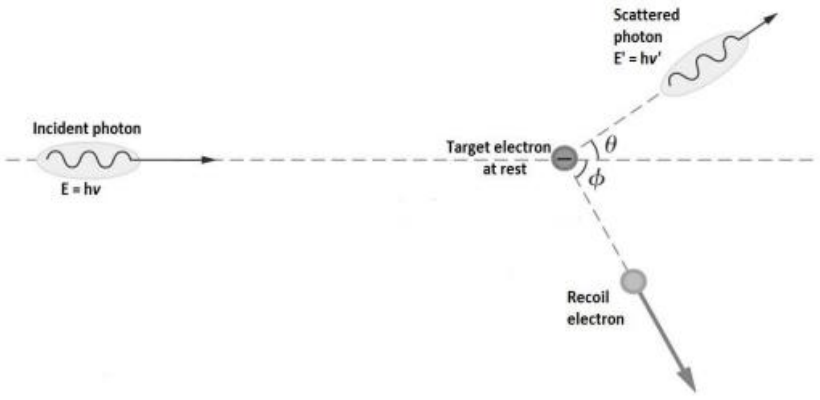

Figure 3.4: Illustration of Compton scattering
(Mahuvana, 2016)

By the law of conservation of energy, the energy before and after collision must be equal, as expressed in equation (3.19).

$$hf + m_0c^2 = hf' + mc^2 \qquad (3.19)$$

Where hf is the energy of the incident photon, m_0c^2 the rest mass energy of the electron; with m_0 being the rest mass of the electron at rest and c being the speed of light. hf' is the energy of the scattered photon where f' is the frequency of the scattered photon and mc^2 the energy of the energy of the scattered electron where m is the relativistic mass of the electron which is the mass when the electron is in motion.

By the law of conservation of linear momentum in the direction of the incident photon, the initial momentum in the x direction is equal to the final momentum in the same direction. Given that $\frac{hf}{c}$ is the momentum of the incident photon, zero is the momentum of the electron at rest before impact, $\frac{hf'}{c}\ \text{Cos}\ \square$, the x component of the momentum of the scattered photon and $mv\ \text{Cos}\phi$, the x component of the momentum of the recoil electron, where v is the velocity of the electron, it follows that;

$\frac{hf}{c} + 0 = \frac{hf'}{c}\ \text{Cos}\ \square + mv\ \text{Cos}\phi$ or upon rearranging;

$$h(f - f'\ \text{Cos}\ \square) = mvc\ \text{Cos}\ \phi \qquad (3.20)$$

Applying the law of conservation of momentum in the direction at right angle to the incident photon;

$$hf'\text{Sin}\ \square = mvc\ \text{Sin}\ \phi \tag{3.21}$$

Substituting equations (3.30) and (3.21) in equation (3.19) and solving reduces to equation (3.22):

$$\frac{1}{f'} - \frac{1}{f} = \frac{h}{m_o c^2}(1 - \text{Cos}\square) \tag{3.22}$$

Since $c = f\lambda$, Equation 3.22 can be re-written as:

$$\Delta\lambda = \lambda' - \lambda = \frac{h}{m_e c}(1 - \text{Cos}\square) \tag{3.23}$$

Where λ and λ' are the wavelengths of the incident photon and scattered photon respectively, and Δλ is the change in the wavelength of the Compton photon.

Multiplying the denominators of equation (3.22) by h, it may be expressed as:

$$\frac{1}{hf'} - \frac{1}{hf} = \frac{1}{m_e c^2}(1 - \text{Cos}\square) \tag{3.24}$$

This simplifies to:

$$hf' = \frac{hf}{(1+\alpha(1-\text{Cos}\square)} \tag{3.25}$$

Equation 3.25 represents the energy of the scattered photon, where $\alpha = \frac{hf}{m_e c^2}$is the ratio of the incident photon energy to the rest mass energy of the electron.

The difference between the energy of the incident photon hf and the scattered photonhf'gives the kinetic energy of the of the Compton electron (hf_e) given by equation (3.26).f_e is the frequency of the Compton electron.

$$\text{Kinetic Energy}, hf_e = hf - hf' \quad (3.26)$$

Combining this with equation (3.25), equation (3.26) therefore becomes;

$$\text{Kinetic Energy}, \ hf_e = hf\frac{\alpha(1-\text{Cos}\ \theta)}{(1+\alpha(1-\text{Cos}\ \theta)} \quad (3.27)$$

When the scattering angle θ=0, the photon moves straight without deflection and when the angleθ=180^0, the photon scatters back from the direction of origin.

It can be noted that, Compton Scattering only predominates at moderate energies, (IAEA, 2003).

3.1.5.3 Pair production

In pair production, all the photon energy is completely absorbed in the material and as a result used to create an electron-positron pair. This is illustrated in Figure 3.5.

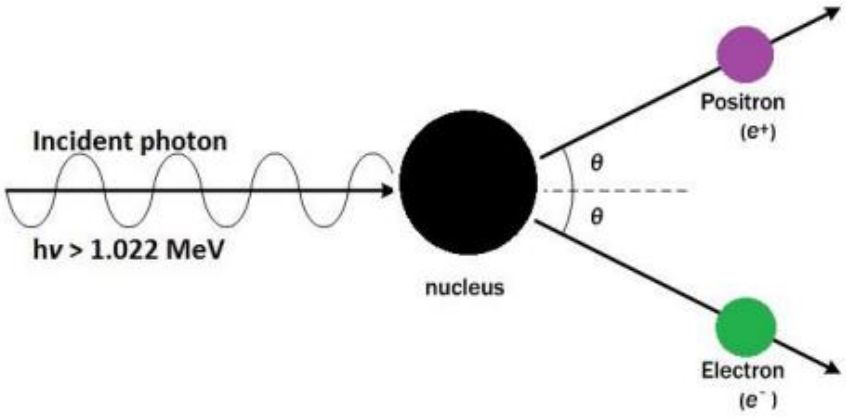

Figure 3.5:Illustration of pair production
(Mahuvana, 2016)

In order to conserve energy and momentum, pair production must take place in the Coulomb field of a nucleus. Pair production takes place when the photon energy is

either equal to or exceeds 1.022 MeV. It therefore has a threshold energy of $2m_0c^2$,equal to 1.022 MeV, which is the combination of the rest mass energies of the two electrons at rest. If the photon energy is exactly 1.022 MeV, then two particles would be created and remain at rest with no kinetic energy, (Dhobi *et al.,* 2020). Therefore, energy would be completely converted to mass. If photon energy is however greater than this, the energy difference is transferred to the electron –positron pair as kinetic energy. Pair production therefore dominates at higher energies. This process can be represented using equation (3.28) as follows;

$$hf = 2m_ec^2 + K_e^- + K_e^+ \qquad (3.28)$$

hf is the energy of the incident photon, K_e^- and K_e^+ are the kinetic energies of the electron and the positron respectively immediately after creation.

Figure 3.6 illustrates the dominant regions where the three gamma radiation interactions take place.

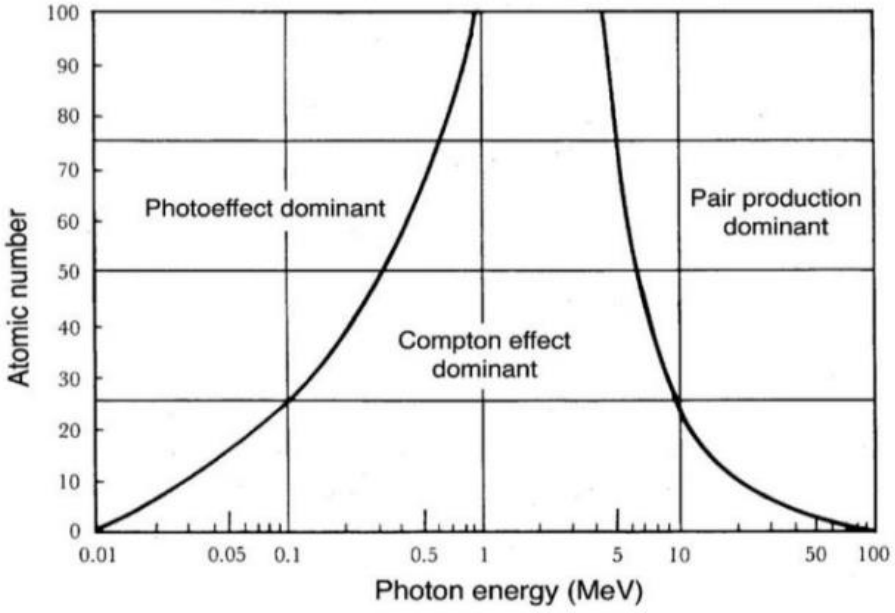

Figure 3.6: The energy dependence of the three types of gamma ray interactions (Mahuvana, 2016)

3.2 Radon and thoron movement in homes

Entry of radon in dwellings is mainly through soil gas which may pass through cracks and gaps in the building, exhalation from building materials, outdoor air and usage of groundwater. It accumulates in rooms according to the strength of its emanation and its dilution by ventilation. Figure 3.7 illustrates its entry in to indoor air. Entry of thoron on the other hand mainly occurs if the soil is in direct contact with indoor air as in the case of most traditional dwellings in Kenya, constructed using raw soil. Depending on the geology of the area, soils may contain enough thorium and radium to produce significant exhalation of the radon isotopes. This leads to significant concentration of the decay products. The progenies are solid in nature and attach themselves to aerosols in air. When inhaled, they are logged to the inner walls and membranes of the respiratory system and cause constant damage to the sensitive tissues of the respiratory track due to their alpha decay leading to possibility of

developing lung cancer. Inhaled radon progeny is considered to be the major source of background radiation exposure that accounts for over 50% radiation dose to the general population, (Hashim *et al.,* 2020).

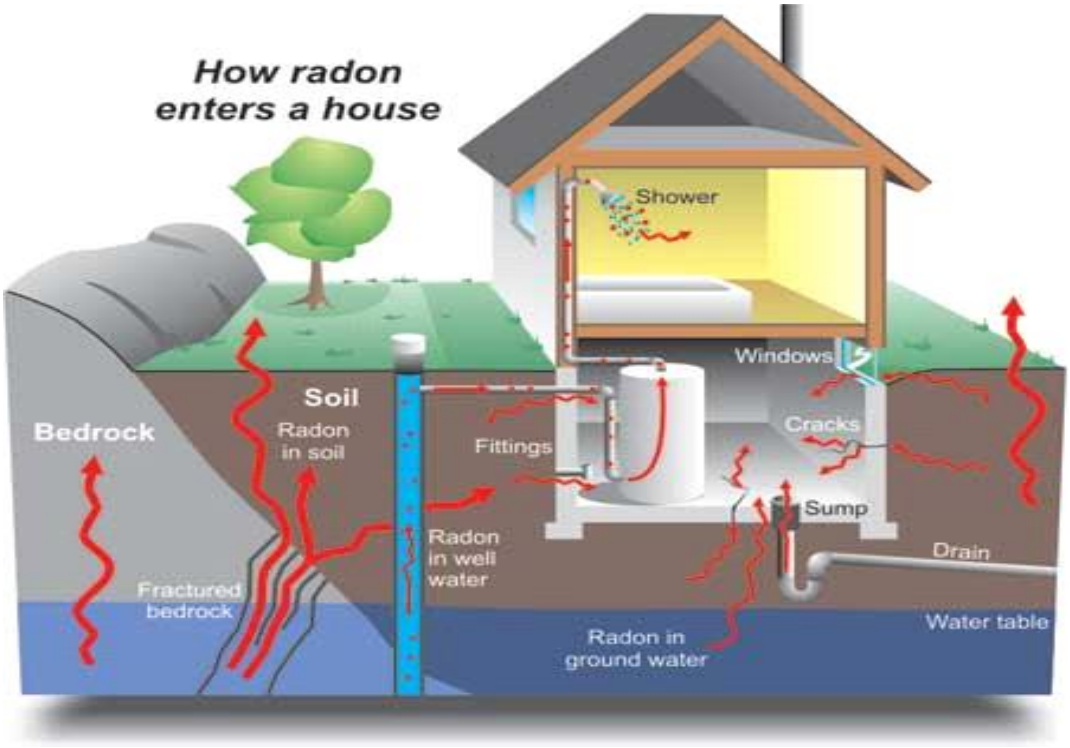

Figure 3.7:Radon entry points to a house
(Marcia, 2016)

Soil gas also easily gets into houses due to the pressure difference created indoors as a result of heating and cooking appliances that tend to warm the rooms hence reducing the indoor pressure. As a result, the house acts as a partial vacuum that draws radon and thoron to the indoors through the bare floor or cracks and openings available in case of concrete floors.

Building materials also contain radium and thorium in varying amounts. Upon decay, radon and thoron get their way into indoor air. Also, as the radionuclides decay, the residents get exposed to gamma radiation released in the decay process. The

concentration of gases generated from the building materials depends on the amount of radium and thorium in the materials.

3.3 Metal elements

3.3.1 Heavy metals

A heavy metal is any metal with a specific gravity or atomic weight of 5.0 or more, than that of water. One that is toxic to organisms, or just a metal having high specific weight (Klaus, 2010), and is toxic even at low levels. Heavy metals are part of the earth's crust and find their way to the body through ingestion of water and food or through air. Most of the contamination and exposure is due to anthropogenic activities like industrial production, industrial and domestic use, mining, and smelting operations. Also, the metals are introduced to aquatic systems due to weathering of rocks, volcanic eruptions and human activities. Heavy metals could enter the animal, and human tissue through inhalation, ingestion, and dermal contact. Water sources like rivers, lakes, ground water, and streams get polluted by heavy metals. Once the heavy metals find their way into human body, they tend to bioaccumulate given that they are hard to metabolize hence they tend to be very toxic, (Jadaa and Mohammed, 2023). Symptoms and effects of heavy metals depend on the metal or the metal compound, dose received, route of exposure and the chemical species. They also depend on the gender, age, genetics and the nutritional status of the exposed individual, (Tchounwou *et al.*, 2012). The most significant metals as far as toxicity to human is concerned are arsenic, cadmium, mercury, lead, and chromium. Their exposure can result in multiple organ damage and are therefore classified as human carcinogens. The effects of cadmium are aggravated due to its inability to be excreted by the human body. Acute exposure to cadmium may lead to pneumonitis (lung

inflammation) while chronic or long-term exposure may lead to lung cancer, osteomalacia (softening of bones), proteinuria (excess protein in urine) which is a possibility of kidney damage, skeletal damage and *itai-itai* diseases, hair loss, dermatitis, renal dysfunction or depression, (Koki *et al*., 2015). Lead is the most systemic toxicant that affects several organs in the body; kidneys, central nervous system, hematopoetic system, endocrine system and reproductive system. Acute exposure to lead may result in encephalopathy (brain dysfunction), nausea, and vomiting while chronic exposure may lead to anemia, encephalopathy, and nephropathy (kidney disease). Nervous system is most vulnerable target of lead poisoning, headache, poor attention, and memory loss. Additionally, lead absorbed by pregnant mothers is readily transferred to the developing featus leading to miscarriage, (Jadaa and Mohammed, 2023) should the exposure exceed certain levels. Arsenic which finds its way into the environment through smelting, microelectronic industry, wood preservatives, paints, pesticides, herbicides, and fungicides is also highly toxic. Exposure to Arsenic may lead to impairment of cellular respiration by inhibition of various mitochondrial enzymes. Similarly, exposure to mercury can lead to harm the brain, kidneys, and developing featus. It affects the nervous system, alters brain function and leads to tremors and changes to hearing or vision. Short term exposure to mercury may lead to vomiting, nausea, diarrhea, high blood pressure, skin rashes, lung damage, or hair loss, (Jaishankar *et al.*, 2014)

3.3.2 Essential elements

These are the nutrients required by human body for various biological and physiological functions. They include but not limited to Nickel (Ni), Cobalt (Co), Copper (Cu), Iron (Fe), Magnesium (Mg), Manganese (Mn), Potassium (K), Sodium

(Na), Zinc (Zn), Potassium (K), Calcium (Ca) and Sodium (Na). Inadequacy in supply of the micronutrients may lead to deficiency diseases or syndromes while excess intake may be toxic. Iron is present in all body cells as a component of haemoglobin and myoglobin which acts a carrier of oxygen in the blood and muscles. Iron deficiency for instance results in retardation in body growth and anaemia. Zinc is a constituent of more than 200 enzymes and helps in nucleic acid metabolism, cell replication, tissue repair and growth, (MacDonald, 2000). It plays a role in production, storage and secretion of individual hormones. Excess intake of Zn nevertheless interferes with the absorption and utilization of Fe and Cu. It also leads to gastric cancer and development of solid tumors in the stomach, cervix, ovary, prostrate and the lungs.

Copper assists in iron absorption and mobilization. Insufficient dietary copper leads to elevated lipid levels and impaired heart functions. Chromium on the other hand is needed by the body for normal carbohydrate metabolism, a biological function closely associated with that of insulin. Its deficiency leads to glucose intolerance, impaired lipid metabolism, and high circulating insulin levels. Manganese functions as a cofactor activation, a large number of enzymes forming metal enzyme complexes and an integral part in certain metalloenzymes (enzyme proteins containing metal ions) and involved in regulation of carbohydrate metabolism. Nickel is found in RNA (Ribonucleic acid) and involved in protein structure or function. It helps in Prolactic production thus aids in human breast milk production as well as adrenaline and glucose metabolism, (Kumar and Trivedi 2016). It improves bone strength and production of red blood cells. Deficiency of Ni is however associated with liver and kidney diseases. Ni toxicity is said to lead to skin allergies, lung fibroids and lung

cancers, (Kumar and Trivedi 2016). Cobalt helps in the absorption and processing of vitamin B_{12}, aids in repair of myelin (surrounds and protects nerve cells), helps in formation of haemoglobin (red blood cells). It also regulates and stimulates production of some enzymes like the thyroxin (a thyroid hormone). It is used to form amino acids and some proteins in nerve cells and in the creation of neurotransmitters. Deficiency of Co leads to disturbances in Vitamin B_{12} synthesis. It may also as a result cause anaemia and hypofunction of thyroid and increase in risk of developmental abnormalities in infants. Excess intake of Co on the other hand may lead to increase in the action of thyroid and bone marrow leading to overproduction of erythrocytes, fibrosis in lungs and asthma, (Czarnek *et al*., 2016).

Magnesium is an essential mineral and electrolyte for human nutrition. It is needed for more than three hundred biochemical reactions in the body. It assists maintain normal nerve and muscle function, keeps heartbeat steady, bones strong, supports a healthy immune system and adjusts blood glucose levels. It also helps in the production of energy and protein. Deficiency in magnesium brings about nausea, vomiting, loss of appetite, general tiredness and weakness. Long term deficiency may affect bone density, digestive system, nerve and muscle function as well as brain function. Deficiency may also prevent bone growth in children and increase the risk of osteoporosis and bone fracture in old people, (Fiorentini *et al.*, 2021) Calcium helps in bone development, keeping them healthy, enables muscles to contract, heart to beat and also assists in blood clot. About ninety-nine per cent of calcium in the body is found in bones. Deficiency in calcium is referred to as hypocalcemia, a condition in which the blood has too little calcium. This may lead to muscle cramps, tingling in the lips and limbs as well as confusion. Furthermore, long term deficiency may lead

to oestroporosis, alterations in brain, dental changes and cataracts, (Khan, 2023). Hypercalcemia is a condition where the blood has too much calcium. This may lead to poor bone health, kidney stones or abnormal heart and brain function. Potassium in the body regulates fluid balance and controls electric activity of the heart and other muscles. It also decreases the risk of stroke, reduces formation of kidney stones, protects against the loss of muscle mass, lowers blood pressure and preserves bone mineral density. It also balances acids and bases in the body plus aids in Ca absorption. It also helps in carbohydrate and glucose metabolism. Low potassium intake leads to high blood pressure and cardiovascular diseases, loss of appetite, nausea, vomiting, fatigue, and increases levels of anxiety. Excess K is however eliminated in urine though high intake from supplements may lead to gastrointestinal problems like diarrhoea, nausea and cramping. Large doses may lead to kidney problem, low blood pressure, urine retention and loss of central nervous system.

Sodium balances fluids in the body and sends nerve impulses needed for muscle contractions and enzyme operation. It also assists in glucose absorption, improves heart performance and brain function. Deficiency in Na may nonetheless cause the nervous system to shut down, muscular irritability, lethargy, low blood pressure, weight loss, confusion, dizziness, vomiting and headache, (Gagnon and Delpire 2021). The kidneys have considerable flexibility in removing excess sodium and can accommodate intakes greater than the minimum requirements. However, excess sodium intake can cause acute and long-term health effects such as dryness of mucous membranes, violent inflammatory reaction and ulceration in the gastrointestinal tract, along with dehydration and congestion of internal organs and brain, central nervous system disturbances (such as convulsions, confusion, and coma). Excess Na intake

also increases the risk of stomach cancer and hypertension, high blood pressure, chances of lung infection and swelling of neural tissues and nerves, (Veniamakis *et al.,* 2022).

3.4 Detection and measurement

3.4.1 Gamma ray spectrometry

Gamma ray spectrometry helps in identification and quantification of gamma emitting isotopes in different materials. One can be able to detect several radionuclides present in a sample. Basically, spectral lines are obtained from the spectrum whose amplitudes are proportional to the level of concentration of the radionuclides. Since each radionuclide has a particular energy associated with it, then their position on the energy axis helps identify the type of the radionuclide from the spectrum.

3.4.1.1 NaI (Tl) scintillation detector

Sodium Iodide detector uses the principle of emission of light by scintillator materials when radiation falls on it. The detection system consists of the NaI (Tl) crystal, a photomultiplier tube (PM) connected to a high voltage (HV) supply, preamplifier, amplifier, and a Multi-Channel Analyzer (MCA) interfaced with a personal computer as shown in Figure 3.8, (Cheruiyot, 2014). The sample placed in the detector consists of radionuclides which upon decay, they emit gamma rays. When radiation strikes the scintillator material, it causes it to emit photons of visible light. Thus, when a gamma ray interacts with the NaI crystal it deposits energy and this energy is what causes the photons to be given off. These photons then go through the crystal and strike the photocathode which then emits photoelectrons by the process of photoelectric effect. The scintillation crystal is coupled to a photomultiplier tube (PMT). When the photon hits the photocathode it in turn causes an electron to be ejected from the photocathode.

The PMT itself consists of a photocathode, a focusing grid, an array of dynodes and an anode housed in an evacuated glass tube. The photocathode converts the light flashes produced by radiation in the scintillation crystal into electrons. The grid focuses these electrons onto the first dynode; some photoelectrons are emitted and then directed towards the second dynode in the PMT. This electron multiplication process is repeated at the second dynode and the photoelectrons accelerated towards the third dynode and so on. An electron avalanche therefore develops so that a sizeable number of electrons eventually hit the anode at the bottom of the dynode chain as shown in Figure 3.8.

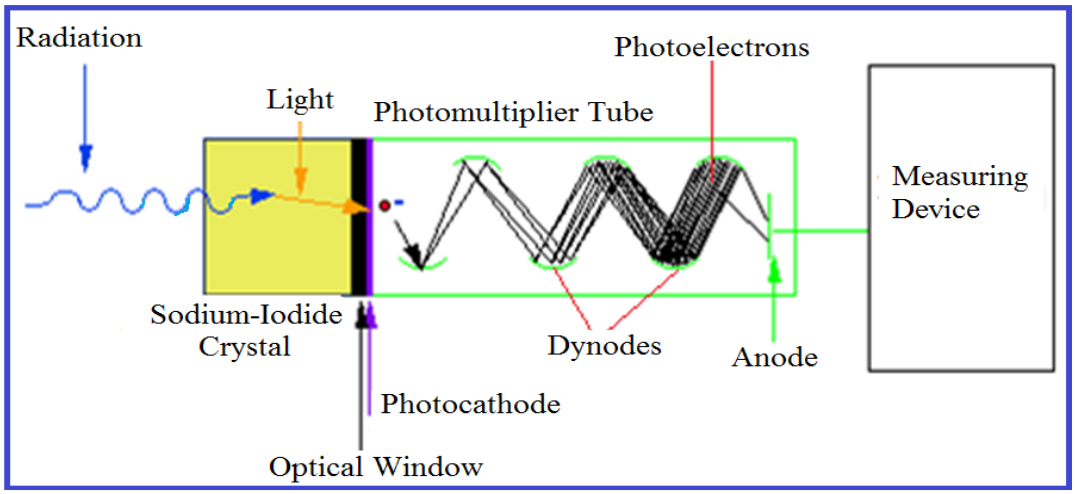

Figure 3.8:Schematic diagram of a photomultiplier tube
(Cheruiyot, 2014; Zoomie, 2015)

These electrons flow, which constitutes an electric current that generates a voltage, which is measured by an electronic circuitry. This output voltage, is directly proportional to the energy deposited in the scintillation crystal by the gamma radiation. This current is still small for detection. It is first strengthened by the pre-multiplier and further amplified by the amplifier. The amplifier further amplifies and increases the height of the pulses. The multichannel analyzer collects data and

produces the output. The MCA, which is interphased with a computer, collects pulses in all ranges of voltage and displays the data on the screen of a computer. The output signal or pulse has amplitude that is proportional to the energy of the incident photon from the radionuclides whose concentration is being determined. A schematic diagram of NAI (TI) detector is shown in Figure 3.9.

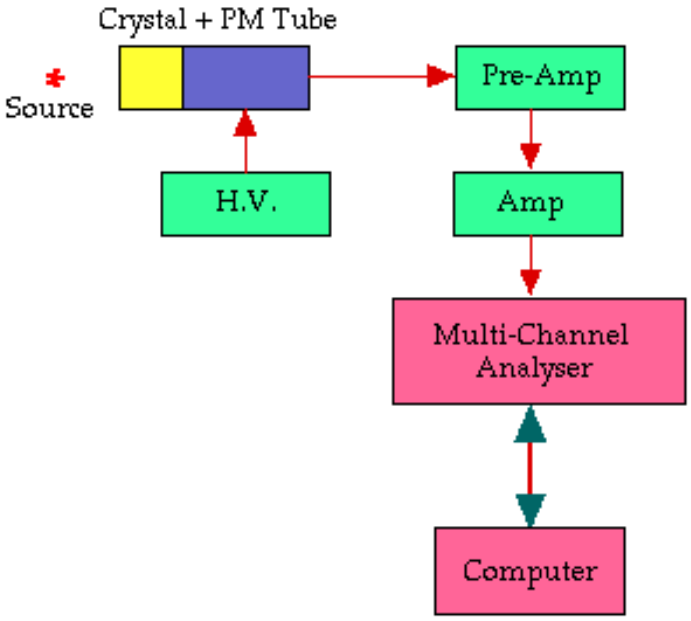

Figure 3.9:Schematic diagram of NAI (TI) detector

Basic Physics of Nuclear Medicine/Scintillation Detectors. (2021, May 28).

The output observed on the screen of the computer is an energy spectrum of the detected radiation. Since individual radionuclides emit specific gamma ray energies, gamma ray spectra obtained can be used to diagnose the source of the radiation, and hence the radionuclides present in a material. The detector has an analog-to-digital converter (ADC) whose purpose is to sort the pulses by their heights into specific channels where each channel represents a specific range of energy in the spectrum. The number of detected signals for each channel represents the spectral intensity of

the radiation in this energy range. The multichannel analyzer output is sent to a computer, which stores, displays, and analyzes the data such as energy calibration, peak area and net area and resolution calculation. Therefore, measuring the size of the output pulse helps us get to know how much energy was deposited in the crystal and as a result get to know the radionuclide that emitted the gamma ray that was detected.

3.4.1.2 Energy calibration

The sodium iodide detector was calibrated before using it for radiation detection. This was done in order to assign energies to channel numbers. Energy calibration was done using Cs-137 (662 keV) and Co-60 (1170 KeV and 1332 KeV). The obtained spectrum was calibrated for energy by setting regions of interest (ROI) around the peaks of interest. A linear fit of photon energy against channel number using a linear equation of the form shown in equation (3.29) was used to obtain the energy calibration parameters. The equation of the linear fit is only valid in the energies of interest.

$$Y = B + A\,X \tag{3.29}$$

Where Y is the gamma energy, X the channel number while A and B are constants. The energy calibration graph obtained in this work is as shown in Figure 3.10.

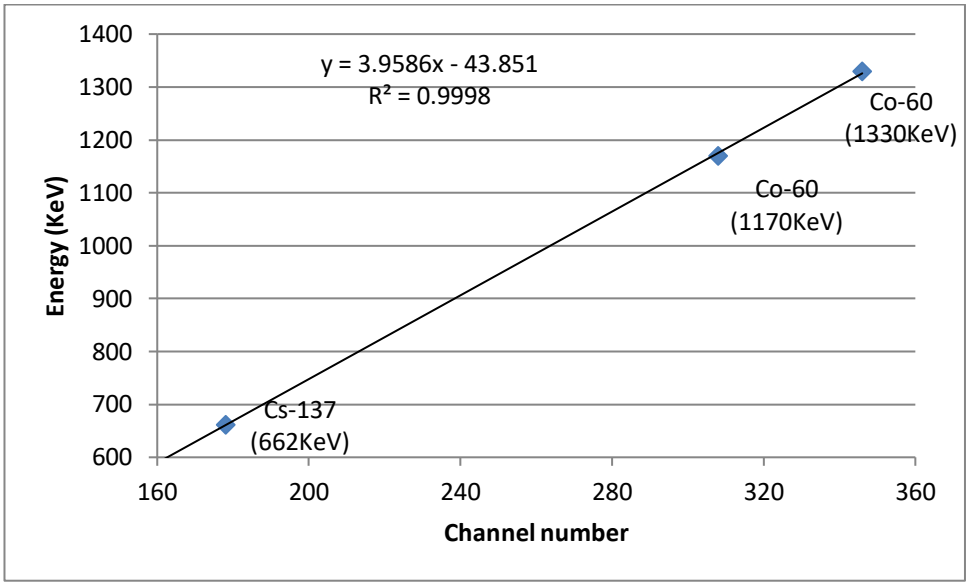

Figure 3.10: Energy calibration graph showing a linear fit

3.4.1.3 Detector efficiency

Efficiency is the fraction of photons of a given energy from a source, contributing to the corresponding full energy peak observed in the spectrum. The efficiency depends on the sample geometry, distance from detector, density and size. In this study, certified standard reference materials; RGK-1, (Potassium Sulphate), RGTh-1, (Thorium ore) and, RGU-1 (Uranium Ore) from the International Atomic Energy Agency were used for efficiency calibration of the detector. The decay products and gamma lines used for evaluation of the efficiency were: Bi-214 at 609 KeV, 1120 KeV and 1765 KeV for Ra-226, Tl-218 at 2614 for Th-232 and K-40 at 1461 KeV. The net counts, N, for a given photo peak was determined from the region of interest (ROI) around the peak of interest and the gross and net counts generated. To account for the background correction, a sample containing distilled water was used and run the same way as the samples. Equation (3.30) was used to determine the detector efficiency at different energies of interest.

$$\varepsilon = \frac{N}{T \times A_R \times M_R \times P_\gamma} \quad (3.30)$$

Where;

ε = absolute photopeak efficiency

N = Net counts in photopeak, after appropriate background subtraction

T= Live time, the time during which the system is available for processing a pulse

A_R = Activity concentration of the standard reference material at the collection time

M_R= Mass of the standard reference sample

P_γ = branching ratio, the statistical chance that a particular γ-ray is emitted per decaying nucleus

The radionuclides decay from the reference materials was corrected using equation (3.31).

$$(A) = A_0 e^{-\lambda t} \quad (3.31)$$

Where A is the activity concentration at the counting time; A_0 the activity concentration at the certificate time; λ the decay constant given by; $\lambda = \frac{\ln(2)}{T½}$ with T½ being the half-life.

Certificate time is the time at which the certificate of the reference material was issued or when the reference material was prepared. Count time is the time at which the reference material was used to determine the efficiency. Efficiency versus energy curve was then generated and efficiencies at different energies of interest determined

from the curve using the equation of fit as indicated in the graph as shown in Figure 3.11

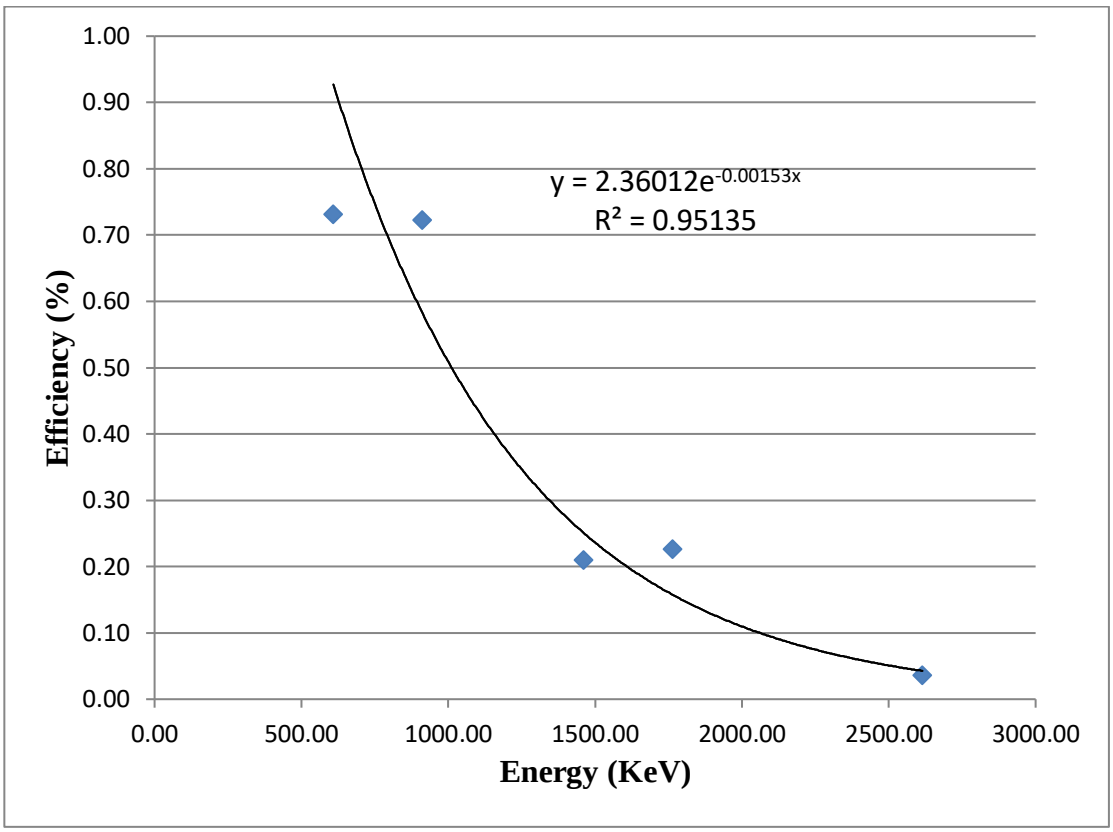

Figure 3.11:Efficiency versus energy curve from RG series reference materials

3.4.1.4 Activity concentration

The efficiencies determined from the equation were then used to calculate the activity concentration using equation (3.32) for the different radionuclides of interest, (Garba *et al.*, 2023; Lee *et al.*, 2023; Lolila and Mazunga, 2023);

$$A_S = \frac{N}{T \times \varepsilon \times M_S \times P_\gamma} \qquad (3.32)$$

Where A_S is the activity concentration of the sample and M_S is the mass of the sample.

3.4.2 Alpha detectors

3.4.2.1 Solid State Nuclear Track Detectors (SSND)

Radon and thoron concentration levels were measured using passive integrating radon–thoron discriminative monitors, (RADUET), (Kudo *et al*., 2015; Nkoulou II *et al.*, 2023; Hashim *et al.*, 2020). The measurement of the concentration of the isotopes is based on passive sampling. The monitor is made up of two different diffusion chambers, a high and a low diffusion chamber. Each chamber comprises of an electroconductive plastic, cylindrical in shape, with an inner volume of about 30 cm^3. A detecting material, CR-39 (one of the solid-state nuclear track detectors (SSND)) is fixed at the bottom with sticky clay. CR-39 (Columbia Resin -39) (Polyallyl diglycol carbonate or PADC) is a material made of polymer or plastic. It has a good sensitivity; stability against various environmental factor sand has a high degree of optical clarity. RADUET consists of a pair of detectors placed in a low-diffusion chamber and a high diffusion chamber as illustrated in Figure 3.12 and Plate 3.1

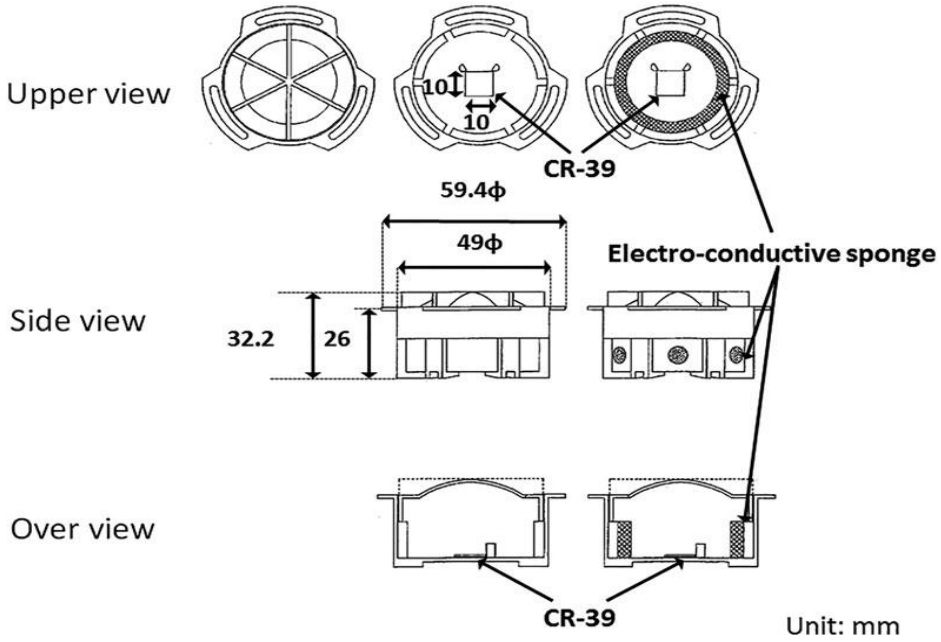

Figure 3.12: An overview of the RADUET

(Kudo *et al.*, 2015; Hosoda *et al.*, 2017; Nkoulou II *et al.*, 2023).

Plate 3.1: An overview of the RADUET

Alpha particles formed by integration of radon, thoron and their progeny transfer their energy by ionizing or exciting the atoms in the polymer which leaves damaged patches on the CR-39 chip called tracks. The track densities formed on each of the detectors

depends on the concentration of radon and thoron in the indoor air. The two isotopes are separated using the two chambers based on their different half-lives. Radon gets into the low air-exchange rate chamber through a microscopic or very small air gap which only allows a small quantity of thoron. During radon calibration, both chambers of RADUET (low air-exchange rate and high air-exchange rate) are used. Two conversion factors, one for the low exchange rate (f_{Rn1})chamber, and another one for the high exchange rate (f_{Rn2}) chamber are therefore obtained.

Thoron detection is facilitated by opening six holes of 6 mm in diameter on the side of the other chamber called the high air-exchange rate chamber. The holes are covered using an electroconductive sponge. In this high air-exchange rate chamber, radon, and thoron get in and both radioactive gases form tracks on the CR-39 placed at the bottom of the chamber. In the calibration of detectors using thoron, both RADUET chambers are again used obtaining two conversion factors; one for the low exchange rate (f_{Tn1}) chamber and the other for the high exchange rate (f_{Tn2}) chamber.

To determine the concentration levels of radon and thoron in the study region, the RADUET monitors were installed in the dwellings for three months, (Nkoulou II *et al.,* 2023.

Once the monitors have been retrieved from the field, they are transported to the laboratory for analysis. They are chemically etched in a 6 M NaOH solution at 60^0C for 24 h in order to expose and help identify the alpha tracks. The etching makes the alpha tracks more uniform in shape and size and easily visible. Figure 3.13 shows a typical image of alpha tracks formed in a detector.

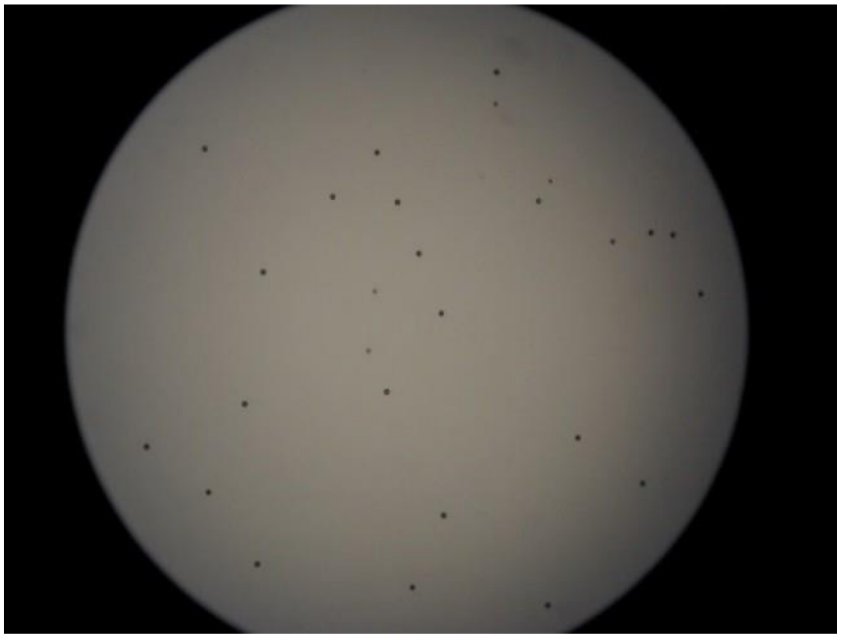

Figure 3.13: An image of tracks formed in the detector

After etching, the detectors are removed from the holders and cleaned with clean running cold water and finally rinsed in distilled water. A microscope and a software called J method, (Tokonami *et al.,* 2005; Janik *et al*., 2013), were used to determine the track density on the detectors. A CCD (Charge Coupled Device) camera is usually mounted on a microscope. A monitor for viewing the images and a control unit are also mounted. Ten images of the same detector are taken, at different points and then transferred to the computer. The J-Method software, a Java-based image processing program is then used to compute the track densities of images.

The average radon and thoron concentrations for each set of monitors are then simultaneously determined using equations (3.33) and (3.34), (ISO, 2014; Nkoulou II *et al.,* 2023);

$$\overline{C_{Rn}} = \left(d_L - \bar{b}\right)\frac{f_{Tn2}}{t\times(f_{Rn1}\times f_{Tn2} - f_{Rn2}\times f_{Tn1}} - \left(d_H - \bar{b}\right)\frac{f_{Tn1}}{t\times(f_{Rn1}\times f_{Tn2} - f_{Rn2}\times f_{Tn1}} \quad (3.33)$$

$$\overline{C_{Tn}} = \left(d_H - \bar{b}\right)\frac{f_{Rn1}}{t\times(f_{Rn1}\times f_{Tn2} - f_{Rn2}\times f_{Tn1}} - \left(d_L - \bar{b}\right)\frac{f_{Rn2}}{t\times(f_{Rn1}\times f_{Tn2} - f_{Rn2}\times f_{Tn1}} \quad (3.34)$$

Where, $\overline{C_{Rn}}$ and $\overline{C_{Tn}}$ are the mean concentrations of radon and thoron during the exposure period in Bq m^{-3}, d_L and d_H are the alpha track densities (track cm^{-2}) for the low and high air-exchange-rate chambers, respectively. f_{Rn1} and, f_{Tn1} are the conversion factors from alpha track densities to radon and thoron activity concentration for the low exchange-rate air chamber [(tracks cm^{-2} h^{-1})/(Bqm^{-3})]. f_{Rn2} and f_{Tn2} are the conversion factors from alpha track densities to radon and thoron activity concentration for the high exchange-rate air chamber [(tracks cm^{-2} h^{-1}) /(Bqm^{-3})], t is the exposure time in days and $\bar{b}$ is the background of the alpha track density (track cm^{-2}) on the CR-39 detector.

The background b is determined experimentally by reading the number of tracks on the CR-39 that have not been exposed to radon and have been processed under the same physico-chemical and counting conditions.

It is worth noting that, in equations (3.33) and (3.34);

f_{Tn1} is used for correction of radon concentration in low exchange rate chamber

f_{Tn2} is used for correction of radon concentration in high exchange rate chamber

f_{Rn1} is used for correction of thoron concentration in low exchange rate chamber

f_{Rn2} is used for correction of thoron concentration in high exchange rate chamber

3.4.2.2. Thoron progeny monitor

Thoron progeny was detected using a thoron progeny monitor shown in Figure 3.14 and Plate 3.2.

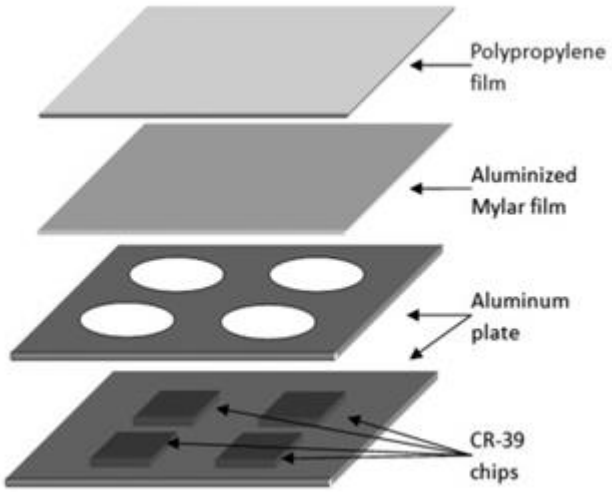

Figure 3.14:An overview of thoron progeny monitor
(Janik *et al.*, 2013)

Plate 3.2: An overview of thoron progeny monitor

For radiation detection, four 1 cm by 1 cm CR-39 chips are installed in the monitor and are shielded with aluminum -vaporized Mylar film of an air-equivalent thickness of 71 mm. This thickness is adjusted only to allow the detection of the 8.8 MeV (alpha energy of the highest magnitude among all the natural radionuclides) alpha particles produced from ^{212}Po, the thoron progeny.

The monitor was exposed by hanging on the wall for three months. Thoron progeny in indoor air deposits on the detector over the time forming tracks of alpha particles. The detecting principle of alpha energy emitted from ^{212}Po, thoron progeny is demonstrated in Figure 3.15;

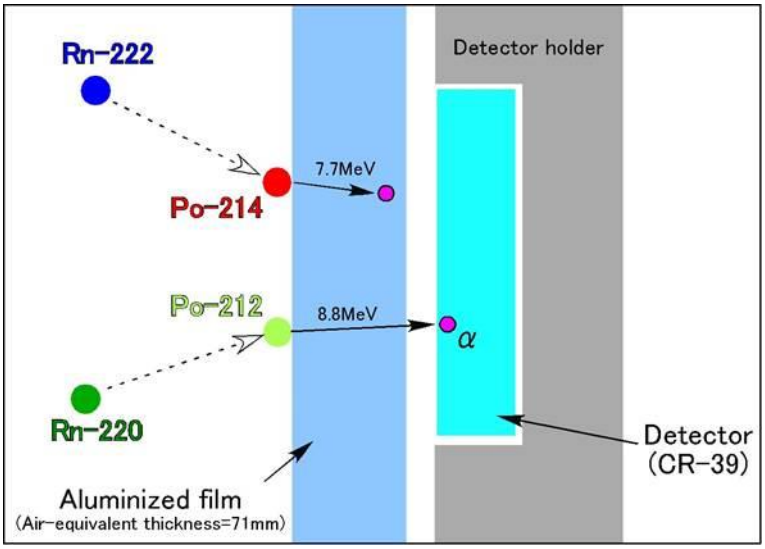

Figure 3.15: Detecting principle of alpha energy emitted from ^{212}Po,
(Tokonami, 2020)

After retrieval, the CR-39 chips were treated in a similar manner as those of the RADUET monitors. The concentration of the thoron progeny is calculated as the equilibrium equivalent thoron concentration (EETC) using equation (3.35).

$$\mathrm{EETC} = \frac{D}{C \times T} \qquad (3.35)$$

Where D is the track density in tracks/mm^2; C is the conversion factor experimentally obtained as 0.0106 tracks/mm^2/ (Bq/m^3 day), T the exposure period in days and EETC the equilibrium equivalent thoron concentration, in Bqm^{-3}.

3.4.3 Atomic Absorption Spectrometry

Atomic absorption spectroscopy is an analytical technique that measures concentration of metal elements using the absorption of optical radiation (light) by free atoms in the gaseous state. It is used to determine the concentration of metals in liquid samples. It is based on the absorption of light by free metallic ions.

3.4.3.1 Flame atomic absorption spectroscopy

For the water sample to be analysed, it has to be atomized either using a flame or a graphite tube. The flame atomic absorption spectrometer uses the principle that, atoms generated in an atomizer can absorb radiation at specific wavelength. The atoms are then irradiated by optical radiation whose source could be an element-specific line radiation source. Hollow cathode lamps are used as radiation sources that contain a tungsten anode and a hollow cylindrical cathode made of the element whose concentration is to be determined. Each particular element has its own unique lamp which must be used for analysis. The atoms absorb ultraviolet or visible light and make transitions to higher energy levels. The concentration of the analyte is determined by the amount of absorption. The nebulizer sucks up the liquid sample where it is aspirated, aerosolized and mixed with combustible gas, acetylene and air. The air-acetylene flame has a temperature of about 2300^0C. When metals are exposed to heat, they absorb light emitted from the source. At the atomizer, atomization takes place where aerosol particles are separated to individual molecules and further to atoms attributable to the high temperatures of the flame. The radiation then passes

through a monochromator or a wavelength selector which separates the element-specific wavelength of light which is absorbed by the sample and excludes other wavelengths. The ability to select the specific light assists in the determination of the selected element amidst others. The selected light from the monochromator is directed to the detector which converts the light to an electrical signal that is proportional to the light intensity. This is further amplified by the amplifier and then sent to computer for display. A block diagram of the flame atomic absorption spectrometer is shown in Figure 3.16.

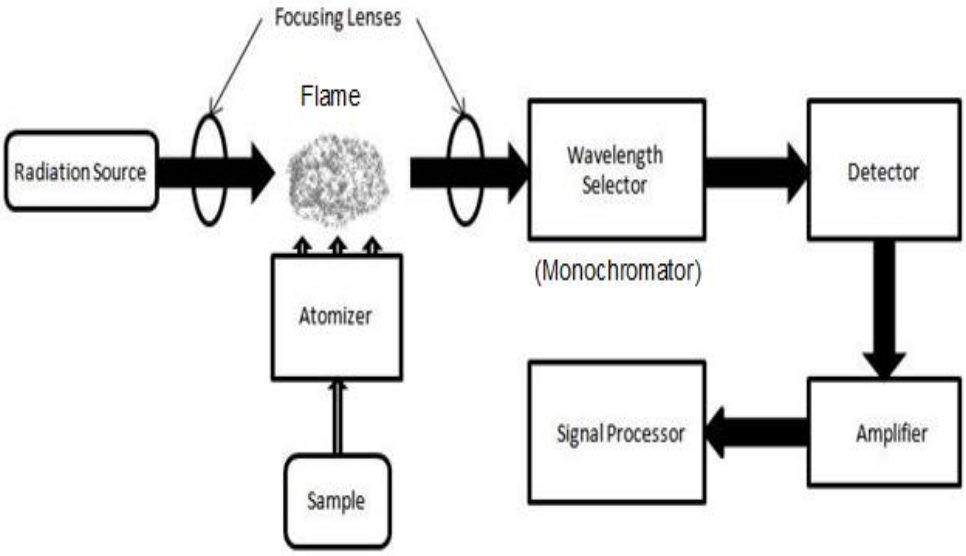

Figure 3.16: Atomic absorption spectrometer

(Gavong *et al.*, 2019)

CHAPTER FOUR: MATERIALS AND METHODS

4.1 Geology of the sampling region

The current study focused on Kilimambogo region. It is in the border of Kiambu and Machakos counties and in the vicinity of fourteen falls, Delmonte pineapple farms, and the Oldonyo Sabuk National Park, located along the slopes of the Mountain. The geology of the study region is characterized by Kerichwa Tuff volcanic rocks as well as basalt igneous rocks with the mountain region being dominated by undifferentiated basement rock (gneisses) which is formed from sedimentary rocks. A geology map showing the study region is shown in Figure 4.1.

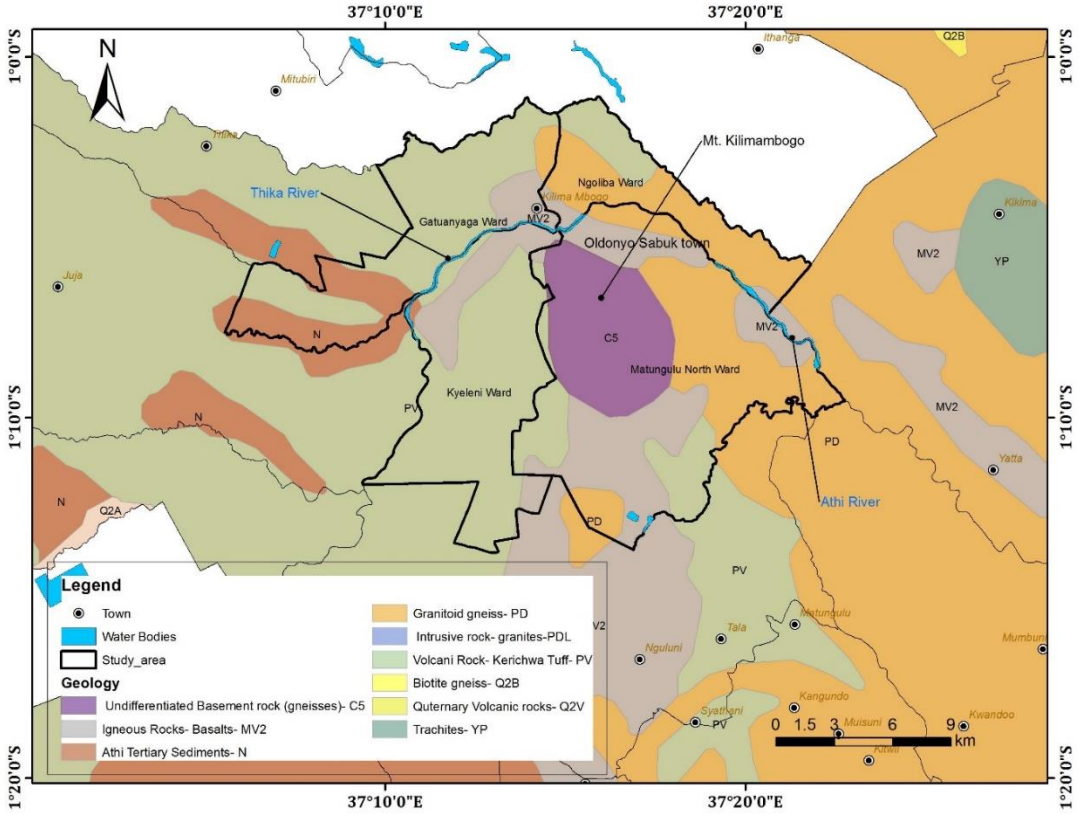

Figure 4.1: Geology map of the study area (Department of mining, Kenya, 2023)

4.2 Activity concentration of ^{226}Ra, ^{232}Th and ^{40}K in soil, rock and cassava samples

4.2.1 Sampling

The sampling points were selected along the slopes and the environs of Mt. Kilimambogo, in Ngoliba and Gatuanyaga wards in Kiambu county, and Kyanzavi in the upper Matungulu ward in Machakos county, Kenya by purposeful random sampling technique. The samples were collected mainly in Maguguni, Kilimambogo, Ndula, Ol-DonyoSabuk, Kitini, and Ngoliba villages within the environs of Kilimambogo Mountain. The longitudes and latitudes of the sampling locations were determined using a portable GPS (Global Positioning System) receiver, read within 300s, (Baochuan *et al*., 2015). The rock samples were sampled from different quarries in the regions and along the slopes of the mountain.

Soil samples and the cassava plants were randomly collected from the various points and farms in the region. Soil samples were collected between the depths of 15 cm to 20 cm after removing the surface loam soil which consists of dead leaves, roots, and organisms.

4.2.2 Sample preparation

The rock and soil samples were separately crushed and thoroughly mixed to ensure homogeneity and sieved in a 1 mm mesh sieve. Samples were oven dried at about 110^{o}C for about 24 hours to completely remove the moisture (or until the samples attained a constant weight upon weighing). About 500 g of each of the samples were then put in clean and dry plastic containers, sealed and stored for approximately 30 days. This was to ensure that radioactive equilibrium between ^{226} Ra and ^{232}Th and

their daughter radionuclides was reached, (Kebwaro, 2009), and that, radon and thoron gases did not escape from the samples.

The outer skin of the cassava tubers was removed, washed clean, and cut into small pieces. The cassava stems and leaves were also washed and cut into small pieces, sun and oven dried and then ground. The samples were then packed and sealed in airtight plastic containers and similarly stored for about 30 days before analysis.

4.2.3 Sample analysis

Equation (3.32) described previously in section 3.4.1.3 was used to determine the activity concentration of the environmental samples, (Isinkaye and Emelue, 2015). The minimum detection activity concentration was determined using equation (4.1), (Jibiri and Biere, 2011).

$$\mathrm{MDA} = \frac{4.66\sqrt{\mathrm{B_C}}}{\varepsilon \mathrm{P_\gamma M_{BS} T}} \qquad (4.1)$$

Where T is the counting time; ε is detector efficiency at the given energy of interest; P_γ is the absolute probability; M_{BS} the mass of the blank sample used for background determination and B_C the background counts.

4.2.4 Radiological risk evaluation of NORM

Radiological risks associated with NORM in building materials such as rocks and soils were determined using the radium equivalent activity and the external hazard indices.

4.2.4.1 Radium equivalent activity (Ra_{eq}) and External hazard index (Hex)

The activity concentration of ^{226}Ra, ^{232}Th and ^{40}K is not uniformly distributed throughout the soils. Radium equivalent activity (Ra_{eq}) therefore defines this non-uniformity in respect to the exposure of radiation from the concentrations of ^{226}Ra, ^{232}Th and ^{40}K, given by equation (4.2) (Alashrah 2016; Kamunda *et al*., 2016; Lee *et al.,* 2023; Lolila and Mazunga, 2023);

$$\mathrm{Ra_{eq}} = \mathrm{A_{Ra}} + 1.43\ \mathrm{A_{Th}} + 0.077\ \mathrm{A_K} \qquad (4.2)$$

Where A_{Ra}, A_{Th} and A_K are the activity concentrations of ^{226}Ra, ^{232}Th and ^{40}K respectively. The maximum value of Ra_{eq} in soil is estimated to be less than 370 Bq kg^{-1}suggested by UNSCEAR, (2019) for safe use of building materials, in order to limit the annual exposure of 1.5 mGy, (Baochuan *et al*., 2015; Isinkaye and Emelue, 2015; Alashrah, 2016; Kamunda *et al*., 2016; Faanu *et al.*, 2016; Lee *et al*., 2023; Lolila and Mazunga, 2023; Garba *et al.*, 2023). For ease of comparison, equation (4.2) is modified by making the reference level to be unity and the resulting equation named as the external hazard index, (H_{ex}). That is:

$$\mathrm{H_{ext}} = \frac{\mathrm{Ra_{eq}}}{370\ \mathrm{Bq\ kg^{-1}}} \qquad (4.3)$$

This results to equation (4.4);

$$\mathrm{H_{ext}} = \frac{\mathrm{A_{Ra}}}{370} + \frac{\mathrm{A_{Th}}}{259} + \frac{\mathrm{A_K}}{4810} \qquad (4.4)$$

For safe use of building materials, H_{ex} should not exceed 1 in order for the residents to receive insignificant dose.

4.2.4.2 External exposure due to soil and rock samples

There exists a risk of external exposure inside dwellings from the building materials used in the region. As a result, there is indoor risk due to gamma irradiation. This was evaluated using equation (4.5), (UNSCEAR, 2000; Chege, 2014; Lee *et al.,* 2023; Mwalongo *et al.,* 2023);

$$D_{IN} = 1.4 \times F_d \times t \times \sum F_i C_i \quad (4.5)$$

Where D_{IN} is the external exposure indoors, $\sum F_i C_i$ is the absorbed gamma dose rates (nGy h^{-1}) with F_i being 0.462, 0.604, and 0.047 nGyh^{-1}/Bq Kg^{-1} for ^{226}Ra, ^{232}Th and ^{40}K which are the absorbed dose conversion factors for the radionuclide i, C_i is the corresponding activity concentration. F_d is the outdoor gamma dose conversion factor, (=0.7 nGyh^{-1}/ Sv h^{-1}). Outdoor dose is then converted to the indoor dose by a factor of 1.4 implying that the indoor dose is 1.4 times higher than the outdoor dose. t(h y^{-1}) is the indoor occupancy factor taken as 60% in Kenya, (Mustapha *et al.,* 2002; Kinyua *et al.,* 2011; Chege *et al*., 2015).

4.2.4.3 Internal exposure due to consumption of radionuclides in cassava

The risk received from the intake of naturally occurring radionuclides present in cassava tubers and leaves by the residents was calculated as the effective dose using equation (4.6) as follows;

$$D = q \times \sum C_i F_i \quad (4.6)$$

Where D is the effective dose in mSvy^{-1}. C_i is the concentration of the radionuclides in cassava tubers and leaves and F_i is the corresponding dose coefficients equivalent

to 2.8×10^{-4} mSv Bq^{-1} for ^{226}Ra, 2.3×10^{-4} mSv Bq^{-1} for ^{232}Th and 0.062×10^{-4} mSv Bq^{-1} for ^{40}K for the public; q is the ingested rates of the cassava tubers and the leaves per annum, taken to be 45 kg and 25 kg per annum.

4.3 Radon and Thoron concentration

4.3.1 Sampling

Mud- built houses, iron sheet- built houses and stone - built modern houses were randomly sampled in the study area. The monitors were installed in three different types of dwellings, that is; mud- built, iron sheet- built and stone - built modern houses. An example of a mud walled dwelling is shown in Plate 4.1.

Plate 4.1: Mud walled dwellings in the sampling region

Each monitor was tied to a string which was used to hang them near the walls, such that, they are at a height of about 2 m above the floor. The monitors were left in dwellings for a period of three months, after which they were removed, repacked in

air-tight casings, (Chege, 2014), and taken to the laboratory in the Graduate School of Health Sciences, Hirosaki University in Japan for analysis.

4.3.2 Analysis

All the CR-39 RADUET detectors for radon, thoron, and thoron progeny measurements were chemically etched in a 6 M NaOH solution at 60 ^{o}C for 24 h in order to expose and identify the alpha tracks. The track density was determined using a microscope and computer software, (Mehta *et al*., 2014; Kudo *et al*., 2015, Hosoda *et al*., 2017). Calibration factors were used to convert track densities to radon, thoron, and thoron progeny concentrations. Calibration factors are those quantities that convert track densities to activity concentration of the samples.

4.3.3 Annual effective dose due to radon (E_{Rn}) and thoron (E_{Tn}) progenies.

The annual effective dose received by residents living in Kilimambogo as a result of exposure to progenies of radon and thoron was estimated using equations (4.7) and (4.8) respectively as discussed by UNSCEAR report, (Tokonami *et al.,* 2004; Kudo *et al*., 2015; Hashim *et al.,* 2020).

$$(\mathrm{E_{Rn}}) = \mathrm{C_R(Bq\ m^{-3})} \times 0.4 \times 8760\mathrm{h} \times 0.6 \times \mathrm{DCF_{Rn}} \times 10^{-6} \quad (4.7)$$

$$(\mathrm{E_{Tn}}) = \mathrm{EETC} \times 8760\ \mathrm{h} \times 0.6 \times \mathrm{DCF_{Tn}} \times 10^{-6} \quad (4.8)$$

Radon and thoron progenies dose conversion factors (DCF) were taken to be 9 nSv $(\mathrm{Bqm^{-3}h})^{-1}$ and 40 nSv $(\mathrm{Bq\ m^{-3}\ h})^{-1}$ respectively, indoor occupancy factor in Kenya as 0.6 and 8760 as the number of hours per annum, EETC is the equilibrium equivalent thoron concentration, (thoron progeny) and 10^{-6} converts nSv to mSv. 0.4 is the equilibrium factor which converts radon to radon progeny. The total effective dose

therefore is the sum of the effective doses due to exposures to indoor radon and thoron progenies

4.4 Physico chemical analysis of water samples

4.4.1 Sampling

River water was fetched along Athi and Thika rivers and Matathia stream, while the borehole water samples were fetched randomly from the available boreholes within the region. Water samples were collected using 1000 ml new PVC bottles. Before use, the bottles were cleaned and rinsed off with 10% nitric acid. They were then rinsed off using distilled water and with the sample water on site before collection. Groundwater and surface water was sampled in the wet and dry seasons as the locals normally do. The samples were then transported to the laboratory, at Kenyatta University and appropriately acidified using concentrated nitric acid for preservation, (Chege, 2014).

4.4.2 Sample preparation

The analysis of pH was done *in situ* with a pH meter. For analysis of heavy metal, preserved water samples were stored for at least 72 hours before analysis began. This facilitated in liberation of any metals that could have adsorbed on to the surfaces of the bottles. Samples were prepared by adding 2 ml concentrated nitric acid and 1 ml concentrated hydrochloric acid to 100 ml of each sample. The resulting solution was then heated to a solution temperature of 95 ^{o}C until the volume reduced to 20 ml. Digestion removes organic materials present in the water samples and also augments the release of metals adsorbed on particulate matter. The concentrate was allowed to cool, topped up to 100 ml using double distilled water, and filtered using 0.45µm pore size filters into a 100 ml conical flask. This procedure was repeated for all the other

samples. A blank sample was similarly prepared using double distilled water for background check, (Islam *et al.*, 2023).

4.4.3 Analysis

Analysis of heavy metals present in water samples was determined using a flame atomic absorption spectrophotometer (AAS). A portion of each sample and a blank was put in plastic containers. The samples were aspirated into the acetylene – air flame of the AAS with a cathode lamp corresponding to each metal of interest as a source of light, one at a time and the absorbance of light measured in each case. The concentration of the given metal was obtained in reference to the calibration curve less the concentration of the blank. The procedure was repeated with cathode lamps that corresponded to each metal of interest, (Chege, 2014; Islam *et al.*, 2023). The elements analyzed included; Copper (Cu), Potassium (K), Manganese (Mn), Cadmium (Cd), Zinc (Zn). Calcium (Ca), Nickel (Ni), Iron (Fe), Lead (Pb), Magnesium (Mg), and Sodium (Na). The concentration levels of the elements in water samples were determined using Atomic Absorption Flame Emission spectrophotometer (AA-6200) except for K and Na whose analysis was done using a flame photometer.

4.4.4 Quality Assurance

Different stock and standard solutions of the heavy metals of interest were prepared. Calibration of the instrument was done using the standard solutions and deionized water for all the elements analyzed. Blank samples made from only reagents and double distilled water were also analyzed to eliminate any background of the heavy metals resulting from digestion process. This ensured that determination of

concentration of heavy metals was accurate. A calibration curve for each element was obtained by plotting absorbance readings against the corresponding levels of concentrations and used to determine the concentration of the trace elements in the samples. A calibration curve for Cd standard for instance is shown in Figure 4.2.

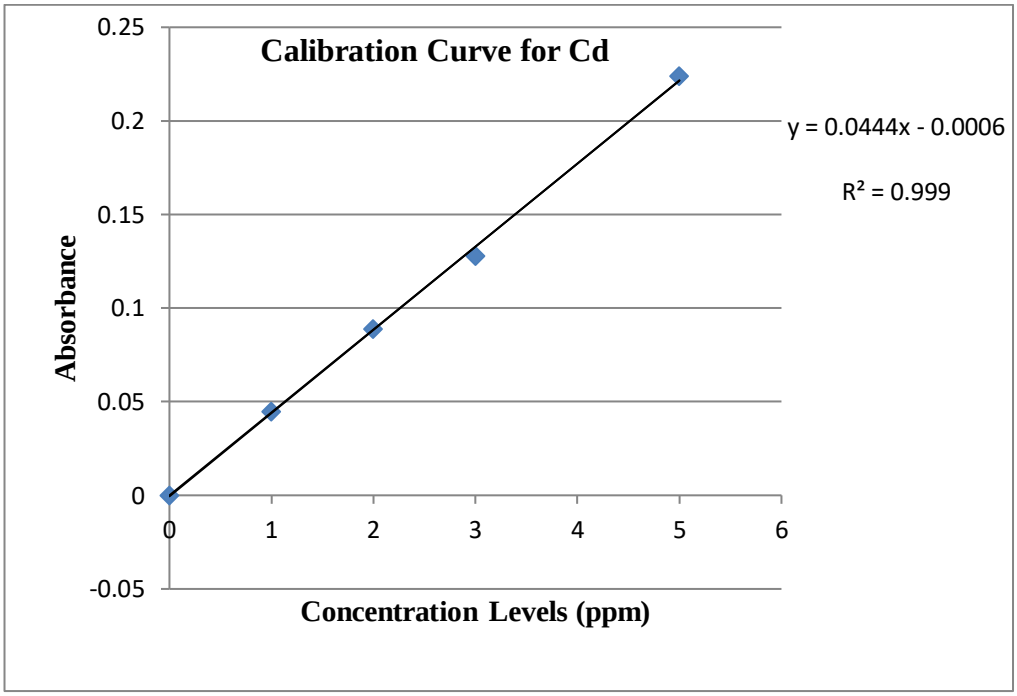

Figure 4.2: Calibration curve for Cd standard

4.5 Determination of concentration of the elements

Concentration levels of different elements in different samples were obtained from the AAS readings using equation (4.9), (Mwangi, 2013);

$$\text{Concentration of sample} = \frac{\text{AAS reading} \times 100}{\text{Mass of sample}} \qquad (4.9)$$

4.6 Exposure and risk assessment due to the metal elements

The daily exposures to heavy metals were assessed for non-carcinogenic and carcinogenic effects. Non-carcinogenic effects include respiratory system irritant

action, liver and kidney toxicity, changes in the central nervous system and fertility disorders, (Konchakova *et al.,* 2016). Two toxicity risk indices are the slope factors (SF) for carcinogenic risks and reference doses (R_fD) for non-carcinogenic characterization. Industrial activities release heavy metal contaminated wastes into water sources leading to severe water pollution, (Aziz *et al.,* 2023). Their main exposure pathways include intake through consumption of water and through skin absorption either through bathing or swimming, (Koki *et al.,* 2015). The health risk of heavy metals through drinking water was assessed using the measured concentration of heavy metals in water as follows;

4.6.1 Chronic daily intake (CDI)

The daily human exposure to heavy metals in mg kg^{-1} d^{-1} through the drinking water pathway was calculated using equation (4.10), (Koki *et al*., 2015; Maigari *et al*., 2016; Wanjala *et al.*, (2020); Kipng'eno 2022; Mohammadi *et al.,* 2019; Mohammed *et al.,* 2023); The chronic daily intake was used to estimate both carcinogenic and non-carcinogenic risks associated with intake of water by residents in the study region.

$$\mathrm{CDI} = \frac{C_i \times IR \times ED \times EF}{BW \times AT} \qquad (4.10)$$

Where C_i is the heavy metal concentration in mg L^{-1}; IR the average daily water ingestion rate taken as 1.488 L d^{-1} for adults; EF the exposure frequency (350 d y^{-1}); ED the exposure duration (66.7 years, the average life expectancy in Kenya), WHO, (2016); BW the body weight in kg (70 kg for both men and women) and AT the average exposure, (AT=ED×365 for carcinogenic and, AT=30×365 for non-carcinogenic risks in adults).

4.6.2 Non-cancer risks

4.6.2.1 Hazard quotients (HQ)

The non-carcinogenic risks were determined by evaluating the hazard quotients (HQ) using equation (4.11). (Koki *et al.,* 2015; Bhuvaneshwari *et al*., 2016; Maigari *et al*., 2016; Mohammadi *et al.,* 2019; Mohammed *et al.,* 2023). It is the quotient between the chronic daily intake and the reference dose (R_fD). Reference dose also called the acceptable daily intake (ADI) is the approximate exposure incurred daily over an entire lifetime, without appreciable risk for the general public including all subgroups like infants and children. It is expressed in milligrams per kilogram of body weight per day (mg/kg/day).

$$\mathrm{HQ} = \frac{\mathrm{CDI}}{\mathrm{R_fD}} \qquad (4.11)$$

The risk is unacceptable if HQ >1, (Adamu *et al.*, 2015).

4.6.2.2 Hazard index (HI)

The potential risk to the population as a result of intake of several elements was determined using the chronic hazard index (HI) given by equation (4.12). The sum of multiple metal exposures is taken to be proportional to the level of adverse effects, (Koki *et al.,* 2015; Maigari *et al*., 2016; Bhuvaneshwari *et al*., 2016; Mohammadi *et al.,* 2019; Munene *et al.*, 2023; Mohammed *et al.,* 2023).

$$\mathrm{HI} = \sum_{i=1}^{n} \mathrm{HQ_i} \qquad (4.12)$$

HI should not exceed one. 1 <HI <5 shows a level of concern while 10<HI<100 indicates that there is need for additional data gathering and research since it is an indication of extreme levels of pollution.

4.6.3 Cancer risks

4.6.3.1 Incremental Lifetime Cancer Risk

The carcinogenic risks associated with the intake of the carcinogenic agents in water were calculated based on the USEPA, (2011) human risk assessment model. Cancer risks indicate the probability of a population developing any type of cancer due to intake of the carcinogens. This was determined as the Incremental Lifetime Cancer Risk (ILCR) using equation (4.13), (Koki *et al*., 2015; Munene *et al.*, 2023; Mohammed *et al.,* 2023).

$$\mathrm{ILCR} = \mathrm{CDI} \times \mathrm{CSF} \qquad (4.13)$$

CDI is the average daily intake of the carcinogens in mg/kg Bw/day which is an indication of the lifetime average daily dose of exposure to the heavy metals; discussed in section 4.6.1 above. CSF is the cancer slope factors which indicate the risk produced by a lifetime average dose of 1 mg/kg Bw/day and is heavy metal dependent. The acceptable cancer risk from heavy metal intake regulation is between 10^{-6} to 10^{-4} (Wanjala *et al.*, 2020). The cumulative cancer risks due to the exposure of several carcinogenic heavy metals was determined using equation (4.14), (Adamu *et al.,* 2015; Koki *et al.,* 2015).

$$\mathrm{ILCR_{TOTAL}} = \mathrm{ILCR_1} + \mathrm{ILCR_2} + \cdots + \mathrm{ILCR_n} \qquad (4.14)$$

Where n= 1,2…. n is the number of elements.

4.7 Dose analysis using RESRAD code

RESRAD ONSITE family of codes is a computer model that estimates radiation doses and risks from RESidual RADioactive materials developed by the Argonne National Laboratory (ANL), (Kaimboj *et al.,* 2018) It uses pathway analysis to evaluate

radiation exposure and associated risks. It supports an ALARA (as low as reasonably achievable) analysis. The external ground pathway was used to determine the exposure of the target population.

Different exposure scenarios can be considered in analysis of the doses. These scenarios affect the release of radioactivity from the contaminated zones and determine the amount of exposure received by the exposed individuals. Exposure scenarios are patterns of human activity that can affect the release of radioactivity from the contaminated zone and the amount of exposure received at the exposure location. In the current study, only the resident farmer and the quarry worker scenarios were considered. The resident farmer spends most of his time in the contaminated zone. He spends about fourteen hours outdoor on the contaminated site. The quarry worker on the hand spends approximately eight hours daily on site since it is assumed that he resides in a different zone outside the contaminated site under consideration. In both cases, only the direct radiation pathway was considered in calculating the radiation dose received by the residents, (Hassan, 2023).

RESRAD ONSITE code uses a database of 38 radionuclides which account for ingrowth of daughters from initially-present parent radionuclides. The radionuclides of interest in the current study were radium (^{226}Ra), thorium (^{232}Th) and their daughter products and the singly occurring radioactive potassium (^{40}K). The code tries to model a site using various variables such as occupancy and shielding factors, area and shape factors, depth and cover factors as well as thickness of the contaminated and the uncontaminated zones. Erosion and leach rates are also included. These variables have default values assigned but the user can change to suite site specific needs. The main

input parameters included the measured mean activity concentrations of ^{226}Ra, ^{232}Th and ^{40}K, as measured in the soil and quarry rock samples from the study region.

RESRAD uses the actual radionuclide concentrations to estimate the Total Effective Dose Equivalent (TEDE). The total dose received by an individual as a result of exposure from the external, inhalation, and ingestion pathways should not exceed 25 mrem y^{-1}. RESRAD offers nine major environmental pathways for dose assessment. These include external exposure directly from the ground, exposure from inhalation of particulates and radon and ingestion of soil, water, plant, meat, milk and aquatic foods, (Yu *et al*., 2001; Yu 2012; Kaimboj *et al.*, 2018). The exposure pathways for an onsite resident are demonstrated in Figure 4.3.

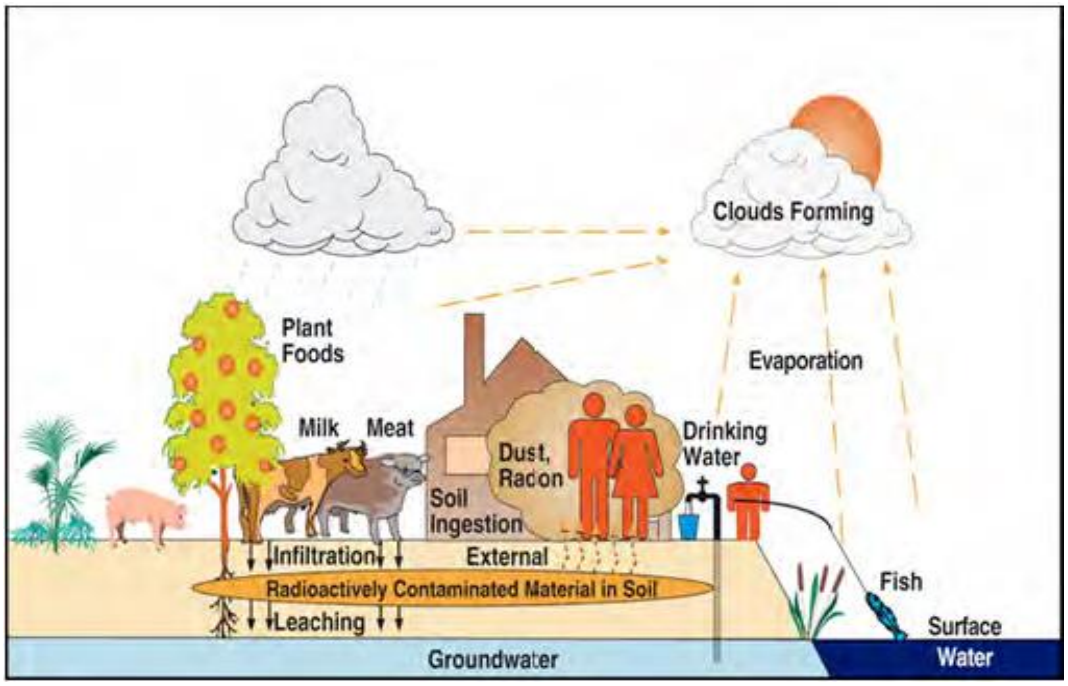

Figure 4.3 Exposure pathways for an onsite resident (Yu *et al*., 2001)

The program uses equation (4.15) to calculate the effective dose of radionuclides, (Yu *et al*., 2001; Yu, 2012; Kipng'eno, 2022).

$$(\mathrm{Dose})_{i,p}(t) = \mathrm{DCF}_{i,p} \times \mathrm{ETF}_{i,p}(t) \times \mathrm{SF}_i(t) \times \mathrm{S}_i(0) \quad (4.15)$$

Where $DCF_{i,p}$ is the dose conversion factor; $ETF_{i,p}$ (t) is the environmental transport factor; $SF_i(t)$ the source factor, $S_i(0)$, the soil concentration at time, t = 0.The environmental transport factor is the ratio between the annual intake rate and the soil concentration of the radionuclide i, at a time t. Source factor is the ratio of soil concentration of radionuclide i at time t, to the concentration at time t=0.

Soil concentration is determined by the ingrowth and decay processes of the individual radionuclides and the leaching process caused by infiltration of rain and water used for irrigation. Source factor is therefore the product of the ingrowth and decay factor, $ID_i(t)$, and the leaching factor, LF_i (t) as in equation (4.16):

$$\mathrm{SF}_i(t) = \mathrm{ID}_i(t) \times \mathrm{LF}_i(t) \quad (4.16)$$

CHAPTER FIVE: RESULTS AND DISCUSSION

5.1 Activity concentration of ^{226}Ra, ^{232}Th and ^{40}K in rock and soil samples

5.1.1 Soil samples

The distribution of activity concentration of ^{226}Ra, ^{232}Th and ^{40}K in soil samples as measured in Kilimambogo and Gatuanyaga regions was tabulated in Table 5.1. The mean activity concentration of ^{226}Ra, ^{232}Th, and ^{40}K in the soil samples were 54 ± 6 Bq kg^{-1}, 58 ± 4 Bq kg^{-1} and 776 ± 54 Bq kg^{-1} in Kilimambogo region and 35 ± 5 Bq kg^{-1}, 32 ± 3 Bq $kg^{-1}$and 430 ± 38 Bq kg^{-1} in Gatuanyaga region respectively.

Table 5.1: Summary statistics of activity concentrations of ^{226}Ra, ^{232}Th and ^{40}K in soil samples

Specific activity concentration of the radionuclides in soil samples (Bqkg^{-1})			
	^{226}Ra (Bq kg^{-1}) Mean (Range)	^{232}Th (Bq kg^{-1}) Mean (Range)	^{40}K (Bq kg^{-1}) Mean (Range)
Soil samples from Kilimambogo region	54 ± 6 (25 ± 4-103 ± 25)	58 ± 4 (29±2– 74±5)	776 ± 54 (298±6 – 1495±32)
Soil samples from Gatuanyaga region	35 ± 5 (21 ± 5– 59 ±10)	56 ± 5 (27 ± 2– 101±6)	430 ± 38 (108 ± 2–1011 ± 50)
Minimum detectable activity concentration (MDA)	2.78 ± 0.07	3.82 ± 0.29	2.68 ± 1.21

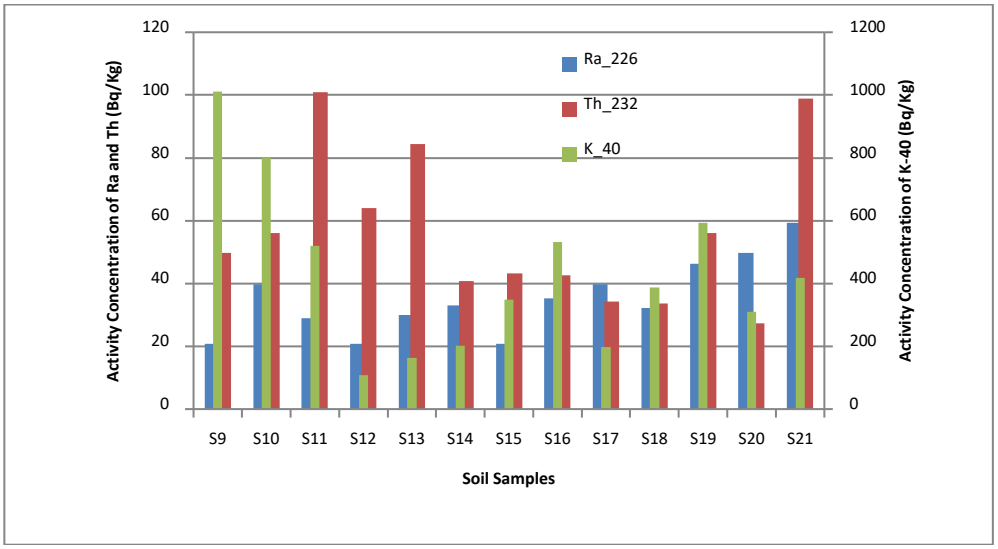

Figure 5.1: Distribution of activity concentration of ^{226}Ra, ^{232}Th and ^{40}K in soil samples from Gatuanyaga region

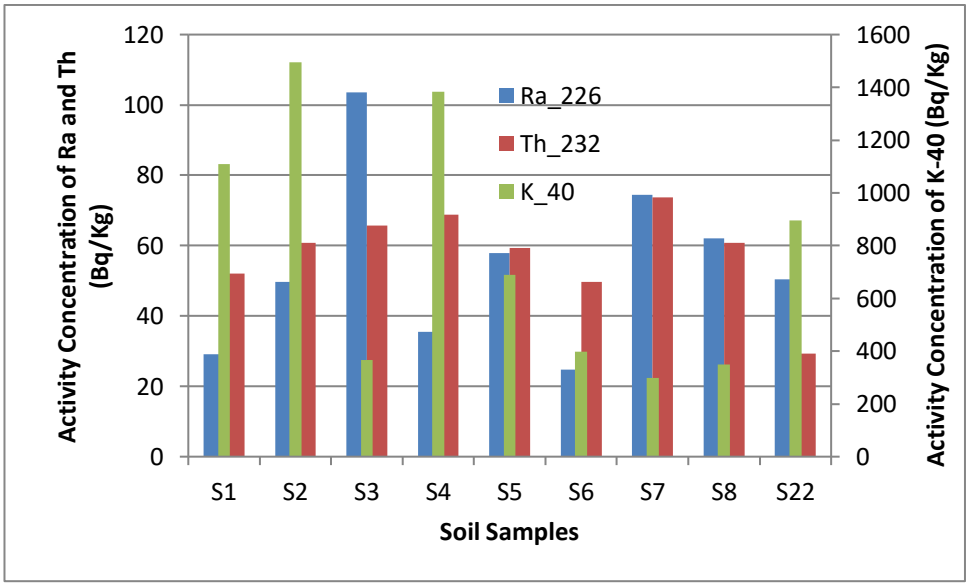

Figure 5.2: Distribution of activity concentration of 226Ra, 232Th and 40K in soil samples from Kilimambogo region

In Kilimambogo region, ^{226}Ra and ^{40}K in 78% and 56% of the samples exceeded the world averages of 33 Bq kg^{-1}, 45 Bq kg^{-1} and 420 Bq kg^{-1}respectively. In Gatuanyaga region, ^{226}Ra, ^{232}Th, and ^{40}K in 54%, 8%, and 38% of the samples exceeded the world

average values. In Gatuanyaga region, highest concentration levels of ^{226}Ra, ^{232}Th, and ^{40}K in samples were measured in samples S21, S11 and S9, collected in Makutano, Ngoliba and Maguguni cultivated farms. Extensive use of phosphate fertilizers in cultivated soils is a likely reason of the relatively high concentration of the natural radionuclides in the soils. However, lowest concentration levels of ^{226}Ra, ^{232}Th, and ^{40}K were recorded in S12, S20 and S12 samples respectively. The samples were collected from Ngoliba and Maguguni (Powerline) areas which had not been cultivated. Besides, these areas are also sandy which does not have retention capacity of elements. In Kilimambogo region, highest concentration levels of ^{226}Ra, ^{232}Th, and ^{40}K were measured in samples S2, S3 and S7 respectively. S2 and S3 were collected along the slopes of Kilimambogo Mountain, while S7 on the other hand indicated highest concentration of thorium which was collected from the base of the same mountain. This region is characterized by clay soil where thorium easily adsorbs as compared to other types of soils. The large surface of clay makes it easy for metals to adsorb on it. Hence thorium content in soil increases with increase in clay content in soil. Lowest levels of ^{226}Ra, ^{232}Th, and ^{40}K in the region were measured in the samples S6, S7 and S22. All the samples were collected in Kitini village at the base of the mountain in abandoned farms.

5.1.2 Rock samples

Rock samples were collected from quarries in Makutano, Ndula, and Maguguni villages in Gatuanyaga region, as well as along the slopes of Mount Kilimambogo and its environs which is generally a rocky area. The distribution of activity concentration of ^{226}Ra, ^{232}Th and ^{40}K in the rock samples is shown in Table 5.2. The mean activity concentration of ^{226}Ra, ^{232}Th and ^{40}K in the quarry rock samples from Gatuanyaga

region were 39 ± 5 Bq kg^{-1}, 76 ± 7 Bq $kg^{-1}$and 723 ± 23 Bq kg^{-1} recording maximum values of 68 ± 12 Bq kg^{-1}, 142 ± 12 Bq $kg^{-1}$and 1161 ± 46 Bq kg^{-1}in ^{226}Ra, ^{232}Th and ^{40}K respectively. ^{226}Ra, ^{232}Th and ^{40}K in 56%, 44%, and 9% of the samples exceeded the world average values of 33 Bq kg^{-1}, 45Bq $kg^{-1}$and 420 Bq kg^{-1}respectively. The mean activity concentration of ^{226}Ra, ^{232}Th and ^{40}K in the rock samples collected in Kilimambogo region were 35 ± 6 Bq kg^{-1}, 56 ± 7 Bq $kg^{-1}$and 645 ± 32 Bq kg^{-1}recording maximum values of 70 ± 10 Bq kg^{-1}, 208 ± 12 Bq $kg^{-1}$and 1,181 ± 56 Bq kg^{-1} respectively.^{226}Ra, ^{232}Th and ^{40}K present in 50%, 25% and 81% of the samples exceeded the world averages. In Gatuanyaga region, highest concentrations in ^{226}Ra, ^{232}Th and ^{40}K were recorded in the samples, R9, R13 and R19 collected in the Maguguni (Powerline), Matathia and Ndula (Makongo) villages respectively. The area is characterized by granitoid gneiss sedimentary rocks which could be the reason for enhanced levels of radionuclides in the samples. In Kilimambogo region, highest concentrations in ^{226}Ra, ^{232}Th and ^{40}K were recorded in the samples, R3, R23 and R5 respectively. The samples were collected along the slopes of the mountain near the Ol-Donyo Sabuk area which is characterized by different kinds of Basalt Igneous rocks known to be enriched in different kinds of radionuclides.

The minimum detectable activity concentration (MDA) for ^{226}Ra, ^{232}Th and ^{40}K in all samples were 2.78 Bq kg^{-1}, 3.82 Bq kg^{-1} and 2.67 Bq kg^{-1} respectively.

Table 5.2:Summary statistics of activity concentrations in the rock samples

	Specific activity concentration in rock samples ($Bqkg^{-1}$)		
	^{226}Ra ($Bq\ kg^{-1}$) Mean (Range)	^{232}Th ($Bq\ kg^{-1}$) Mean (Range)	^{40}K ($Bq\ kg^{-1}$) Mean (Range)
Rock samples from Gatuanyaga region	39 ± 5 (8 ± 2 – 68 ± 12)	76 ± 7 (37 ± 2 – 142 ± 12)	723 ± 23 (225 ± 5 – 1161 ± 46)
Rock samples from Kilimambogo region	35 ± 6 (8 ± 2 – 70 ± 10)	56 ± 7 (6 ± 2 – 208 ± 12)	645 ± 32 (76 ± 2 – 1,181 ± 56)
Minimum detectable activity concentration (MDA)	2.78 ± 0.07	3.82 ± 0.29	2.68 ± 1.21

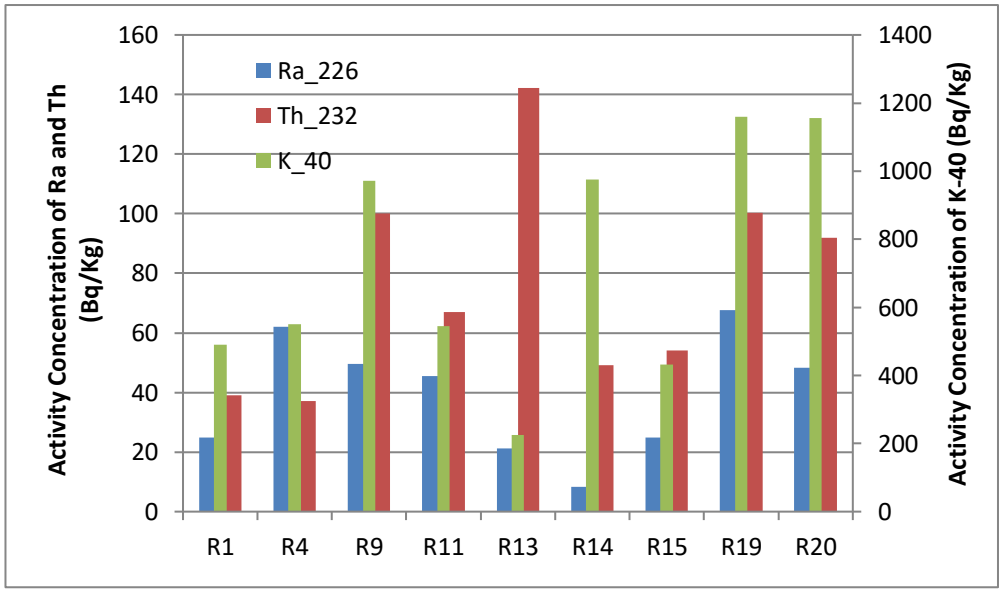

Figure 5.3: Distribution of activity concentration of ^{226}Ra, ^{232}Th and ^{40}K in quarry rock samples from Gatuanyaga region in Kiambu County.

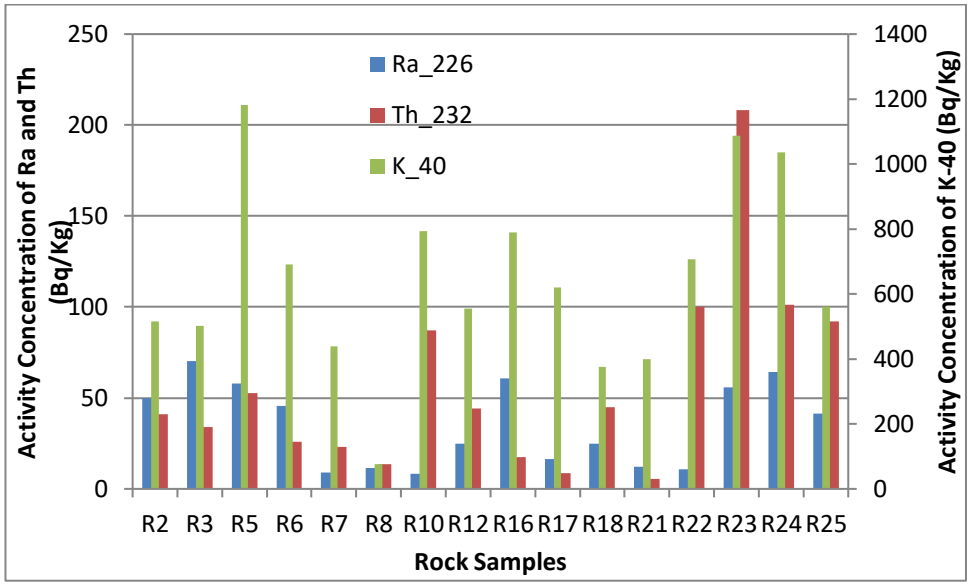

Figure 5.4:Distribution of activity concentration of ^{226}Ra, ^{232}Th and ^{40}K in rock samples from Kilimambogo region

The concentration levels of ^{226}Ra and ^{232}Th were higher than those reported in Kanana village in Kwale, Kenya, (Chege, 2014), though lower than those reported in Homa Mountain, (Otwoma *et al.*, 2012). ^{232}Th concentration levels were lower than those reported in Homa mountain (Otwoma *et al.*, 2012) and Mrima hill, (Chege, 2014), though higher than levels reported in Kanana village (Chege, 2014). The mean activity concentration levels reported in this study were higher than the world average values of 33Bq kg^{-1}, 45Bq kg^{-1} and 420 Bq kg^{-1}of ^{226}Ra, ^{232}Th and ^{40}K reported by UNSCEAR (2000).

For comparison purposes, some samples were transported to laboratory of Hirosaki University, Japan for analysis. The mean and range of the activity concentration of the rock and soil samples measured using HPGe detector in the laboratory of Hirosaki University, Japan are tabulated in Table 5.3.

Table 5.3: Summary statistics of activity concentrations of ^{226}Ra, ^{232}Th and ^{40}K in the rock and soil samples measured in Hirosaki University Japan, (2018)

	Activity concentration of rock and soil samples		
	^{226}Ra (Bq kg^{-1}) Mean (Range)	^{232}Th (Bq kg^{-1}) Mean (Range)	^{40}K (Bq kg^{-1}) Mean (Range)
Soil Samples	42 (29 - 66)	62 (32 - 125)	526 (267- 1040)
Rock Samples	19 (1 - 47)	40 (1 - 93)	661 (55 - 1342)

5.1.3 Radiological risk assessment due to NORM in rock and soil samples

5.1.3.1 Radium equivalent activity (Ra_{eq}) and external Hazard index (H_{ex})

The mean and range of radium equivalent activity and the corresponding external hazard index (H_{ex})from rock and soil samples were computed and tabulated in Table 5.4. The mean external hazard index of the soil samples from Kilimambogo and Gatuanyaga regions were 0.39 ± 0.08 and 0.31 ± 0.20 with a range of 0.25 - 0.50 and 0.14 - 0.93 respectively. That of the quarry rock samples and other types of rocks had mean values of 0.40 ± 0.13 and 0.34 ± 0.18 with maximums of 0.62 and 0.78respectively. All samples recorded hazard indices of less than unity as recommended hence building materials from soil and rocks pose no radiological risks to the dwellers.

Table 5.4: Summary of radium equivalent (Ra_{eq}) and external hazard indices (Hex) due to rock and soil samples

	Ra_{eq} (Bq kg^{-1})	H_{ex}
Rock samples from Gatuanyaga region	203 ± 67 (118 – 300)	0.55 ± 0.18 (0.32 - 0.81)
Rock samples from Kilimambogo region	165±99 (37–437)	0.45±0.27 (0.10 - 1.18)
Soil samples from Kilimambogo region	197±40 (127–252)	0.53±0.11 (0.34-0.68)
Soil samples from Gatuanyaga region	149±43 (104–233)	0.40±0.12 (0.28-0.63)

5.1.3.2 External exposure due to soil and rock samples

The external annual effective dose received indoors by dwellers was calculated using equation (4.5) and results summarized in Table 5.4 for rock and soil samples in the two regions. The mean doses of soil samples from Kilimambogo and Gatuanyaga regions were 0.50 ± 0.11mSv $y^{-1}$and 0.36 ± 0.11 mSv y^{-1} with maximums of 0.67 mSv $y^{-1}$and 0.55 mSv y^{-1}respectively. The average external doses received indoors due to rock samples from Kilimambogo and Gatuanyaga regions were 0.41 ± 0.24 mSv $y^{-1}$and 0.50 ± 0.16 mSv y^{-1}recordingmaximum levels of 1.04 and 0.70 mSv y^{-1} respectively. The doses received by the residents were within or lower than the total exposure limit of 1 mSv y^{-1}recommended by the ICRP, (2007) for safety of members of the public. This means that, soil and rocks in the region does not pose any radiological risks to the residents and can therefore be used for agricultural purposes and for construction of dwellings.

5.1.4 Cassava crop

5.1.4.1 Activity Concentration

Table 5.5 summarizes the mean and range of ^{226}Ra, ^{232}Th and ^{40}K concentrations in cassava tubers, stem, and leaves sampled from the entire study region. In tubers, the mean activity concentrations of ^{226}Ra, ^{232}Th and ^{40}K in the samples were 46 ± 5 Bq kg^{-1}, 105 ± 13 Bq $kg^{-1}$and 555 ± 13 Bq kg^{-1} Maximum concentration levels of 89, 166 and 721 Bq $kg^{-1}$of the respective radionuclides were measured in the samples, R8, R2 and R1 respectively. Radium in the tubers would be expected to be higher but the bark which accumulates more radium was removed upon preparation of the samples. In the stem, the mean concentrations of ^{226}Ra, ^{232}Th and ^{40}K in the samples were 55 ± 1 Bq kg^{-1}, 52 ± 9 Bq kg^{-1} and 541 ± 13 Bq kg^{-1} in the stem. Maximum levels of 117, 69 and

869 Bq kg^{-1} were recorded in the samples S3, S5 and S8respectively. Levels in the leaves were 46 ± 6 Bq kg^{-1}, 68 ± 9 Bq kg^{-1} and 586 ± 41 Bq kg^{-1} recording maximum levels of 110 Bq kg^{-1}, 105 Bq kg^{-1} and 1052 Bq kg^{-1}in the respective radionuclides which were measured in the samples, L2, L8 and L8.^{226}Ra present in 56%, 67% and 56% in tubers, stem, and leaf samples exceeded the world average of 33 Bq kg^{-1}respectively. Radium accumulates more in the bark or stem hence the mean of stem samples was higher than in tubers and leaves. ^{232}Th present in 11% and 33% of tubers and leaf samples exceeded the world average of 45 Bq kg^{-1} respectively. On the other hand, ^{40}K in 67%, 33%, and 67% of tubers, stem, and leaf samples exceeded the world average of 420 Bq kg^{-1} respectively. The enhanced concentration levels of the radionuclides in plants are likely to be due to heavy application of fertilizes to the soil by farmers to improve crop yield. High ^{40}K is also expected since potassium is an important element required by crops for growth and plant development. Low levels of potassium in plants are normally observed in light sandy soils due to the high solubility of potassium leading to its leaching from the soil. Potassium is likely to dissolve more in moist soils leading to enhanced leaching and reducing the amount of exchangeable potassium available for plants uptake.

Radionuclides are mainly transferred to the plants via root uptake and foliar deposition. Since the soil in the region has been found to contain reasonable levels of the radionuclides, then these elements are available for root uptake by crops grown therein. The mean concentration of ^{226}Ra in stem than in leaves could be due to continuous accumulation of ^{226}Ra through root uptake. The tubers were peeled during the sample preparation before analysis hence the radionuclides that accumulate in the

bark of the tuber were not accounted for. Similarly, the tubers are peeled while cooking or eating hence reducing the intake doses.

Table 5.5: Summary statistics of activity concentrations of ^{226}Ra, ^{232}Th and ^{40}K in different parts of cassava samples

Average specific activity concentration and range in cassava samples			
	^{226}Ra Bq kg^{-1} Mean (Range)	^{232}Th Bq kg^{-1} Mean (Range)	^{40}K Bq kg^{-1} Mean (Range)
Cassava tubers	46 ± 5 (8±0.2 – 89±3)	105 ± 13 (37 ±4 –166±39)	555 ± 13 (243±3–721±12)
Cassava stem	55±1 (8 ± 0.2- 117 ± 4)	52±9 (27 ± 2- 69± 8)	541 ±13 (346 ± 6– 869 ± 14)
Cassava leaves	46 ±6 (11 ±0.4– 110 ±2.8)	68±9 (18 ± 2-105 ±24)	586±41 (274 ± 5- 1052 ±27)

The activity concentration of the cassava tubers and leaves measured by HPGe detector in the laboratory of Hirosaki University were comparable to the values measured by the NaI (Tl) detector. The mean and range of the measured samples were tabulated in Table 5.6 below.

Table 5.6: Activity concentration of radionuclides in cassava samples measured in Hirosaki University laboratory

	^{226}Ra (Bq kg^{-1}) Mean (Range)	^{232}Th (Bq kg^{-1}) Mean (Range)	^{40}K (Bq kg^{-1}) Mean (Range)
Cassava tubers	1.1 (0.73 – 1.5)	2.1 (1.9 – 2.2)	282 (243 – 321)
Cassava leaves	5 (4 – 6)	14 (11 – 17)	429 (375 – 482)

5.1.4.2 Internal exposure due to consumption of radionuclides in cassava

The average annual effective dose received by Kilimambogo residents as a result of intake of radionuclides contained in cassava tubers and leaves was also estimated using equation (4.17) and the results tabulated in Table 5.7. The annual consumption of the tubers and leaves per individual was approximated to be 45 kg y^{-1} and 25 kg y^{-1} respectively. The mean annual effective dose received from the consumption of

cassava tubers and leaves were 1.82 ± 0.60 mSv y^{-1} and 0.81 ± 0.30 mSv y^{-1} and recording a total dose of 2.63 ± 0.7 mSv y^{-1} from the consumption of the cassava crop by the residents. This was more than eight-fold higher than the world average ingestion dose of 0.3 mSv y^{-1} reported by the Canadian Nuclear Safety Commission, (2020). The highest dose reported due to tuber and leaf consumption was 2.80 mSv y^{-1} and 1.32 mSv y^{-1} respectively. 78% and 33% of the tuber and leaf samples recorded doses higher than the recommended level of 1 mSv y^{-1}. Consumption of tubers by the residents contributed the highest dose since they are consumed either when raw, roasted or, as a snack or food. The consumption of radionuclides by the residents may not cause immediate health hazards but may do so in future due to accumulation in body tissues with time. The bioaccumulation of radium and thorium in the plants is influenced by the soil pH hence the variation in the concentration was not consistent since different areas have different pH levels. Acidic soils (with low pH) have been reported to enhance availability of radium and thorium.

Table 5.7: Internal exposure due to consumption of cassava crop by the residents

	Cassava tubers	Cassava leaves	Total Average
Mean (mSv y^{-1})	1.82 ± 0.60	0.81 ± 0.30	2.63 ± 0.70
Minimum	0.91 ± 0.30	0.40 ± 0.20	0.66 ± 0.40
Maximum	2.80 ± 0.80	1.32 ± 0.70	2.06 ± 0.11

The total ingestion dose of 2.63 ± 0.70 mSv y^{-1} received by residents as a result of consumption of cassava contributes to 42.1% of the total dose received by the resident from measured sources in this study. Residents in Kilimambogo and Gatuanyaga should be advised to reduce the intake of cassava in order to reduce the exposure risks.

5.2 Activity concentration in air

5.2.1 Radon, thoron and thoron progeny concentration

The concentration levels of radon, thoron, and thoron progeny expressed as Equilibrium Equivalent Thoron Concentration (EETC) were measured in mud-built houses, iron sheet –built and modern or stone-built houses. The summary of the statistics is tabulated in Table 5.8. The mean radon concentration levels in the mud-walled, iron sheet -walled, and stone-walled dwellings were measured to be 67 ± 11 Bq m^{-3}, 60 ± 10 Bq m^{-3}, and 75 ± 10 Bqm^{-3} respectively. These values were significantly lower than the lower limit of 100 Bqm^{-3} and higher limit of 300 Bqm^{-3} set by the World Health Organization, (WHO, 2009) for indoor radon. The mean radon levels are however higher than the world average levels of 40 Bqm^{-3}, (Wanjala, 2021).

Table 5.8: Summary of the survey measurements for radon, thoron and EETC concentrations

Radionuclide concentrations	Mud-walled houses(N=19)	Stone-walled houses(N=12)	Iron sheet-houses(N=9)
Radon concentration (Bqm^{-3})	67 ± 11 (37 - 126)	75 ± 10 (42 -163)	60 ± 10 (38 - 84)
Thoron concentration (Bqm^{-3})	195 ± 36 (LOD - 973)	161 ± 31 (LOD - 1130)	(71±24) (LOD - 385)
EETC(Bqm^{-3})	11.5 ± 2.1 (0.8 - 29.1)	6.9 ± 1.0 (0.9 - 30.2)	2.6 ± 0.5 (1.0 - 9.4)

Figure 5.5 shows a graphical representation of the indoor gases in the mud-walled houses.

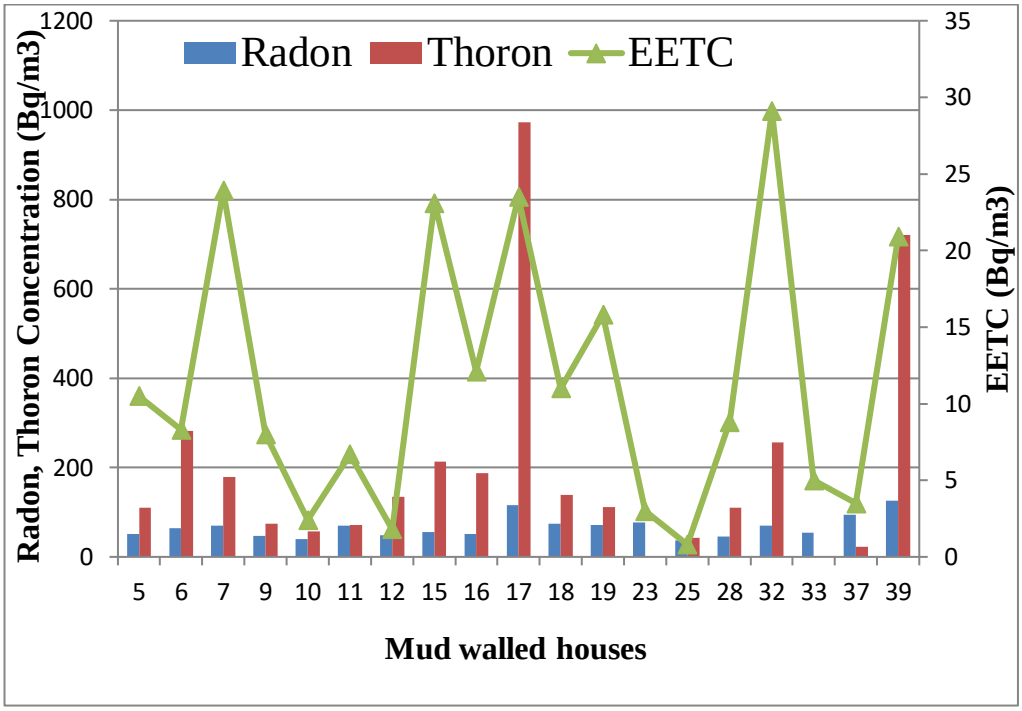

Figure 5.5: Radon, thoron and EETC concentration in mud- walled dwellings.

The highest measured mean radon concentration was in stone-walled dwellings (75 ± 10 Bqm^{-3}), followed by mud-walled houses, (67 ± 11 Bqm^{-3}) and lowest was recorded in iron sheet- walled houses, (60 ± 10 Bq m^{-3}). In the stone-walled houses, radon exceeded the 100 Bq m^{-3} limit only in one house, (8%), (No. 30), while in mud-walled houses, it exceeded the 100 Bq m^{-3} in 2 houses, (11%), (no 17 and no 39) which had bare earthen floors. The earthen floors made it easier for the gases to sip through the bare floors compared to the cement floors. Even so, all the iron sheet-walled houses recorded radon levels below 100 Bqm^{-3}. With a relatively longer half-life, radon is able to accumulate for longer periods in stone-walled houses without escape as compared to the other types of dwellings.

Concentration of thoron levels was highest recorded in mud-walled houses (195 ± 36 Bqm^{-3}), followed by the stone-walled houses, (161 ± 31 Bqm^{-3}) while the least mean level was measured in iron-sheet walled dwellings (71 ± 24 Bqm^{-3}). The mean

concentration levels measured in mud-walled and stone-walled houses exceeded the lower limit of 100 Bqm^{-3} but lower than the higher limit of 300 10 Bqm^{-3}. In stone-walled dwellings, thoron exceeded 300 Bq m^{-3} in 2 houses, (17%), (no. 22 and 30). Additionally, the building stones of house no 30 were joined with mud (or raw soil) instead of concrete and is also located along the slopes of Mount Kilimambogo. Both houses had bare earthen floors. Consequently; it was easy for the radioactive gases to seep into the houses without escape. On the other hand, house no. 13 had the least detectable level of thoron concentration and had a concrete cemented floor. This sealed off the entry of soil gas into the house hence reducing the concentration levels. In the case of mud-walled houses, thoron exceeded 100 Bq m^{-3} in 12 houses; (63%), out of which, 2 (11%) of them exceeded 300 Bq m^{-3}. In Iron sheet- walled houses however, thoron concentration was above the detection limit only in house no. 24 (385 Bqm^{-3}), which was observed to have an earthen floor at the time this survey was conducted. Thoron measured in all dwellings was far much higher than the world average reported by UNSCEAR, (2000). Thoron has a very short half-life and since the mud walls are porous, the gas easily accumulates in the mud-walled houses as compared to other types of dwellings. The gas is however unable to pass through the stone walls before decay.

Highest equilibrium equivalent thoron concentration, EETC (thoron progeny) level was measured in mud - walled dwellings, (11.5 ± 2.1 Bq m^{-3}), followed by stone-walled dwellings, (6.9 ± 1.0 Bqm^{-3}), and lowest was reported in iron sheet-walled houses (2.6 ± 0.5 Bqm^{-3}).

The reported high concentration levels of thoron and EETC in mud houses could be attributed to the high exhalation rate from the ground and soil bricks. Generally,

metals are considered to be barriers of radon isotopes hence together with their progenies, they do not easily pass through the metallic walls. Therefore, houses constructed using iron sheets were considered safest types of dwellings with the lowest mean concentration levels of the isotopes.

Radon concentration in indoor air largely depends on the concentration of ^{226}Ra, its emanation and exhalation rate. It can also be influenced by some environmental factors such as humidity, day time and geology, inflow of soil gas and ventilation of the house. On the other hand, thoron varies significantly due to its short half-life. The levels of the isotopes have also been reported to vary with season with highest values being recorded in the cold seasons and lowest being reported in hot seasons. Studies done in Garhwal Himalaya reported higher radon and thoron levels in mud houses as compared to wooden houses, (Ramola *et al*., 2016). EETC levels in the same study were reported to be highest in mud-built houses and lowest in cemented houses, which is consistent with the results of the present study. In this study, it was observed that, dwellings with concrete cemented floors recorded the lowest concentration levels. This is because cemented floors lower the entry of the gases and act as radon and thoron barriers except in floors that have cracks and joints. Stone-built and iron sheet-built houses with bare earthen floors recorded higher radon and thoron levels since the soil pores of the floors are open, thus making entry of radon and thoron gases into the dwellings easier, (Kumar *et al.*,2018). The variation of the radioactive gases was also observed to vary with the time of the day with concentration levels going higher during the day and night, (Suman *et al.*, 2021). Consequently, the residents need to construct houses with good ventilation. This would significantly reduce exposure by allowing the radioactive gases to escape from the dwellings.

Correlation between radon and thoron was also determined. A positive correlation was observed between radon and thoron, (R^2 = 0.5151), (Figure 5.6) and also between thoron and EETC, (R^2=0.3797), (Figure 5.7). The relatively low correlation between thoron and its progeny is an indication that the concentration level of thoron progeny cannot be obtained from thoron gas using the equilibrium factor as in the case of radon.

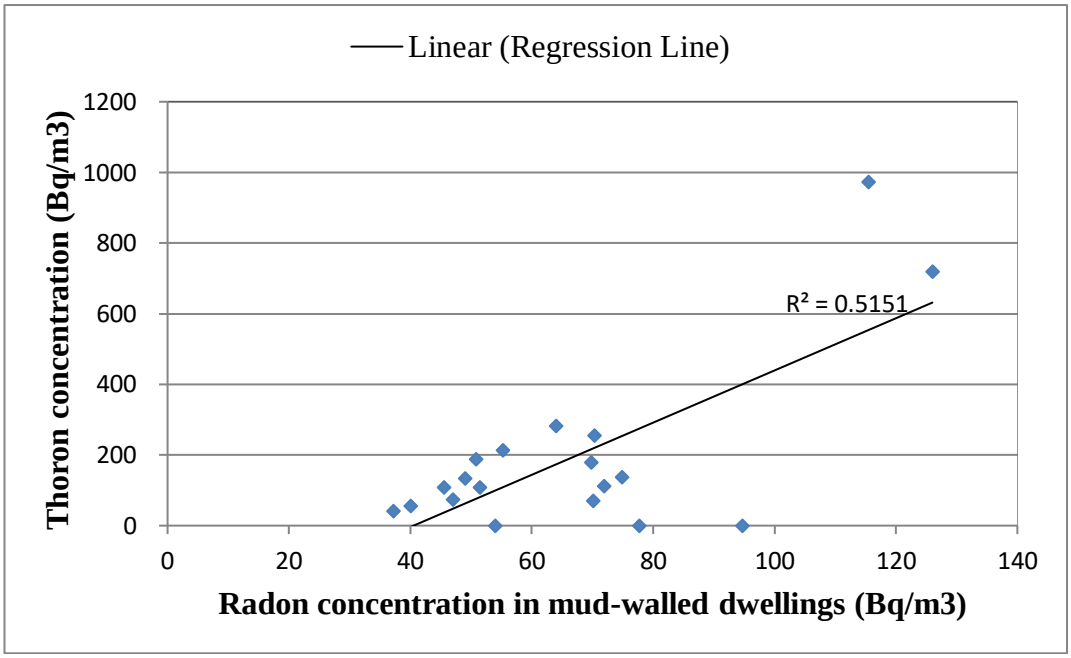

Figure 5.6: Variation of thoron with radon concentration in mud-walled dwellings

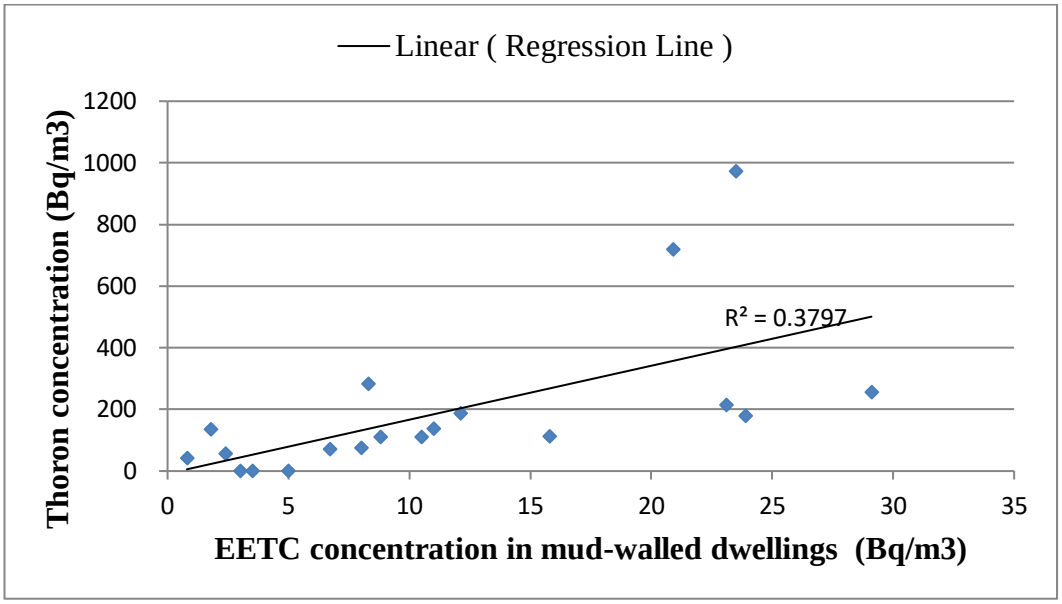

Figure 5.7: Variation of thoron with EETC concentration in mud-walled dwellings

5.2.2 Internal exposure due to radon and thoron progeny

The annual effective doses received by residents from radon and thoron were estimated from their respective progenies. Thoron progeny was directly measured in the dwellings while radon progeny was estimated using the equilibrium factor since both have been observed to be stable. The doses received from radon progeny was reported to be 1.3 ± 0.2 mSv y^{-1}, 1.1 ± 0.1 mSv y^{-1} and 1.4±0.2 mSv y^{-1} while that due to thoron progeny was reported to be 2.4 ± 0.4 mSv y^{-1}, 0.5 ± 0.1 mSv y^{-1} and 1.5 ± 0.2 mSv y^{-1} in mud-walled, iron sheet-walled and stone-walled houses respectively. The total doses were estimated to be 3.7 ± 0.4 mSv y^{-1}, 2.9 ± 0.3 mSv y^{-1} and 1.6 ± 0.2 mSv y^{-1} in the respective dwellings. The doses were observed to be comparable in stone-walled and mud - walled houses but lowest in iron sheet -walled houses. Since metals act as radon barriers, when a depressurization condition arises in a house, radon does not easily seep through the metallic walls. On the contrary, if the floor is earthen, the gases easily seep through the floor and very little or none if the floor is cemented.

Table 5.9 summarizes the annual effective doses in the different types of dwellings measured in the survey.

Table 5.9: Summary of the annual effective doses due to radon and thoron progenies

Annual effective doses	Mud-walled houses (N=19)	Stone-walled houses (N=12)	Iron sheet-houses (N=9)
Annual effective dose: radon progeny($mSvy^{-1}$)	1.3±0.2 (0.7 - 2.4)	1.4±0.2 (0.8 - 3.1)	1.1±0.2 (0.7 - 1.6)
Annual effective dose: thoron progeny($mSvy^{-1}$)	2.4±0.4 (0.2 - 6.1)	1.5±0.2 (0.2 - 6.3)	0.5±0.1 (0.2 - 2.0)
Total annual effective dose ($mSvy^{-1}$)	3.7±0.4 (0.9 - 8.5)	2.9±0.3 (1.0 - 9.4)	1.6±0.2 (0.9 - 3.6)

The overall mean measured dose from radon and the decay products in all the dwellings was 2.73 mSv y^{-1}, more than double the world average of 1.2 mSv y^{-1} as reported by the Canadian Nuclear Safety Commission, (2020) and comparable to that of all other natural sources of ionizing radiation of 2.4mSv, (UNSCEAR, 2008). However, the total average dose received by residents living in mud-built houses was more than 3 $mSvy^{-1}$, the dose action level set by the International Commission on Radiological Protection (ICRP). The doses from the three types of dwellings exceeded 1 mSv y^{-1}, the proposed dose limit set by WHO. These were however comparable to doses reported in Betare- Oya Gold mining areas of Eastern Cameroon, which were 2.63 ± 0.77 and 1.32 ± 0.88 1 mSv y^{-1} for radon and thoron progenies respectively, (Nkoulou II *et al.,* 2023). The results of the study reveal that, residents living in iron sheet - walled houses with cemented floors received the lowest doses from inhalation of the radon isotopes hence such houses are considered safer than the other types of dwellings. Residents living in mud houses and uncemented houses should cement

their dwellings or consider improving ventilation of their houses to reduce exposure risk.

5.3 Elemental concentration in water

5.3.1 pH and concentration of elements in water sources

Water samples from surface and boreholes sources from the two regions were compared for the wet and dry seasons. pH values ranged between 6.32 - 7.32 mg L^{-1} and 6.93 -7.64 mg L^{-1} in the borehole and surface samples respectively. WHO (2011) recommends pH levels of 6.5 to 8.5 and only 50% of the samples were reported to have values below 6.5.

The mean, range (minimum and maximum), and standard deviations of the elemental concentrations of the various elements collected from borehole and surface water sources in the dry and wet seasons are tabulated in Tables 5.10 - 5.13. Generally, the mean values were reported to be higher in both borehole and surface samples during the dry season as opposed to the wet season except for Cd, Cu, Mn, and Ni. Most of the mean values were comparable with the acceptable limits proposed by the WHO, in both types of water sources except for sodium which was higher by a ratio of 35 and 58 times in the borehole and surface water samples respectively. All the mean values were higher than the permissible limits provided by the World Health Organization except for Na. In all seasons, Cu, Fe, Mn and Pb exceeded WHO limits in all the samples, (WHO, 2011). Na exceeded the limit in all samples only in the dry season while Cd exceeded all samples in the wet season. This is due to the fact that sodium is highly soluble and easily dilutes in the rainy season. More than 50%, 60% and 36% of the samples contained Ca, Mg and Zn beyond the acceptable limits.

Table 5.10: Mean, range (min and max) and standard deviation of elemental concentration in borehole samples collected during the wet season

Samples	K	Na	Cd	Ca	Cu	Fe	Mg	Mn	Ni	Pb	Zn
Mean (mg L^{-1})	43.5	1.5	6.4	134	16.9	7.8	101.9	9.0	6.9	42.0	3.5
Min (mg L^{-1})	1.0	0.1	4.4	37.1	5.0	5.9	35.5	0.5	BD	10.7	0.8
Max (mg L^{-1})	209	6.0	8.0	277	29.1	9.1	229.2	19.8	16.1	121.4	8.2
Std Dev	71.1	2.1	1.1	93.5	7.8	1.1	82.2	6.3	5.09	34.0	2.6
WHO limits	-	3	0.003	75	2	0.13	50	0.4	0.07	0.015	3

BD=Below Detection

Table 5.11: Mean, range and standard deviation of elemental concentration in borehole samples collected during the dry season

Samples	K	Na	Cd	Ca	Cu	Fe	Mg	Mn	Ni	Pb	Zn
Mean (mgL^{-1})	50.0	52.9	2.1	143.5	11.4	8.3	135.0	7.5	5.2	61.8	5.8
Min (mg L^{-1})	3.5	8.7	BD	2.9	4.0	4.7	42.7	0.7	0.4	25.0	1.6
Max (mg L^{-1})	213.6	188.4	3.4	457.2	20.1	13.1	318.1	14.5	8.7	87.5	27.3
Std Dev	67.2	59.6	1.1	143.6	4.6	3.1	95.4	4.4	2.9	17.1	7.9
WHO limits	-	3	0.003	75	2	0.126	50	0.4	0.07	0.015	3

Table 5.12: Mean, range and standard deviation of elemental concentration in surface samples collected during the wet season

Samples	K	Na	Cd	Ca	Cu	Fe	Mg	Mn	Ni	Pb	Zn
Mean (mg L^{-1})	25.7	1.0	5.3	100.4	19.9	7.2	82.3	8.5	9.0	42.3	3.2
Min (mg L^{-1})	0.7	0.1	3.4	43.9	6.5	4.8	35.1	2.4	2.2	19.6	0.7
Max (mg L^{-1})	217.1	6.5	8.1	247.8	30.9	8.5	272.6	18.9	15.2	110.7	12.9
Std Dev	67.4	1.9	1.6	65.9	7.3	1.2	74.7	5.1	3.9	26.5	3.6
WHO limits		3	0.003	75	2	0.126	50	0.4	0.07	0.015	3

Table 5.13: Mean, range and standard deviation of elemental concentration in surface samples collected during the dry season

Samples	K	Na	Cd	Ca	Cu	Fe	Mg	Mn	Ni	Pb	Zn
Mean (mg L^{-1})	55.8	56.6	1.5	168.9	15.8	8.7	145.8	7.4	4.0	70.5	3.0
Min (mg L^{-1})	2.6	5.4	BD	52.3	4.3	5.1	48.9	0.7	BD	16.1	0.3
Max (mg L^{-1})	209.3	183.6	3.9	469.5	35.3	12.1	303.0	14.4	10.4	175.0	6.5
Std Dev	67.7	62.6	1.6	139.3	8.7	2.1	94.7	4.7	4.0	45.6	2.2
WHO limits		3	0.003	75	2	0.126	50	0.4	0.07	0.015	3

Calcium and magnesium are important elements in the biological processes of human body and are not classified as heavy metals. These elements reported the highest concentrations in both seasons and in both sources ranging from 134.9 ppm to 145.8 ppm in Mg and 143.5 ppm to 168.8 ppm in Ca. The highest concentrations of Mg exceeded 300 ppm while that of calcium was more than 400 ppm. This to a larger extent contributes to the hardness in water and at the same time is good for the prevention of calcium and magnesium deficiency among residents who consume the water. For borehole samples in the wet season, the mean Zn concentration was comparable to the WHO limit of 2.6 mgL^{-1}, Mn exceeded the limit by twenty times, Fe by 62 times, Ni by 98 times while Cd and Pb exceeded by more than 2,000 times. Cd only exceeded in the surface sources in the dry season by 500 times while Pb by 4700 times in the same season, (WHO, 2011). These concentration levels are of concern to the members of the public who consume water from these sources. These levels are way too high compared to the levels reported in Mrima Hill, (Chege, 2014).

5.3.2 Chronic daily dose (CDI)

The observed chronic daily dose of the elements in drinking water should not exceed the proposed reference dose. This is the approximate exposure incurred daily over an entire lifetime, without appreciable risk for the general public. The chronic daily intake of borehole water in the dry and wet seasons were determined using equation (4.10) and are tabulated in Tables 5.14 and 5.15 respectively. The mean of the CDI in the dry season were 1.02 ± 1.37, 1.08±1.22, 0.04±0.02, 2.92 ± 2.93, 0.23 ± 0.09, 0.17 ± 0.06, 2.75 ± 1.94, 0.15 ± 0.09, 0.11 ± 0.06, 1.26 ± 0.35 and 0.12 ± 0.16 for K, Na, Cd, Ca, Cu, Fe, Mg, Mn, Ni, Pb and Zn respectively. The mean of the CDI in the wet season were 0.89 ± 1.45, 0.03 ± 0.04, 0.13 ± 0.02, 2.72 ± 1.91, 0.34 ± 0.16, 0.16 ±

0.02, 2.08 ± 1.68, 0.18 ± 0.13, 0.14 ± 0.10, 0.96 ± 0.69, 0.07 ± 0.05 for the respective elements. The CDI levels for Ca, Cu, Fe and Mg in all samples in both seasons were lower than the reference levels proposed by WHO. That of Zn, Pb and Mn was observed to be more than the reference level by at least 10%, 20% and 70% respectively. CDI was less that the proposed level in all samples in the dry season while on the contrary; only 10 % of the samples in the wet season had CDI levels lower than the recommended levels.

Table 5.14:Chronic daily intake (CDI) for borehole water samples in the dry season

Element	K	Na	Cd	Ca	Cu	Fe	Mg	Mn	Ni	Pb	Zn
Mean ($mg\ kg^{-1}\ d^{-1}$)	1.02	1.08	0.04	2.92	0.23	0.17	2.75	0.15	0.11	1.26	0.12
Min ($mg\ kg^{-1}\ d^{-1}$)	0.07	0.18	0.00	0.06	0.08	0.10	0.87	0.01	0.01	0.51	0.03
Max ($mg\ kg^{-1}\ d^{-1}$)	4.35	3.84	0.07	9.32	0.41	0.27	6.48	0.30	0.18	1.78	0.56
Std Dev	1.37	1.22	0.02	2.93	0.09	0.06	1.94	0.09	0.06	0.35	0.16
WHO, 2011 R_fD	-	-	0.1	41.4	2	0.3	11	0.14	0.02	0.35	0.3

Table 5.15:Chronic daily intake (CDI) for borehole water samples in the wet season

Element	K	Na	Cd	Ca	Cu	Fe	Mg	Mn	Ni	Pb	Zn
Mean ($mg\ kg^{-1}\ d^{-1}$)	0.89	0.03	0.13	2.72	0.34	0.16	2.08	0.18	0.14	0.86	0.07
Min ($mg\ kg^{-1}\ d^{-1}$)	0.02	0.00	0.09	0.76	0.10	0.12	0.72	0.01	0.00	0.22	0.02
Max ($mg\ kg^{-1}\ d^{-1}$)	4.25	0.12	0.16	5.64	0.59	0.19	4.67	0.40	0.33	2.48	0.17
Std Dev	1.45	0.04	0.02	1.91	0.16	0.02	1.68	0.13	0.10	0.69	0.05
WHO, 2011 R_fD	-	-	0.1	41.4	2	0.3	11	0.14	0.02	0.35	0.3

Tables 5.16 and 5.17 show the internal chronic daily intake of surface water in the dry and wet seasons. The mean of the CDI by the residents from the surface water in the dry season were 1.14 ± 1.38, 1.15 ± 1.2, 0.03 ± 0.03, 3.44 ± 2.84, 0.32 ±0.18, 0.18 ± 0.04, 2.97 ± 1.93, 0.15 ± 0.10, 0.08 ± 0.08, 1.44 ± 0.93, 0.06 ± 0.05 for K, Na, Cd, Ca, Cu, Fe, Mg, Mn, Ni, Pb and Zn respectively. The mean of the CDI by the residents from the surface water in the wet season were 0.76 ± 1.53, 0.03 ± 0.04, 0.10 ± 0.03, 2.20 ± 1.37, 0.40 ± 0.14, 0.14 ± 0.03, 1.97 ± 1.74, 0.18 ± 0.01, 0.18 ± 0.08, 1.09 ± 0.91, 0.08 ± 0.08 for the respective metals. The chronic daily intake for Ca, Cu, Fe, Mg and Zn was less than the proposed limits in all the samples in both seasons. That of Cd, Mn, Ni and Pb was observed to exceed the proposed reference levels by at least 45%, 55%, 36% and 9% respectively.

Table 5.16: Chronic daily intake (CDI) for surface water samples in the dry season

Element	K	Na	Cd	Ca	Cu	Fe	Mg	Mn	Ni	Pb	Zn
Mean ($mg\ kg^{-1}\ d^{-1}$)	1.14	1.15	0.03	3.44	0.32	0.18	2.97	0.15	0.08	1.44	0.06
Min ($mg\ kg^{-1}\ d^{-1}$)	0.05	0.11	0.00	1.07	0.09	0.10	1.00	0.01	0.00	0.33	0.01
Max ($mg\ kg^{-1}\ d^{-1}$)	4.27	3.74	0.08	9.57	0.72	0.25	6.18	0.29	0.21	3.57	0.13
Std Dev	1.38	1.28	0.03	2.84	0.18	0.04	1.93	0.10	0.08	0.93	0.05
WHO, 2011 R_fD	-	-	0.1	41.4	2	0.3	11	0.14	0.02	0.35	0.3

Table 5.17: Chronic daily intake (CDI) for surface water samples in the wet season

Element	K	Na	Cd	Ca	Cu	Fe	Mg	Mn	Ni	Pb	Zn
Mean ($mg\ kg^{-1}d^{-1}$)	0.76	0.03	0.10	2.20	0.40	0.14	1.97	0.18	0.18	1.09	0.08
Minimum ($mg\ kg^{-1}d^{-1}$)	0.01	0.00	0.06	0.89	0.13	0.10	0.71	0.05	0.04	0.40	0.01
Maximum ($mg\ kg^{-1}\ d^{-1}$)	4.43	0.13	0.16	5.05	0.63	0.17	5.56	0.38	0.31	3.35	0.26
Std Dev	1.53	0.04	0.03	1.37	0.14	0.03	1.74	0.10	0.08	0.91	0.08
WHO,2011 R_fD	-	-	0.1	41.4	2	0.3	11	0.14	0.02	0.35	0.3

Elevated heavy metal concentrations in water sources were associated with weathering of rocks, application of fertilizers and pesticides especially in Africa to enhance crop yield. In addition, (Zhou *et al.,* 2020).

5.3.3 Non carcinogenic risks

5.3.3.1 Hazard quotients

The non-carcinogenic risks resulting from intake of elements present in water were estimated by evaluating the hazard quotients and hazard indices for adult residents using equation (4.11). Tables 5.18 and 5.19 show the measured hazard quotients (HQ) for the borehole water samples in the dry and wet seasons respectively. The mean of HQ for borehole water sources in the dry season were 0.44 ± 0.22, 0.07 ± 0.07, 0.12 ± 0.05, 0.56 ± 0.21, 0.25 ± 0.18, 1.10 ± 0.63, 5.27 ± 2.98, 3.60 ± 0.99, 0.40 ± 0.53andin the wet season were 1.31 ± 0.23, 0.07 ± 0.05, 0.17 ± 0.08, 0.53 ± 0.07, 0.19 ± 0.15, 1.31 ± 0.92, 7.05 ± 5.19, 2.44 ± 1.98 and 0.24 ± 0.18 for Cd, Ca, Cu, Fe, Mg, Mn, Ni, Pb and Zn respectively. Hazard quotients measured in Ca, Cu, Fe and Mg were less than the proposed limit of 1. On the contrary, Mn, Ni and Pb exceeded the limit in at least 60%, 80% and 80% of the samples respectively.

Table 5.18: Hazard quotients (HQ) for borehole water samples in the dry season

Elements	Cd	Ca	Cu	Fe	Mg	Mn	Ni	Pb	Zn
Mean	0.44	0.07	0.12	0.56	0.25	1.10	5.27	3.60	0.40
Min	0.00	0.00	0.04	0.32	0.08	0.09	0.44	1.46	0.11
Max	0.69	0.23	0.21	0.89	0.59	2.11	8.86	5.10	1.86
Std Dev	0.22	0.07	0.05	0.21	0.18	0.63	2.98	0.99	0.53

*WHO limit of 1 in all elements,

Table 5.19: Hazard quotients (HQ) for borehole water samples in the wet season

Elements	Cd	Ca	Cu	Fe	Mg	Mn	Ni	Pb	Zn
Mean	1.31	0.07	0.17	0.53	0.19	1.31	7.05	2.44	0.24
Min	0.90	0.02	0.05	0.40	0.07	0.08	0.00	0.62	0.05
Max	1.62	0.14	0.30	0.62	0.42	2.88	16.40	7.07	0.56
Std Dev	0.23	0.05	0.08	0.07	0.15	0.92	5.19	1.98	0.18

*WHO limit of 1 in all elements

Tables 5.20 and 5.21 show the measured hazard quotients (HQ) for the surface water samples in the two seasons. The mean of HQ for surface water sources in the dry season were 0.30 ± 0.33, 0.08 ± 0.07, 0.16 ± 0.09, 0.59 ± 0.14, 0.27 ± 0.18, 1.07 ± 0.68, 4.11 ± 4.10, 4.10 ± 2.66 and 0.20 ± 0.15 and in the wet season were 1.05 ± 0.34, 0.05 ± 0.03, 0.20 ± 0.07, 0.47 ± 0.09,0.18 ± 0.16, 1.29 ± 0.73, 9.10 ± 3.77, 3.11±2.59 and 0.26 ± 0.27 for Cd, Ca, Cu, Fe, Mg, Mn, Ni, Pb and Zn respectively. The mean index of three elements (Mn, Ni, Pb) and four elements (Cd, Mn, Ni and Pb) exceeded the proposed limit of 1 in the surface water samples in the dry and wet seasons respectively. The hazard quotients measured in all samples for Ca, Cu, Fe, Mg and Zn were less than the proposed limit of 1. On the contrary, Mn, Ni, Pb and Cd exceeded the limit in at least 55%, 91%, 91% and 45% of the samples respectively. HQ levels greater than 1 indicates a health risk for the general public when they consume the water without treatment.

Table 5.20: Hazard quotients (HQ) for surface water samples in the dry season

Elements	Cd	Ca	Cu	Fe	Mg	Mn	Ni	Pb	Zn
Mean	0.30	0.08	0.16	0.59	0.27	1.07	4.11	4.10	0.20
Min	0.00	0.03	0.04	0.35	0.09	0.09	0.00	0.94	0.02
Max	0.79	0.23	0.36	0.82	0.56	2.09	10.63	10.19	0.44
Std Dev	0.33	0.07	0.09	0.14	0.18	0.68	4.10	2.66	0.15

*WHO limit of 1 in all elements

Table 5.21: Hazard quotients (HQ) for surface water samples in the wet season

Element	Cd	Ca	Cu	Fe	Mg	Mn	Ni	Pb	Zn
Mean	1.05	0.05	0.20	0.47	0.18	1.29	9.10	3.11	0.26
Min	0.65	0.02	0.07	0.32	0.06	0.35	2.22	1.14	0.05
Max	1.64	0.12	0.32	0.58	0.51	2.75	15.51	9.57	0.88
Std Dev	0.34	0.03	0.07	0.09	0.16	0.73	3.77	2.59	0.27

5.3.3.2 Hazard indices

The potential risk to the population due to intake of several elements in the drinking water was determined using the hazard index (HI). The sum of multiple metal exposures is assumed to be proportional to the level of adverse effects for the population. The hazard indices were evaluated using equation (4.12) and the results tabulated in Table 5.22 for borehole and surface water samples in the two regions. The mean hazard indices were 11.80 ± 4.19, 13.30 ± 4.82, for the borehole samples in dry and wet season and 10.89 ± 4.46 and 15.71 ± 4.93 for the surface samples in the dry and wet season respectively. The hazard indices in all the samples were higher than the proposed reference value of 1. The total hazard index is less than 100 but more than 10 indicating that the water sources are highly polluted and that there is need for further sample analysis to inform the general public and policy makers on possible intervention measures.

Table 5.22: Mean and range of hazard indices in borehole and surface sources in the dry and wet seasons

Season	Borehole dry	Borehole wet	Surface dry	Surface wet
Mean	11.80	13.30	10.89	15.71
Range	4.43 – 16.31	6.09 - 22.36	4.80 - 19.35	7.83 - 22.58
Std Dev	4.19	4.82	4.46	4.93

*WHO limit of 1

5.3.4 Cancer risks

5.3.4.1 Chronic Daily Intake for metal carcinogens

This is the average daily heavy metal intake taken by the residents over a lifetime and obtained using equation (4.10). The average daily intake of heavy metals due to the metal carcinogens, cadmium, nickel, and lead were estimated for the dry and wet seasons in the different types of water sources. The summary of the mean and range of the lifetime average daily dose is shown in Table 5.23. The mean from borehole water samples in the dry season were 0.04 ± 0.02, 0.11 ± 0.06 and 1.26 ± 0.35 and those in the wet season were 0.31 ± 0.02, 0.14 ± 0.10 and 0.86 ± 0.69 for Cd, Ni and Pb respectively.

Table 5.23: Mean and range of Chronic Daily Intake (CDI) in water samples

CDI	Cd	Ni	Pb
Borehole water samples in the dry season (Mg/kg Bw/d)	0.04 ± 0.02 (0.00 – 0.07)	0.11 ± 0.06 (0.01 – 0.18)	1.26 ± 0.35 (0.51 – 1.78).
Borehole water samples in the wet season (Mg/kg Bw/d)	0.31 ± 0.02 (0.09 – 0.16),	0.14± 0.10 (0.00 – 0.33)	0.86± 0.69 (0.22 – 2.48)
Surface water samples in the dry season (Mg/kg Bw/d)	0.03± 0.03 (0.00 – 0.08),	0.08 ± 0.08 (0.00 – 0.21)	1.44 ± 0.93 (0.33 – 3.57)
Surface water samples in the wet season (Mg/kg Bw/d)	0.10 ± 0.03 (0.06 – 0.16)	0.18 ± 0.08 (0.04 – 0.31)	1.09 ± 0.91 (0.40 – 0.28)
WHO, 2011 RfD	0.003	0.02	0.35

The mean of surface water sources in the dry season were 0.03± 0.03, 0.08 ±0.08 and 1.44 ±0.93 and those from the wet season were 0.10 ± 0.03, 0.18 ± 0.08 and 1.09 ± 0.91 for Cd, Ni and Pb respectively. The CDI values were significantly higher than the proposed reference limits by 3 to 100 fold.

5.3.4.2 Incremental lifetime cancer risk (ILCR)

The lifetime cancer risks for the residents as a result of intake of metal carcinogens, Cd, Ni and Pb in borehole and surface water was estimated for both dry and wet seasons using equation (4.13) and (4.14)The summary statistics of the incremental lifetime cancer risks and the total cumulative risks are tabulated in Table 5.24.The mean cancer risks from borehole water in the dry season were 0.02 ± 0.01, 0.10 ± 0.05 and 0.01 ± 0.00 with a cumulative cancer risk of 0.13 ± 0.06 from the three metal carcinogens. The risks from the borehole samples in the wet season were 0.05 ± 0.01, 0.13 ± 0.09and 0.007 ± 0.006 for Cd, Ni and Pb respectively with a cumulative cancer risk of 0.19 ± 0.09. The mean cancer risks from surface water sources in the dry season were 0.01 ± 0.01, 0.07 ± 0.07 and 0.01 ± 0.01 with a cumulative risk of 0.10 ± 0.07. In the wet season, the mean values were 0.04 ± 0.01, 0.17 ± 0.07 and 0.01 ± 0.01 for Cd, Ni and Pb with a cumulative risk of 0.21 ± 0.06.

Table 5.24: Incremental lifetime cancer risk (ILCR) and cumulative risks through intake of borehole and surface water from Kilimambogo region

ILCR	Cd	Ni	Pb	Cumulative risks
Borehole water samples in dry season	0.02 ± 0.01 (0.00 – 0.03)	0.10 ± 0.05 (0.01 – 0.16)	0.01 ± 0.00 (0.00 – 0.02)	0.13 ± 0.06 (0.03 -0.19
Borehole water samples in wet season	0.05 ± 0.01 (0.03 – 0.06)	0.13 ± 0.09 (0.00 – 0.30)	0.007 ± 0.006 (0.002 – 0.021)	0.19± 0.09 (0.05 – 0.35).
Surface water samples in dry season	0.01±0.01 (0.00 - 0.03),	0.07 ± 0.07 (0.00 – 0.19)	0.01± 0.01 (0.00-0.03)	0.10±0.07 (0.01 – 0.21).
Surface water samples in wet season	0.04±0.01 (0.02-0.06),	0.17±0.07 (0.04-0.28)	0.01±0.01 (0.00-0.03)	0.21 ± 0.06 (0.09-0.32).

These risk levels were greater than the acceptable risks of 10^{-6} to 10^{-4} proposed by USEPA, (2011) by a factor of 1000 to 100,000. This implies that about 10% of the

residents could die of cancer related ailments as a result of ingestion of heavy metals present in water sources. This is an indication that the level of pollution of water sources in the study region is very high leading to very high cancer risks for the residents. Intolerable cancer risks in both children and adults were also reported in well drinking water in Kampala, Uganda, (Bamuwamye *et al*., 2017). Similar study done by Munene *et al* (2023) and Wanjala *et al* (2020) reported very low risk from consumption of water from Sosian river and Ortum, Kenya respectively.

5.4 Dose estimation using RESRAD computer code

The RESRAD computer code was used to simulate the total effective dose equivalent (TEDE) received by the resident farmer and the quarry worker due to the continuous exposure to external gamma radiation, from NORM present in soil and rock samples in the study region. The mean concentrations of ^{226}Ra, ^{232}Th and ^{40}K in soil were used in RESRAD code to determine the total effective dose equivalent (TEDE)for time, t = 0 years, for the resident farmer while the mean levels in the quarry rock samples were used in determination of the dose received by the quarry worker. The assumption was that, the radionuclide concentration was uniform over the specified area, (Yu, 2012)

5.4.1 Resident farmer scenario

An adult resident farmer in Kilimambogo region stays most of the time in the contaminated zone and is assumed to receive the highest dose from the environment. The TEDE was calculated only for external ground at t=0 years. The doses contributed by the radionuclides for the external/ ground pathway are 0.12 mSv y^{-1}, 0.09 mSv y^{-1} and 0.004 mSv y^{-1} from ^{40}K, ^{226}Ra and ^{232}Th and having a total dose of 0.22 mSv y^{-1} for all the radionuclides which is comparable to the dose constrain of 0.25 mSv y^{-1} for

the general public (Yu, 2001). Therefore, this risk is low and does not pose any health risk to the residents. The natural radionuclides were present before human existence. Therefore, from point of birth, a resident of Kilimambogo receives most significant dose from ^{40}K followed by ^{226}Ra and least significantly from ^{232}Th. The doses measured in this study were comparable to a dose of 0.28 mSv y^{-1} reported in Ortum, West Pokot County, Kenya, Wanjala (2021), and higher than 0.048 mSv y^{-1} measured in Khak – Sefid in Ramsar, Iran by Ziajahromi *et al* (2015).

5.4.2 Quarry worker scenario

The total effective dose equivalent of an adult worker, who works in a local quarry for six days a week, spends nine hours on site and works for roughly forty weeks in a year was calculated using the RESRAD computer code. The TEDE was calculated for ground (external) pathway from the mean activity concentration of radionuclides in the quarry samples. The total doses contributed by the radionuclides summed over the external radiation pathway are 0.10 mSv y^{-1}, 0.056 mSv y^{-1} and 0.0039 mSv y^{-1} from ^{40}K, ^{226}Ra and ^{232}Th and having a total dose of 0.16 mSv y^{-1} at t=0 years. This dose is low and does not pose any significant health risk to the quarry workers.

Radiation exposure from ^{40}Kcontributed the highest dose while ^{232}Th contributed the least dose. This is due to the fact that the concentration of thorium in samples was relatively low while that of potassium was relatively high. In Kenya, studies done in Homa Hill analyzing the exposure of different age groups of a resident farmer recorded a total dose of 1.03 mSv y^{-1} for an adult resident, (Otwoma, 2012). Lower doses were measured in Cairo by Hassan (2023) for workers working in a construction power plant, and Kipng'eno, (2022) for Bureti residents in Kericho, Kenya.

5.5 Exposure associated with all pathways in the sampling region

Table 5.25 summarizes the annual effective dose associated with exposure to radioactivity in different matrices in Kilimambogo region. The highest annual effective dose is received as a result of inhalation of radon and thoron progeny which is comparable to the dose received due to ingestion of cassava tubers and water. The dose evaluated using RESRAD software was lower than the sum evaluated using discussed mathematical models. This is due to the fact that RESRAD only involved only the activity concentration of the radionuclides in soil only.

Table 5.25: Summary of annual effective doses from various pathways

(i) External dose received indoors

Region	Soil samples (mSv y^{-1})	Rock samples (mSv y^{-1})
Kilimambogo region	0.50 ± 0.11 (0.31 – 0.67)	0.41 ± 0.24 (0.09 – 1.04)
Gatuanyaga region	0.36 ± 0.11 (0.25 – 0.55)	0.50 ± 0.16 (0.30 – 0.75)

(ii) Total inhalation dose due to indoor radon and thoron progeny

Mud-walled houses (mSv y^{-1})	Stone-walled houses (mSv y^{-1})	Iron sheet -walled houses (mSv y^{-1})
3.7 ± 0.4 (0.9 - 8.5)	2.9 ± 0.3 (1.0 - 9.4)	1.6 ± 0.2 (0.9 - 3.6)

(iii) Ingestion Dose due to water and cassava

Water		Cassava	
Borehole Samples (mg kg^{-1} d^{-1})	Surface Samples (mg kg^{-1} d^{-1})	Tubers (mSv y^{-1})	Leaves (mSv y^{-1})
8.73 ± 0.66 (1.92 – 27.56 0	9.05 ± 0.70 (2.40 – 29.01)	1.82 ± 0.60 (0.91 – 2.80)	0.81 ± 0.30 (0.40 – 1.32)

(iv) Dose from RESRAD simulation Dose from RESRAD

External Ground pathway (mSv y^{-1})	
Resident farmer scenario	Quarry worker scenario
0.22	0.16

Table 5.25 (v) and Figure 5.8 outline a summary of doses received by the residents from all evaluated pathways. Residents receive highest doses from inhalation of radon and decay products, (43.7%) followed by dose form ingestion of cassava, (42.1) and least from external dose received indoors.

(v) Summary of annual effective doses for all pathways

Pathway	**Average inhalation dose (^{222}Rn & ^{220}Rn)**	**Ingestion Dose due to cassava**	**External dose received indoors**
Dose (mSv y^{-1})	2.73	2.63	0.885
% Contribution	43.7%	42.1%	14.2%
UNSCEAR, 2008	^{222}Rn & ^{220}Rn 52%	Food and water ingestion (12%)	^{226}Ra, ^{232}Th & ^{40}K external gamma exposure (20%)

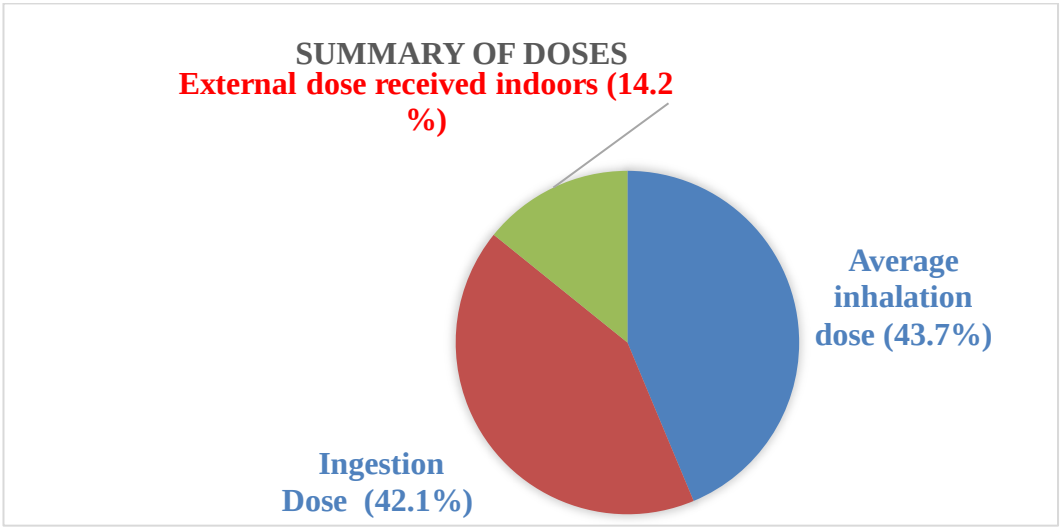

Figure 5.8: Summary of doses from all measured pathways

CHAPTER SIX: CONCLUSIONS AND RECOMMENDATIONS

6.1 Conclusions

The data presented in this research form baseline study on radiation exposure from radionuclide present in air, soil and rock samples and also for elemental concentration levels in borehole and surface water samples. The activity concentrations of the radioisotopes from the two regions were comparable although the concentration of samples from Gatuanyaga region were slightly higher compared to that from Kilimambogo region. The risks received by the general public as a result of exposure to NORM present in rock and soil was determined. The total indoor mean dose received by residents of Gatuanyaga region and Kilimambogo region as a result of exposure to soil and rock samples were 0.91 ± 0.26 mSv y^{-1} and 0.86 ± 0.19 mSv y^{-1} respectively averaging to 0.885 mSv y^{-1}. This contributed to only 14.2% of the total observed dose. This is slightly lower than the total exposure limit of 1 mSv y^{-1} recommended by ICRP (2007) for members of the public. This therefore means that the radiological risk associated with use of soils and rocks from the region is inconsequential. Consequently, soil and rock harvested from the region could safely be used for agriculture and construction of dwellings by the residents.

The doses received due to intake of cassava tubers and leaves are 1.82 ± 0.60 mSv y^{-1} and 0.81 ± 0.30 mSv y^{-1} respectively, totaling to 2.63 mSv $y^{-1.}$ This was about three times higher than the recommended ingestion dose limit of 1 mSv $y^{-1.}$ recommended by ICRP (2007) and more than 8 times the world average ingestion dose of 0.3 mSv y^{-1}, (Canadian Nuclear Safety Commission, 2020; Kinahan *et al.,* 2020). Therefore, ingestion of cassava in the region contributes significantly to the ingestion dose of up

to 42.1% of the total measured dose. Residents could be advised to reduce the intake cassava tubers and leaves in order to reduce the exposure risk.

The annual effective dose received by the residents of Kilimambogo due to exposure of radon and thoron progenies was determined for the three types of dwellings. The mean dose received from radon progeny was comparable in all cases while that from thoron was highest in earthen dwellings and least in the metallic dwellings. This is possibly because radon has a longer half-life and hence takes time to attain stability in any type of dwelling. Thoron on the other hand has a very short half-life, diffuses easily through soil hence the concentration of thoron in mud-walled houses was the highest followed by stone and least in metallic walled dwellings. Residents living in mud-walled dwellings therefore receive the highest mean total dose from the two isotopes of 3.7 ± 0.4 mSv y^{-1} while those that live in metallic dwellings receive the lowest doses of 1.6 ± 0.2 mSv y^{-1}, less than half dose that received by residents in mud walled houses. The average inhalation dose received by the residents was 2.73 mSv y^{-1} constituting 43.7% of the total dose received by residents. Therefore, residents living in mud walled houses are at a higher risk of getting lung cancer than those living in metallic dwellings. Residents living in houses without concrete floors also receive higher doses than those whose houses had cemented floors. To reduce the inhalation dose, residents should consider ensuring that their floors are cemented and do not have cracks. Also, they should ensure their houses are well ventilated by opening their widows throughout the day. This will reduce the radon and thoron gases build up in the houses.

The mean concentration levels of elemental composition in all samples in both seasons far exceeded the limits recommended by WHO, (2011). For instance, that of

Pb and Cd were 4,700 and 500 times higher than the limits. These levels are of great concern and the policy makers need to intervene and advise the public to find alternative means to obtain drinking water. These high levels are attributed to the geology of the area which contains Granitoid Gneiss metamorphic rocks which are known to contain abundant minerals and heavy metals. Additionally, industrial affluents from Thika and Nairobi, which are industrial towns could get into the region through the Athi and Thika rivers. The lifetime cancer risks for the residents as a result of intake of metal carcinogens, Cd, Ni and Pb in borehole and surface water was estimated. The cumulative cancer risk in the borehole samples was 0.12 ± 0.06 and 0.19 ± 0.09 in the dry and wet seasons respectively. Those from surface water sources were 0.10 ± 0.07 and 0.21 ± 0.06 in the dry and wet seasons respectively. In both seasons, the levels of cancer risks were greater than the acceptable risks of 10^{-6} to 10^{-4}, USEPA, (2011) by a factor of up to 100,000. This means that approximately 10% of the residents are likely to die of cancer related ailments due to ingestion of metal carcinogens in water sources. This was higher than the risk reported in Ortum, Kenya, (Wanjala *et al.*, 2019). The total hazard index exceeded 10 implying that the water sources in the region are extremely polluted.

The dose received from the contribution of ^{40}K, ^{226}Ra and ^{232}Th by the resident farmer and the quarry worker in the study area were 0.22 mSv y^{-1} and 0.16 mSv y^{-1} respectively which were lower than the dose constraint of 0.25 mSv y^{-1} used by RESRAD to guarantee radiation safety of the general public.

6.2 Recommendations

i. To reduce inhaled dose, residents of Kilimambogo region could be advised to use alternative building materials other than mud such as iron sheets

according to the outcome of this research. In addition, residents should be advised to have concrete floors in their dwellings and increase ventilation to improve air quality in the dwellings.

ii. The impact of fertilizers on radioactivity levels in crops grown in the region should be investigated in future studies

iii. The water quality from the region indicated extreme pollution. Residents should be advised to get drinking water from alternative sources. They could consider harvesting enough water to run throughout the rainy and dry seasons within the year. However, this comes with financial constraints and therefore residents could be advised on affordable means of purifying drinking water.

iv. The Kiambu and Machakos water departments should investigate the quality of water in the counties and come up with intervention measures to ensure residents consume quality water.

v. Disposal of industrial wastes and effluents from industries in Thika and Nairobi need to be investigated.

vi. To reduce ingestion dose, residents should be advised to reduce intake of cassava tubers and leaves. Similar research should be extended to other crops grown in the region like maize, beans, sorghum, bananas, kales among others.

vii. The outcome of this research can be used as a reference or baseline data. The study could be extended to cover other areas of Kiambu and Machakos counties.

viii. Mapping of radon, thoron and thoron progeny in Kenya is needed in future studies.

REFERENCES

Abdullahi S. Ismail A. F. and Samat S. (2016). Determination of indoor doses and excess lifetime cancer risks caused by building materials containing natural radionuclides in Malaysia. *Nuclear Engineering Technology,* **30**: 1-12.

Adamu C.I., Nganje T.N. and Edet A. (2015). Heavy metal contamination and health risk assessment associated with abandoned barite mines in Cross River State, southeastern Nigeria. *Environmental Nanotechnology, Monitoring and Management,* **3**:10–21.

Ahmed N. K., Abbady A., El-Arabi A.M., Michel R. El-Kamel A. H and Abbay A. G. E. (2006). Comparative study of the natural radioactivity of some selected rocks from Egypt and Germany. *Indian Journal of Pure & Applied Physics,* **44**: 209- 215.

Alashrah S.A. (2016). Radiation properties for red soil in Qassim Province, Saudi Arabia.*Journal of Radiation Research and Applied Sciences,* **30**:1-7.

Al-Zahrani B. M., Alqannas H.S. and Hamidalddin H. (2020). study and simulated the natural radioactivity (NORM) U-238, Th-232 and K-40 of igneous and Sedimentary Rocks of Al-Atawilah (Al-Baha) in Saudi Arabia. *World Journal of Nuclear Science and Technology,* **10:** 171-181.

Avwiri O. G and Agbalagba E.O. (2015). Assessment of natural radioactivity, associated radiological health hazards indices and soil-to-crop transfer factors in cultivated area around a fertilizer factory in Onne, Nigeria. *Environmental Earth Sciences,* **71(4):**1541-1549.

Aziz K. H. H., Mustafa F. S., Omer K. M, Hama S., Hamarawfa R. F. and Rahmana K. O. (2023). Heavy metal pollution in the aquatic environment: efficient and low-cost removal approaches to eliminate their toxicity: a review. *Royal Society of Chemistry,* **13:** 17595-17610.

Badry E. A. (2016). Distribution of heavy metals in contaminated water and bottom deposits of Manzala Lake, Egypt. *Journal of Environmental and Analytical Toxicology,* **6**:1-7.

Bamuwamye M., Ogwok P., Tumuhairwe V., Eragu R., Nazisozi. and Ogwang P. E. (2017). Human health risk assessment of heavy metals in Kamplala (Uganda) drinking water. *Journal of Food Research,* **6(4*):*** 6-16.

Baochuan L., Nanping W., Jianhua W., Shengqing X., Hongtao L., Shijun L. and Rong Z. (2015). In-situ gamma-ray survey of rare-earth tailings dams. A case study in Baotou and Bayan Obo Districts, China. *Journal of Environmental Radioactivity,* **151**: 304-310.

Bekelesi W.C. (2015). Determination of the activity concentration of radon-222 and radon-220 in water and soil samples from Newmont-Akyem Gold mine using Gamma spectrometry. Msc Thesis, University of Ghana.

Bhuvaneshwari R., Selvam A. P, Srimurali S., Padmanaban K. and Rajendran R.B. (2016). Human and ecological risk evaluation of toxic metals in the water and sediment of river Cauvery. *International Journal of Scientific and Research Publications* **6(3)**: 415-421.

Bray F., Ferlay J., Soerjomataram I., Siegel R. L., Torre L. A., and Jemal A. (2020). Global cancer statistics 2018: GLOBOCAN estimates of incidence and mortality worldwide for 36 cancers in 185 countries. CA: *A Cancer Journal for Clinicians,* **68(6):** 394-424.

Cain T. (2017). Nuclear Medicine; https://www.insideradiology.com.au/nuclear-medicine/

Canadian Nuclear Safety Commission, (2020). Fact sheet: Natural background radiation.

Chandrashekara K. and Somashekarappa H. M. (2015). Estimation of radionuclides concentration and average annual committed effective dose due to ingestion for some selected medicinal plants of South India. *Journal of Radiation Research and Applied Sciences,* **9**:68 -77.

Chege M.W. (2014). Modeling radon and thoron exhalation and measurement of total natural radiation exposure in Mrima Hill, Kenya. PhD Thesis, Kenyatta University, Nairobi, Kenya.

Chege M.W., Hashim N. O., Merenga A. S., Meisenberg O. and Tschiersch J. (2015). Estimation of annual effective dose due to radon and thoron concentrations in mud dwellings of Mrima Hill, Kenya. *Radiation Protection Dosimetry,* **167:** 1-3.

Chege M. W., Rathore I. V. S., Chhabra S. C. and Mustapha, A. O., 2009. The Influence of meteorological parameters on indoor radon in selected traditional Kenyan dwellings. *Journal of Radiological Protection,* **29**: 95-103.

Chen J., Lauren B., Renato F. and Jeff W. (2014). Results of simultaneous radon and thoron Measurements in 33 metropolitan areas of Canada. Health Canada, Radiation Protection Bureau, Ottawa, Canada. *Radiation Protection Dosimetry,* **163(2):**210–216.

Cheruiyot L. (2014). Natural radioactivity hazards of building bricks fabricated from clay soil of Bomet District, Bomet County, Kenya. Msc Thesis, Physics Department, Kenyatta University, Nairobi, Kenya.

Czarnek K., Terpiłowska S., and Siwicki A. K. (2016). Selected aspects of the action of cobalt ions in the human body. *Central-European Journal of immunology,* **40(2):** 236–242.

Degu B. G., and Alemu Y. (2021). General overview of radon studies in health hazard perspectives. *Journal of oncology, 2021*, 6659795. https://doi.org/10.1155/2021/6659795

Dhobi S. H., Rangrej J. and Verma S. K. (2020). Energy and nucleus field are two parameter to detemine particles, created in pair production phenomena. *International Journal of Multisiciplinary Sciences and Advanced Technology,* **1(1):** 20-24.

Dilebo W. B., Anchiso M.D., Kidane T. T. and Ayalew M. E. (2023). Assessment of selected heavy metals concentration level of drinking water in Gazer town and selected Kebele, South Ari District, Southern Ethiopia. *International Journal of Analytical Chemistry,* **2023:** 1-12.

Echessa A. C. P. (2020). Biomass-based fertilizer formulation using chemically decomposed agricultural wastes and evaluation of its efficacy in growing maize. PhD Thesis, Kenyatta University, Nairobi, Kenya.

Environmental Protection Agency (EPA, 2017). Radiation protection: Health effects. https://www.epa.gov/radiation/radiation-health-effects

Faanu A., Adukpo O. K., Larbi T. L., Lawluvi H., Kpeglo D. O., Darko E. O., Reynolds G. E., Awudu R. A., Kansaana C., Amoah P. A., Efa A. O., Ibrahim A. D., Agyeman B., Kpodzro R. and Agyeman L. (2016). Natural radioactivity levels in soils, rocks, and water at a mining concession of Perseus gold mine and surrounding towns in Central Region of Ghana. S*pringer Plus*, **5**:98.

Fiorentini, D., Cappadone, C., Farruggia, G., and Prata, C. (2021). Magnesium: Biochemistry, nutrition, detection, and social impact of diseases linked to its deficiency. *Nutrients, 13*(4), 1136. https://doi.org/10.3390/nu13041136

Gagnon, K. B., and Delpire, E. (2021). Sodium transporters in human health and disease. *Frontiers in physiology*, ***11*****:** 1-18.

Garba N. N., Rabi'u N., Aliyu A. S., Kankara U. M., Vatsa A.M., Isma'ila A., and Bello S. (2023). Evaluation of radiological risk associated with local building materials commonly used in Northwestern Nigeria. *Heliyon* **9:** 1-7.

Gavong L. C., Wapwera J. A., Kutshak P. I and Ede R. R. (2019). Speciation study of cadmium and zinc in water and soil samples obtained at the vicinity of Abbatoir, Bukuru and Busa-Buji dumpsites in Jos Metropolis. *International Journal of Research and Innovation in Applied Science,* **4(7):** 2454-6194.

Ghiassi N., M., Mortazavi, S. M., Cameron, J. R., Niroomand-rad, A., and Karam, P. A. (2002). Very high background radiation areas of Ramsar, Iran: Preliminary biological studies. *Health physics*, **82(1),** 87–93.

Hakmana W.S. S. (2007). Development of cosmic ray simulation program - earth cosmic ray shower (ecrs) Department of Physics and Astronomy Dissertations, Georgia State University.

Hashim A. K., Hmood A. N., Ashoor N. I. and Hammood M.N. (2020). Radiation hazards due to radon in the air of buildings surrounding imam hussain holy shrine in Karbala, Iraq. *IOP Conference Series: Materials Science and Engineering*, **928**:072152.

Hashim, N. O. (2001). The levels of radionuclides and elements in selected Kenyan coastal ecosystem. M.Sc. Thesis, Kenyatta University, Nairobi, Kenya.

Hashim N.O., Rathore I.V.S., Kinyua A.M. and Mustapha A.O. (2004). Natural and artificial radioactivity levels in sediments along the Kenyan coast. *Radiation Physics and Chemistry*, **71(3-4):**805-806.

Hassan H. B. (2023). Radiological impact assessment of te-norm generating from combustion of fuel in thermal power plant using RESRAD model. *Arab Journal of Nuclear Sciences and Applications*, **56(1):** 126-132.

Hendry J.H, Simon S.L., Wojcik A., Sohrabi M., Burkart W., Cardis E., Tirmarche M and Hayata I. (2014). Human exposure to high natural background radiation: what can it teach us about radiation risks?. *Journal of Radiological Protection*, **29(0):** A29-A42.

Hosoda, M., Kudo, H., Iwaoka, K., Yamada, R., Suzuki, T., Tamakuma, Y. and Tokonami S. (2017). Characteristic of thoron (^{220} Rn) in environment. *Applied. Radiation and Isotopes.***120**; 7–10.

Ibrahim M.S., Atta E., and Zakaria Kh.M. (2014). Assessment of natural radioactivity of some quarries raw materials in El-Minya Governorate, Egypt. *Arab Journal of Nuclear Science and Applications*, **47(1),** 208-216.

ICRP (2007). ICRP Recommendations By Streffer, C. *Radiation Protection Dosimetry*, **127(1-4):** 2-7.

International Atomic Energy Agency. (2003). Radiation oncology physics: A handbook for teachers and students (Ed. Podgorsak, E. B.). IAEA: Vienna.

Isinkaye M.O. and Emelue H.U. (2015). Natural radioactivity measurements and evaluation of radiological hazards in sediment of Oguta Lake, South East Nigeria. *Journal of Radiation Research and Applied science*, **8**: 459-469.

Islam S., Hassan K., Bhuiyan D. I and Sajeeb M. I. (2023). Heavy metal contamination in surface water and sediment of the Meghna River ecosystem. *International Journal of Advanced Research in Biological Sciences*, **10(4):** 22-45.

ISO, International Organization for Standardization, 2014. Measurement of radioactivity in the environment - air - radon 220: integrated measurement methods for the determination of the average activity concentration using passive solid-state nuclear track detectors. (ISO16641).

Jadaa W. and Mohammed H. (2023). Heavy Metals – Definition, natural and anthropogenic sources of releasing into ecosystems, toxicity, and removal methods – An overview study. *Journal of Ecological Engineering*, **24(6):** 249–271.

Jaishankar, M., Tseten, T., Anbalagan, N., Mathew, B. B., and Beeregowda, K. N. (2014). Toxicity, mechanism and health effects of some heavy metals. *Interdisciplinary toxicology*, ***7*(2),** 60–72. https://doi.org/10.2478/intox-2014-0009

Janik M., Tokonami S., Kranrod C., Sorimachi A., Ishikawa T., Hosoda M., James Mclaughlin J., Chang B. and Kim Y.J. (2013). Comparative analysis of radon, thoron, and thoron progeny concentration measurements. *Journal of Radiation Research*, **54**: 597–610.

Jazzar M.M. and Thabaynehm K. M. (2014). Transfer of natural radionuclides from soil to plants and grass in the western north of West Bank environment-Palestine. *International Journal of Environmental Monitoring and Analysis*, **2(5):** 252-258.

Jibiri N.N. and Biere P.E. (2011). Activity concentrations of ^{232}Th, ^{226}Ra and ^{40}K and gamma radiation absorbed dose rate levels in farm soil for the production of different brands of cigarette tobacco smoked in Nigeria. *Iran Journal of Radiation Research*, **8 (4):** 201-206.

Jibiri N.N., Farai I. P. and Alausa S. K. (2007). Activity concentrations of ^{226}Ra, ^{228}Th, and ^{40}K in different food crops from a high background radiation area in Bitsichi, Jos Plateau, Nigeria. *Radiation and Environmental Biophysics*, 46(1):53-59. doi:10.1007/s00411-006-0085-9

Kamboj S., Gnanapragasam E and Yu C. (2018). User's guide for RESRAD-ONSITE Code Version 7.2; Environmental Assessment Division Argonne National Laboratory, United States Department of Energy.

Kamita M., Bird P., Akinyi B., Kamau R. W., Carter R., Muma S., Adam M., Makori T., Figueroa J. D. and Makokhaa F. (2023). Cancer referrals at African Inland Church Kijabe Hospital, Kiambu County (2014–2020) and the impact of COVID-19. *International Health*, **15**: 547–556.

Kamita M., Mweni S., Nzioka A., Figueroa J. D. and Francis Makokha F. (2020). Analysis of cancer diagnoses from 2015-2019 within Machakos County, Kenya, support establishment of Cancer Centre in 2019 likely changing referral patterns [version 1; peer review: 1 approved]. *Welcome open Research,* **5(290):** 1-10.

Kamunda C., Mathuthu M. and Madhuku M., (2016). An assessment of radiological hazards from gold mine tailings in the Province of Gauteng in South Africa. *International Journal of Environmental Research and Public Health,* **13:**570.

Kebaso G. (2023, February 3). Why cancer has become major crises for Kenyans. *People Daily.* https://www.pd.co.ke/news/why-cancer-has-become-major-crisis-for-kenyans-167949/

Kebwaro M. J., (2009). Gamma ray spectrometric analysis of surface soils around Mrima Hill, Kenya, using NaI (Tl) detector and decomposition technique. M.Sc Thesis**,** Kenyatta University, Nairobi, Kenya.

Kebwaro M. J., Rathore I. V. S., Hashim N. O and Mustapha A.O. (2011). Radiometric assessment of natural radioactivity levels around Mrima Hill, Kenya. *International Journal of the Physical Sciences.* **6(13):** 3105-3110.

Khan A. (2023). Hypocalcemia (Cacium deficiency disease): healthline. https://www.healthline.com/health/calcium-deficiency-disease

Kinyua R., Atambo V. O. and Ongeri R. M. (2011). Activity concentration of K-40, Th-232 and Ra-226 and Radiation exposure levels in the Tabaka soapstone quarries of the Kisii Region, Kenya. *African Journal of Environmental Science and Technology,* **5(9):** 682-688.

Kiplang'at E. (2016). Radioactivity concentrations and dose assessment for soil samples from wheat plantation areas of Narok County, Kenya. M.Sc thesis, Kenyatta University, Nairobi, Kenya.

Kipng'eno R. C. (2022). Effects of human exposure and associated risks due to natural radioactivity and heavy metals in Bureti, Kericho County, Kenya. PhD thesis, Kenyatta University, Nairobi Kenya.

Klaus-J A. (2010). Definition of "Heavy Metals" and their role in biological systems. *Acta Physiol Plant,* **32**:615-619.

Koki I.B., Bayero A.S., Umar A. and Yusuf S. (2015). Health risk assessment of heavy metals in water, air, soil and fish. *African Journal of Pure and Applied Chemistry,* **9(11):** 204-210.

Konchakova N. V., Ushakova N. S. and Aikina T.Y. (2016). Ecological risk assessment of tomsk region groundwater used for drinking purposes. IOP Conference Series: *Earth and Environmental Sciences,* **33**: 1-5.

Kudo H., Tokonami S., Omori Y., Ishikawa T., Iwaoka K., Sahoo S. K., Akata N., Hosoda M., Wanabongse P., Pornnumpa C., Sun Q., Li X. and Akiba S. (2015). Comparative dosimetry for radon and thoron in high background radiation areas in China. *Radiation Protection Dosimetry,* **167:**155–159.

Kumar A., Sharma S., Mehra R. and Mishra R. (2018). Assessment of Indoor radon, thoron concentrations and their relationship with seasonal variation and geology of Udhampur District, Jammu and Kashmir, India. *International Journal of Occupational and Environmental Health,* **23(2):** 1-13.

Kumar S and Trivedi A.V. (2016). A review on role of nickel in the biological system. *International Journal of Current Microbiology and Applied Science,* **5 (3):** 719-727.

Kumar S, Diksha, Sindhu S. S. and Kumar R. (2022). Biofertilizers: An ecofriendly technology for nutrient recycling and environmental sustainability. *Current Research in Microbial Sciences,* **(3):** 1-26.

Lee J., Kim H., Kye Y. U, Lee D. Y., Jo W. S., Lee C. G., Kim J. K., Baek J. H. and Kang Y. R. (2023). Activity concentrations and radiological hazard assessments of 226Ra, 232Th, 40K, and 137Cs in soil samples obtained from the Dongnam Institute of Radiological and Medical Science, Korea. *Nuclear Engineering and Technology,* **55:** 2388-2399.

Lenntech (2016). Heavy metals. https://www.lenntech.com/processes/heavy/heavy-metals/heavy-metals.htm

Lolila F. and Mazunga M. S. (2023). Measurements of natural radioactivity and evaluation of radiation hazard indices in soils around the Manyoni uranium deposit in Tanzania. Journal of Radiation Research and Applied Sciences, **16(100524):** 1-9.

Lorenzo R. W., Dios J. M. B. and Ravina A. R. (2017). Radon and stomach cancer. *International Journal of Epidemiology*, **46(2):** 767-768.

MacDonald R. S. (2000). The role of zinc in growth and cell proliferation. *The Journal of Nutrition*, **130(5):** 1500S-1508S.

Mc Laughlin J., Murray M., Currivan L., Pollard D., Smith V., Tokonami S., Sorimachi A. and Janik M. (2011). Long-term measurements of thoron, its airborne progeny, and radon in 205 dwellings in Ireland. *Radiation Protection Dosimetry,***145**: 189-193.

Mahuvana C. 2016. Monte Carlo evaluation of the dose perturbation effect of various hip prostheses during pelvic megavoltage photon radiotherapy. M. Med. Sc Thesis, University of the Free State, South Africa.

Maigari A. U., Ekanem E. O., Garba I. H., Harami A. and Akan J. C., (2016). Health risk assessment for exposure to some selected heavy metals via drinking water from Dadinkowa dam and river Gombe Abba in Gombe State, Northeast Nigeria. *World Journal of Analytical Chemistry,*.**4(1):**1-5.

Maina, D.M., Kinyua, A.M., Nderitu, S.K., Agola J.O and Mangala M.J. Indoor radon (^{222}Rn) levels in Coastal and Rift Valley regions of Kenya., (2002). International conference on occupational radiation protection: Protecting workers against exposure to ionizing radiation, Geneva, Switzerland. 26-30 August (400-405). IAEA-CN-91.

Marcia L. (2016). Radon dangers. The grove Examiner; https://www.sprucegroveexaminer.com/2016/02/05/radon-dangers

Mathuthu M. and Olobatoke R. (2016). Assessment of heavy Metals and Radionuclide Concentrations in Mafikeng waste water treatment plant. *Journal of Water Resource and Protection,* **8:** 93-99.

Mathuthu M., Kamunda C. and Madhuku M. (2016). Modelling of radiological health risk from gold mine tailings in Wonderfonte in spruit Catchment Area, South Africa. *International Journal of Environmental Research and Public Health*, **13(6):**570.

Maurya P. K. and Malik D. S. (2016). Distribution of heavy metals in water, sediments and fish tissue (Heteropneustis fossilis) in Kali River of western U.P. India. *International Journal of Fisheries and Aquatic Studies,* **4(2):** 208-215.

Mehta V., Singh S. P., Hauhan R. P., and Mudahar G. S. (2014). Measurement of indoor radon, thoron and their progeny levels in dwellings of Ambala District, Haryana, Northern india using solid state nuclear track detectors. *Rom. Journal of Physics-Bucharest,* **59:**834-845.

Merril E. 1997. Environmental radioactivity; from natural, industrial and military sources.3rd edition. *New York Medical Centre; Institute of Environmental Medicine, New York Academic Press.*

Miyaoka A. (2011). Decay of radioactivity. https://depts.washington.edu/imreslab/2011%20Lectures/radioactive_decay_2011_4slidesperpage.pdf

MOH. (2019). Kenya cancer policy 2019-2030. https://www.health.go.ke/wp-content/ uploads/2020/07/Kenya-Cancer-Policy-2020.pdf

Mohammadi A. S., Zarei A., Majidi S., Ghaderpoury A., Hashempour Y., Saghi M. H., Alinejad A., Yousef M., Hosseingholizade N. and Ghaderpoori M. (2019). Carcinogenic and non-carcinogenic health risk assessment of heavy metals in drinking water of Khorramabad, Iran. *Elsevier: MethodsX*, **6:** 1642-1651.

Mohammed A., Seid K. and Woldegbreal B. (2023). Heavy metals accumulation in water and human health risk assessment via the consumption of Labeobarbus intermedius samples from Borkena river, Ethiopia. *The Scientific World Journal,* **2023**: 1-10

Mohammed S. A., Mohamad S. J., Norlaili A. K. and Nisar A. (2015). Distribution of ^{226}Ra, ^{232}Th, and ^{40}K in rice plant components and physico-chemical effects of soil on their transportation to grains. *Journal of Radiation Research and Applied Sciences,* **8**:300-310.

Motari M.K. (2018). Simulation of cosmic ray muon charge ratio at energies up to 10 TeV Using EPOS LHC . PhD *Thesis, Kenyatta University,* Nairobi, Kenya.

Mugaiga A., Jurua E., Oriada R. and Turyahabwa S. (2016). Radioactivity levels and dose rates from rocks in selected mining areas and quarries in Eastern Uganda. *International Journal of Research in Engineering and Technology***, 05**: 2319-1163.

Munene E. M., Hashim N. O. and Ambusso W. N. (2023). Human health risk assessment of heavy metal concentration in surface water of Sosian river, Eldoret town, Uasin-Gishu County Kenya. *Journal of Agriculture Science* and *Technology,* **11(102298):** 1-8.

Musamali E.W (2016). Assessment of human exposure to natural source of radiation on the soil in Tongaren constituency of Bungoma county, Kenya., M.Sc Thesis, Kenyatta University, Nairobi, Kenya.

Mustapha, A.O., Patel, J.P and. Rathore, I.V.S., (2002). Preliminary report on radon concentration in drinking water and indoor air in Kenya. Environ. *Geochemistry-Health,* **24:**387-396.

Mwalongo D. A,·Haneklaus N. H., Carvalho F. P., Lisuma J. B., Kivevele T. T. and Mtei K. M. (2023). Infuence of phosphate fertilizers on the radioactivity of agricultural soils and tobacco plants in Kenya, Tanzania, and Uganda. *Environmental Science and Pollution Research*, **30***:*83004–83023.

Mwangi. (2013). Determination of concentration of selected heavy metals in tilapia fish, sediments and water from Mbagathi and Ruiru Athi River tributaries, Kenya .M.SC Thesis: Applied Analytical Chemistry, Kenyatta University, Nairobi, Kenya.

Nair M.K, Nambi K. S. V., Amma N. S., Gangadharan P., Jayalekshmi P., Sreedharan J. and Varghese C. (2000). Population study in the high natural background radiation area in Kerala, India. *Radiation Research Society,* **152(6):** 145-148.

National Academies of Sciences, Engineering, and Medicine. (2005). Assessment of the scientific information for the radiation exposure screening and education program. Washington, DC: The National Academies Press. https://doi.org/10.17226/11279.

Njinga R. L., Moyo M. N. and Abdulmaliq S. Y. (2013). Analysis of essential elements for plants growth using instrumental neutron activation analysis. *Hindawi Publishing Corporation: International Journal of Agronomy*, **156520:** 1-9.

Nkoulou II J. E. N., Engola L. N., Dallou G. B., Saïdou, Bongue D., Hosoda M., Njock M. G. K. and Tokonami S. (2023). Public exposure to natural radiation and the associated increased risk of lung cancer in the Betare-Oya Gold Mining areas, Eastern Cameroon. *Journal of Radiation Protection and Research*, **2023:** 1-10.

Nwankpa A. C. (2017). Determination of food crops contamination in Osun State, Nigeria due to Radium-226, Thorium-232 and Potassium-40 concentrations in the Environment. *European Journal of Sustainable Development*, **6 (4):** 169-174.

Nyambura C., Tokonami S., Hashim N.O., Chege M.W., Suzuki T., Kudo H. and Hosoda M. (2019). Annual effective dose assessment due to radon and thoron progenies in dwellings of Kilimambogo, Kenya. *Radiation Protection Dosimetry*,**184(3-4):**430-434.

Odongo W. O. G., Chege M., Hashim N., Tokonami S., Chutima K. and Rotich C. (2021). Determination of activity concentration of natural radionuclides and radiation hazards' assessment of building materials in high background radiation areas of Homa and Ruri, Kenya. *The Scientific World Journal*, **2021**: 1-7.

Okedeyi A. S., Gbadebo A.M., Arowolo A.O., Mustapha A.O. and Tchokossa P. (2012). Measurement of gamma –emitting radionuclides in rocks and soils of Saunder quarry site, Abeokuta, Ogun State, Nigeria.*Journal of Applied sciences*, **12 (20)**: 2178-2181.

Olise F.S., Akinnagba D.M and Olasogba O.S (2016). Radionuclides and radon levels in soil and ground water from solid minerals-hosted area, southwestern Nigeria. *Cogent Environmental Science*, **2:** 1-12.

Opiyo A.S. (2009). Radioactivity and elemental analysis of carbonatite rocks from parts of Gwasi area, South Western Kenya. M.Sc Thesis, University of Nairobi, Nairobi, Kenya.

Otwoma D. (2012). An Investigation of the Radioecology of the Carbonatite deposits in the Homa Mountain region in South Nyanza, Kenya. PhD Thesis, University of Nairobi, Nairobi, Kenya.

Otwoma D., Patel, J., Bartilol, S. and Mustapha A. (2012). Estimation of annual effective dose and radiation hazard due to natural radionuclides in mount Homa, southwestern Kenya. Radiation protection Dosimetry Advances Access. Oxford University Press. Pp 1-8.

Pawel D.J. and Puskin J.S. (2004). The U.S. Environmental Protection Agency's assessment of the risks for indoor radon. *Health Physics,* **87**:68-74.

Pentreath, R. (2021). Stable and unstable atoms. In *Radioecology: Sources and Consequences of Ionising Radiation in the Environment* (Cambridge Environmental Chemistry Series, pp. 32-68). Cambridge: Cambridge University Press. doi:10.1017/9781316156124.003

Ramola R. C., Mukesh P., Tushar K., Preeti P., Bossew P., Rosaline M. and Tokonami S. (2016). Dose estimation derived from the exposure to radon, thoron and their progeny in the indoor environment. *Scientific reports,* **6:**31061.

Ramola R.C., Prasad G., Gusain G.S., Rautela B.S., Choubey V.M., Sagar D.V., Tokonami S., Sorimachi A., Sahoo S.K., Janik M. and Ishikawa T. (2010). Preliminary indoor thoron measurements in high radiation background area of Southeastern coastal Orissa, India. *Radiation Protection Dosimety*, **141**: 379-382.

Ravina A. R., Aragones N., Kelsey K. T., Rios M. P., Lamas M. P., Abente G. L., and Dios J. M. B. (2017). Residential radon exposure and brain cancer: an ecological study in a radon prone area (Galicia, Spain). *Scientific Reports,* **7 (3595):** 1-7

Reddy A., Conde C., Peterson C. and Nugent K. (2022). Residential radon exposure and cancer. *Oncology Reviews,* **16(558):** 1-9.

Republic of Kenya. (2023). The National Cancer Control Strategy (2023–2027). Pp 2.

Ruto P.K., Muitta E., Owino A. and Makokha F. W. (2020). Frequency and pattern of all cancer cases at Thika Level Five Hospital in Kiambu County, Kenya. *International Research Journal of Oncology,* **3(4):** 1-9.

Saïdou, Tokonami S., Janik M., Samuel, B. G. Abdourahimi and Joseph E. N. N. (2015). Radon-thoron discriminative measurements in the high natural radiation areas of Southwestern Cameroon. *Journal of environmental radioactivity,**150***: 242–246.

Senthilkumar G., Raghu Y., Sivakumar S., Chandrasekaran A., Prem A. D. and Ravisankar R., (2014). Natural radioactivity measurement and evaluation of radiological hazards in some commercial flooring materials used in Thiruvannamalai, Tamilnadu, India. *Journal of Radiation Research and Applied sciences,* **7**:116-122.

Singh P., Singh S, Sahoo B.K., Sapra B.K. and Bajwa B.S. (2015). A study of indoor radon, thoron and their progeny in Tosham region Haryana, India. *Journal of radiation research and applied sciences,* **8:**226-233.

Solehah A. R., Yasir M. S. and Samat S. B. (2016). Activity concentration, transfer factors and resultant radiological risk of ^{226}Ra, ^{232}Th, and ^{40}K in soil and some vegetables consumed in Selangor, Malaysia Conference Paper. DOI: 10.1063/1.4966802

Suman G., Reddy K. V. K., Reddy S., Reddy C.G. and Reddy P. Y. (2021). Radon and thoron levels in the dwellings of Buddonithanda: a village in the environs of proposed uranium mining site, Nalgonda district, Telangana State, India. *Scientific reports: Nature Portfolio*, **11:** 6199.

Tchounwou P.B., Yedjou C. G., Patlolla A. K. and Sutton D.J. (2012). Heavy metals toxicity and the environment. *National Institutes of Health*.**101:**133-164.

Tokonami S. (2020). Characteristics of Thoron (220Rn) and its progeny in the indoor environment. *International Journal of Environment Research and Public Health, **17**: 1-9.*

Tokonami S., Sun Q., Akiba S., Zhuo W., Furukawa M., Ishikawa T., Hou C., Zhang S., Narazaki Y., Ohji B., Yonehara H. and Yamada Y. (2004). Radon and thoron exposures for cave residents in Shanxi and Shaanxi Provinces. *Radiation Research,* **162:**390-396.

Tokonami S., Takahashi H., Kobayashi Y. and Zhuo W. (2005). Up-to-date radon – thoron discriminative detector for a large-scale survey. *Review of scientific instruments,* **76**: 113505.

UNSCEAR, (2000). Sources and effects of ionizing radiation; United Nation Scientific Committee on the effects of atomic radiation Annex A.B. New York.

UNSCEAR, (2008). United Nations Scientific Committee on the Effects of Atomic Radiation. Sources and Effects of Ionizing Radiation. UNSCEAR 2008 Report to the General Assembly, with Scientific Annexes, (I): New York: United Nations, 2008.

UNSCEAR, (2019). United Nations Scientific Committee on the Effects of Atomic Radiation UNSCEAR 2019 Report to the General Assembly, with Scientific Annexes: New York: United Nations, 2020.

USEPA, (2011). A Citizen's guide to radon: The guide to protecting yourself and your family from radon. United States Environmental Agency, USA.

USNRC (2011): Reactor concepts manual: Biological effects of radiation. United States Nuclear Regulatory Commission Technical Training Centre, **0606:** 1-23.

Veiga R., Sanchesa N., AnjosaR.M, Macarioa K., Bastosa J., Iguatemya M., Aguiarb J.G., Santosb A.M.A., Mosqueraa B., Carvalhoa C., Baptista F. M. and Umisedoc N.K. (2006). Measurement of natural radioactivity in Brazilian beach sands. Radiation Measurements, **41**:189–196.

Veniamakis E., Kaplanis G., Voulgaris P. and Nikolaidis P. T. (2022). Effects of sodium intake on health and performance in endurance and ultra-endurance sports. *International Journal of Environmental Research and Public Health*, ***19*(6):** 1-19.

Wanjala F. O. (2021). Human Exposure and associated risks due to natural radioactivity and heavy metals in Ortum, West Pokot County, Kenya. PhD Thesis, Kenyatta University, Nairobi, Kenya.

Wanjala, F. O., Hashim N O, Otwoma D., Nyambura C, Kebwaro J., Mauring A., Bartilol J. and Chege M. (2019). Human exposure to background radiation in Ortum, Kenya. *Radiation Protection Dosimetry*. ncz264, https://doi.org/10.1093/rpd/ncz264

Wanjala, F.O., Hashim, N.O., Otwoma, D. Nyambura, C., Kebwaro, J., Ndege, M. and Bartilol, S. (2020). Environmental assessment of heavy metal pollutants in soils and water from Ortum, Kenya. *Environmental Monitoring Assessment,* **192:**118.

World Health Organization. (2009). WHO handbook on indoor radon: a public health perspective.

World Health Organization (2011). Guidelines for drinking-water quality. WHO chronicle by Edition, F **38(4),** 104-108.

World Health Organization (WHO), (2016). Ionizing radiation, health effects and protective measures. https://www.who.int/news-room/fact-sheets/detail/ionizingradiation-health-effects-and-protective-measures.

Yamada Y., Sun Q., Tokonami S., Akiba S., Zhuo W., Hou C., Zhang S., Ishikawa T., Furukawa M., Fukutsu K. and Yonehara H. (2006). Radon-thoron discriminative measurements in Gansu Province, China, and their implication for dose estimates. *Journal of Toxicology and environmental Health,* **69**:723-734.

Yu C. (2012). RESRAD family of codes — A suite of tools for environmental radiological dose assessment. Environmental assessment division Argonne National Laboratory, United States Department of Energy. *Environmental Radiological Assistance Directory Web Conference.*

Yu C., A. Zielen A.J., Cheng J.J., LePoire D.J., Gnanapragasam E., Kamboj S., Arnish J., Wallo A., Williams W.A. and Paterson H. (2001) User's manual for RESRAD Version 6, Environmental assessment Division Argonne National Laboratory, United States Department of Energy.

Ziajahromi S., Khanizadeh M and Nejadkoorki F. (2013). Total effective dose equivalent assessment after exposure to high-level natural radiation using the RESRAD code. *Environmental Monitoring and Assessment,* **186 (3):** 1907-1915.

Ziajahromi S., Khanizadeh M. and Nejadkoorki F. (2015). Using the RESRAD code to assess human exposure risk to ^{226}Ra, ^{232}Th, and ^{40}K in soil. *Human and Ecological Risk Assessment: An International Journal,* **21(1):** 250-264.

Zhou Q., Yang N., Ren B., Ding X., Bian H. and Yao X. (2020). Total concentrations and sources of heavy metal pollution in global river and lake water bodies from 1972 to 2017. *Global Ecology and Conservation,* **22**: 1-11.

Zoomie, 2015. How do sodium iodide (scintillation detectors work? Radiation Safety and Healthy Physics Blog. (https://www.ntanet.net/how-do-sodium-iodide-scintillation-detectors-work)

APPENDICES

Appendix 1: Uranium decay series

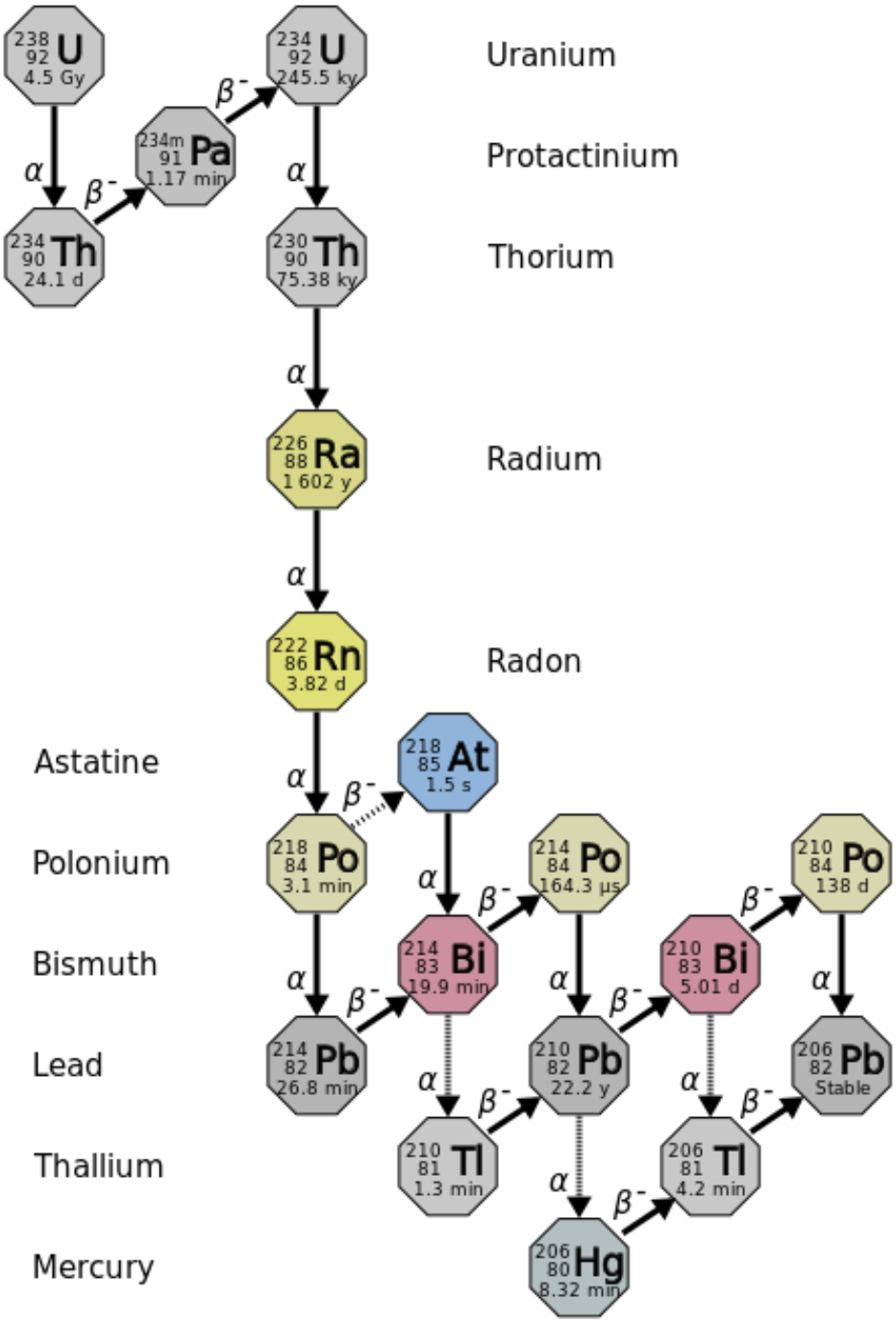

Appendix 2: Actinium decay series

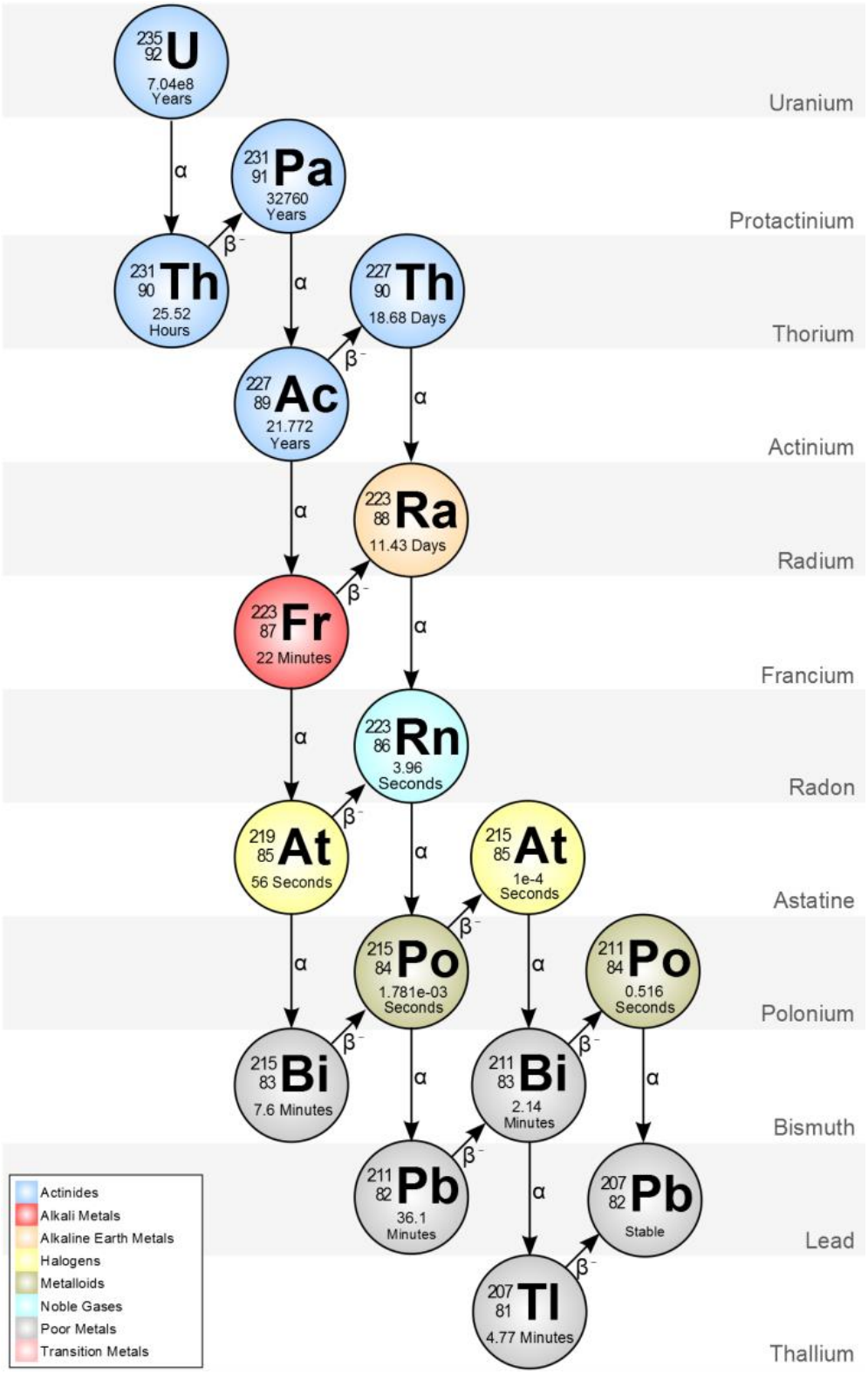

Appendix 3: Thorium decay series

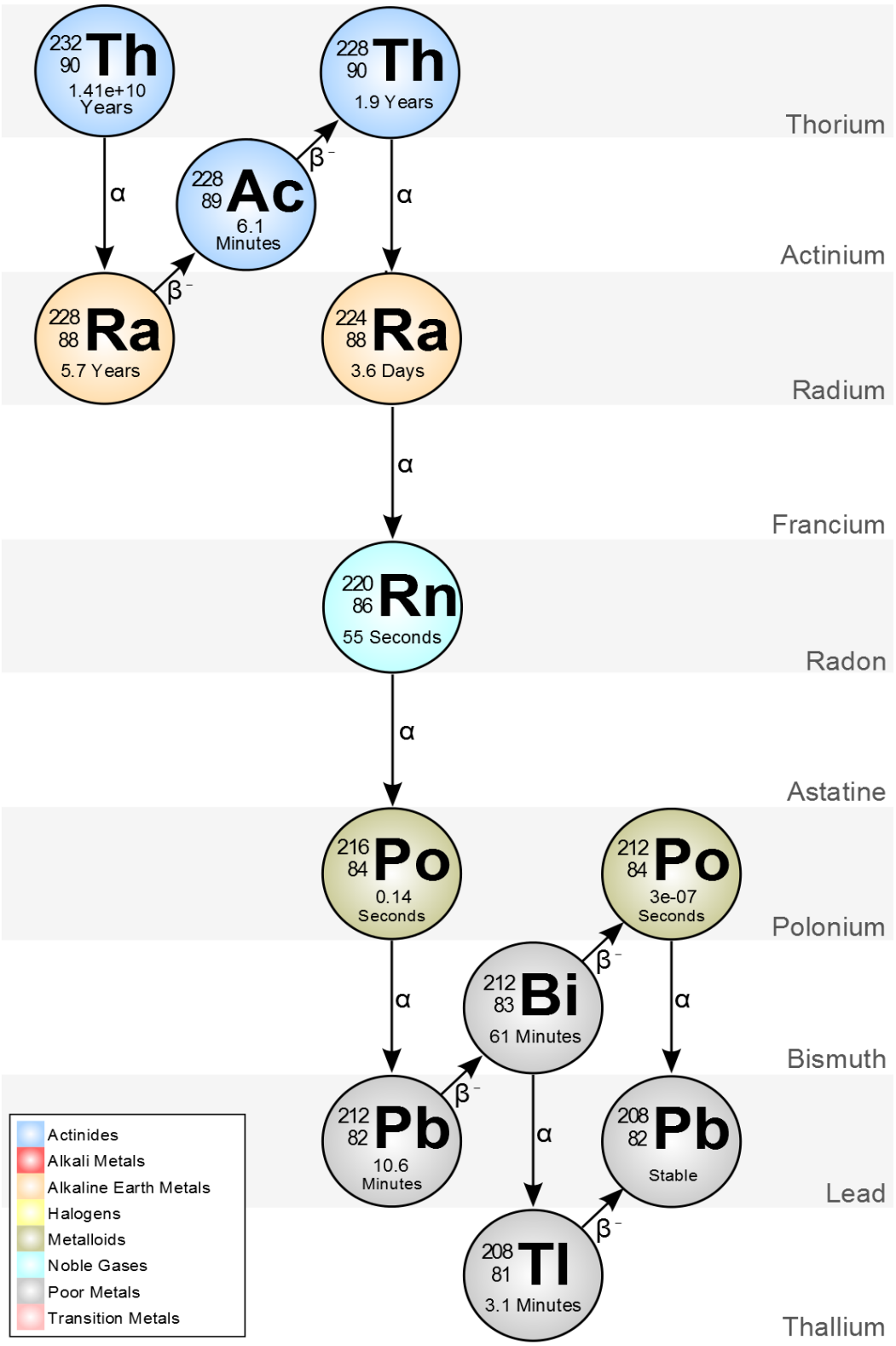

Appendix 4: Neptunium decay series

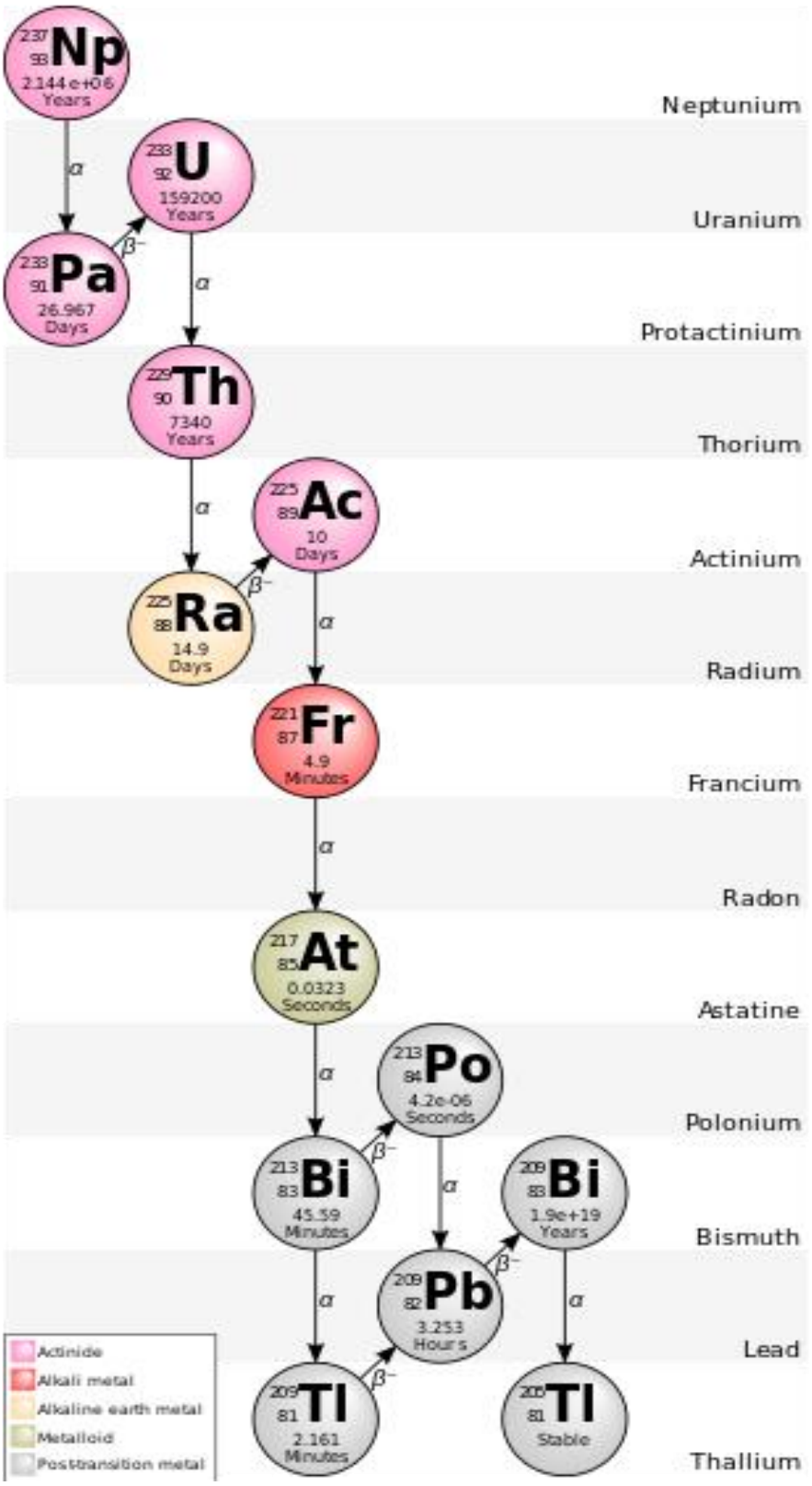

Appendix 5: IAEA reference materials

(a) IAEA RGU -1

IAEA-RGU-1 , Uranium Ore

Inorganic , Ores

- Unit Size: 500g
- Price per Unit: 60 EUR
- Report: IAEA/RL/148
- Date of Release: 1987-01-01

Both, IAEA-RGU-1 and IAEA-RGTh-1 reference materials were prepared on behalf of the International Atomic Energy Agency by the Canada Centre for Mineral and Energy Technology by dilution of a uranium ore BL-5 (7.09% U) and a thorium ore OKA-2 (2.89% Th, 219 µg U/g) with floated silica powder of similar grain size distribution, respectively. No evidence for between-bottles inhomogeneity was detected after mixing and bottling. BL-5 has been certified for uranium, ^{226}Ra and ^{210}Pb confirming that it is in radioactive equilibrium. The agreement between radiometric and chemical measurements of thorium and uranium in OKA-2 shows both series to be in radioactive equilibrium.

Analyte	Value	Unit	95% C.I.	N	R/I/C
^{232}Th	< 4$^{?}$	Bq/kg	-	None	I
^{235}U	228$^{?}$	Bq/kg	226 - 230	None	R
^{238}U	4940$^{?}$	Bq/kg	4910 - 4970	None	R
^{40}K	< 0.63$^{?}$	Bq/kg	-	None	I
K	< 20	mg/kg	-	None	I
Th	< 1	mg/kg	-	None	I
U	400	mg/kg	398 - 402	None	R

(Value) Concentration calculated as a mean of the accepted laboratory means (N) Number of accepted laboratory means which are used to calculate the recommended or information values and their respective confidence intervals

(R/I/C) Classification assigned to the property value for analyte (Recommended/ Information/ Certified)

(?) Natural Radionuclide activity concentration derived from the elemental concentration on basis of isotopic abundance and half-life data

The values listed above were established on the basis of a gravimetric dilution of materials with known uranium, thorium and potassium composition. The details concerning the criteria for qualification as a recommended or information value can be found in the respective report (attached).

(b) IAEA RGTh

IAEA-RGTh-1 , Thorium Ore

Inorganic , Ores

- Unit Size: 500g
- Price per Unit: 60 EUR
- Report: IAEA/RL/148
- Date of Release: 1987-01-01

Both, IAEA-RGU-1 and IAEA-RGTh-1 reference materials were prepared on behalf of the International Atomic Energy Agency by the Canada Centre for Mineral and Energy Technology by dilution of a uranium ore BL-5 (7.09% U) and a thorium ore OKA-2 (2.89% Th, 219 µg U/g) with floated silica powder of similar grain size distribution, respectively. No evidence for between-bottles inhomogeneity was detected after mixing and bottling. BL-5 has been certified for uranium, ^{226}Ra and ^{210}Pb confirming that it is in radioactive equilibrium. The agreement between radiometric and chemical measurements of thorium and uranium in OKA-2 shows both series to be in radioactive equilibrium.

Analyte	Value	Unit	95% C.I.	N	R/I/C
^{232}Th	3250(?)	Bq/kg	3160 - 3340	155	R
^{235}U	3.6(?)	Bq/kg	3.3 - 3.9	145	R
^{238}U	78(?)	Bq/kg	72 - 84	145	R
^{40}K	6.3(?)	Bq/kg	3.1 - 9.5	45	I
K	200	mg/kg	100 - 300	45	I
Th	800	mg/kg	784 - 816	155	R
U	6.3	mg/kg	5.9 - 6.7	145	R

(Value) Concentration calculated as a mean of the accepted laboratory means (N) Number of accepted laboratory means which are used to calculate the recommended or information values and their respective confidence intervals
(R/I/C) Classification assigned to the property value for analyte (Recommended/ Information/ Certified) (?) Natural Radionuclide activity concentration derived from the elemental concentration on basis of isotopic abundance and half-life data
The values listed above were established on the basis of a gravimetric dilution of materials with known uranium, thorium and potassium composition. The details concerning the criteria for qualification as a recommended or information value can be found in the respective report (attached).

(c) IAEA RGK

IAEA-RGK-1 , Potassium Sulfate

Inorganic , Ores

- Unit Size: 500g
- Price per Unit: 60 EUR
- Report: IAEA/AL/148
- Date of Release: 1987-01-01

The IAEA-RGK-1 material is produced from high purity (99.8%) potassium sulphate supplied by the Merck Company. The potassium property value and its uncertainty were obtained from repeated measurements performed at the IAEA Laboratories Seibersdorf and the results confirmed the value certified by Merck. The upper limits for the uranium and thorium property values were estimated by the IAEA Laboratories Seibersdorf using fluorimetry and activation analysis, respectively.

Analyte	Value	Unit	95% C.I.	N	R/I/C
^{40}K	14000?	Bq/kg	13600 - 14400	20	R
K	448000	mg/kg	445000 - 451000	20	R
Th	< 0.01	mg/kg	-	20	I
U	< 0.001	mg/kg	-	20	I

(Value) Concentration calculated as a mean of the accepted laboratory means (N) Number of accepted laboratory means which are used to calculate the recommended or information values and their respective confidence intervals
(R/I/C) Classification assigned to the property value for analyte (Recommended/ Information/ Certified) (?) Natural Radionuclide activity concentration derived from the elemental concentration on basis of isotopic abundance and half-life data
The values listed above were established on the basis of a gravimetric dilution of materials with known uranium, thorium and potassium composition. The details concerning the criteria for qualification as a recommended or information value can be found in the respective report (attached).

Appendix 6: Calibration curves for heavy metal analysis

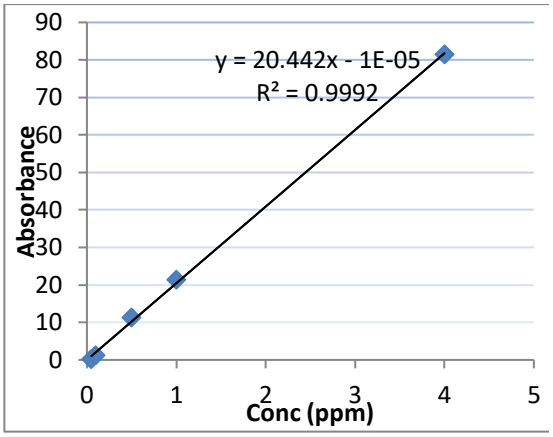

Calibration curve for K analysis

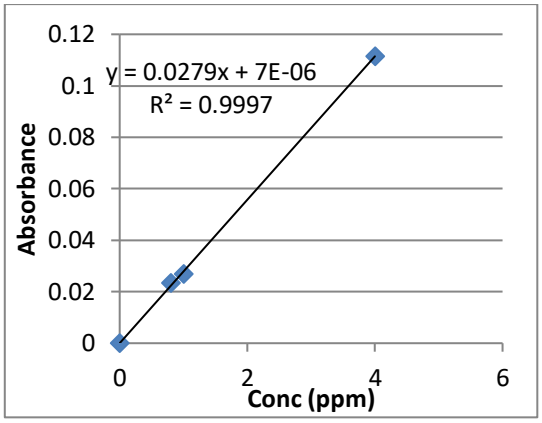

Calibration curve for Ca analysis

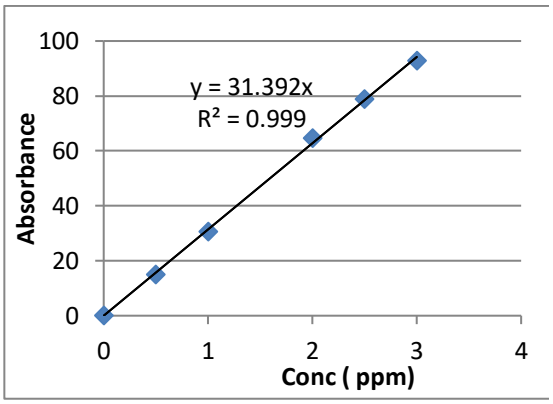

Calibration curve for Na analysis

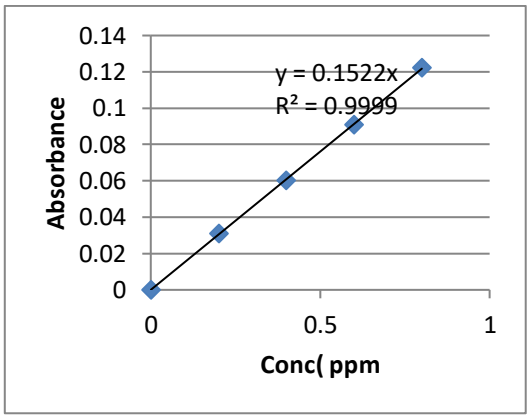

Calibration curve for Fe analysis

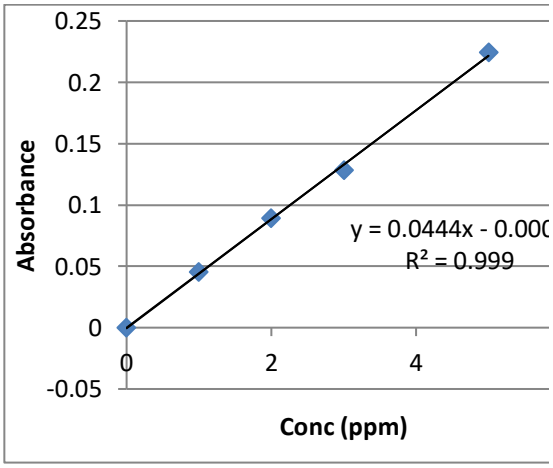

Calibration curve for Cd analysis

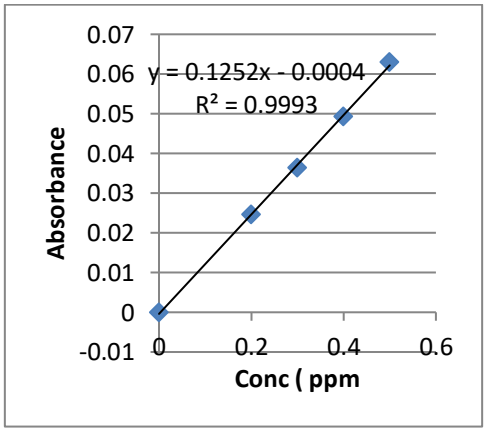

Calibration curve for Mg analysis

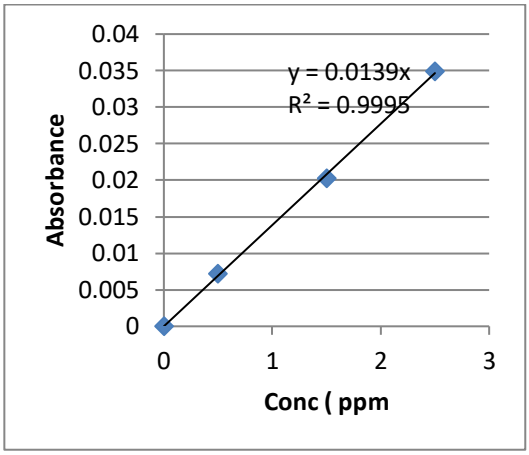

Calibration curve for Cu analysis

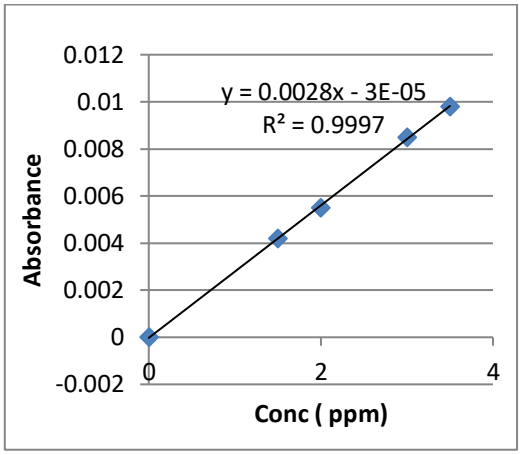

Calibration curve for Pb analysis

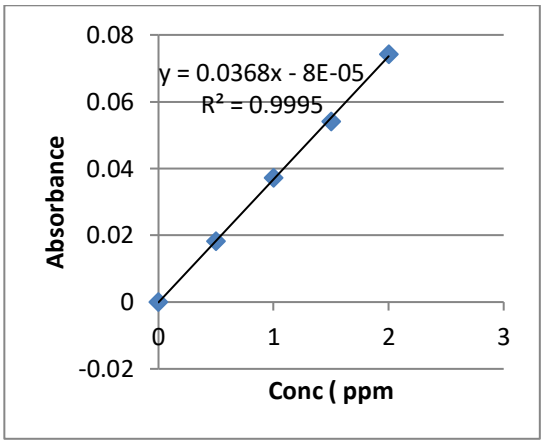

Calibration curve for Mn analysis

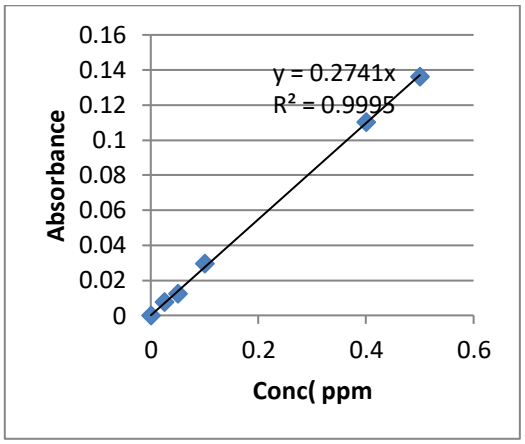

Calibration curve for Zn analysis

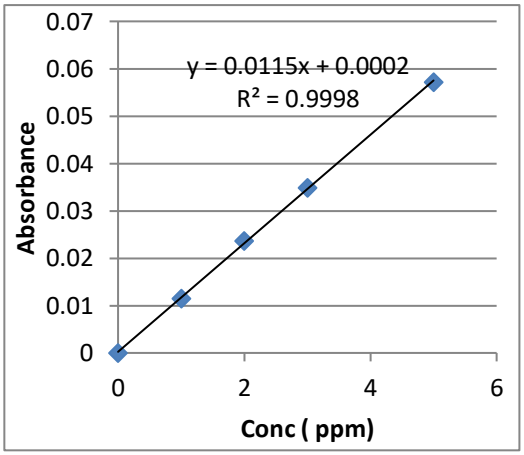

Calibration curve for Ni analysis

Appendix 7: Cancer Cases at Thika level Five Hospital, Kiambu County, Kenya (2013- 2018) (Ruto *et al.*, 2020)

S/No	Type of Cancer	No of Patients	Percentage (%)
1.	Cervix	146	25.44
2.	Breast	88	15.33
3.	Esophagus	88	15.33
4.	Stomach	49	8.54
5.	Prostrate	29	5.05
6.	Liver	26	4.53
7.	Colorectal	22	3.83
8.	Skin	20	3.48
9.	Pancreas	17	2.96
10.	Gall Bladder	10	1.74
11.	Others	79	13.8
	Total	**574**	**100%**

Appendix 8: Cancer Cases at Machakos County Hospitals- 2015-2019 (Kamita *et al.*, 2020)

		Male			Female			Total		
Primary Site	**ICD**	**No. of Cases**	**%**	**Median Age**	**No. of Cases**	**%**	**Median Age**	**No. of Cases**	**%**	**Median Age**
Lip, Oral Cavity and Pharynx	C00-14	12	5.6%	54	6	1.9%	65	18	3.4%	54.5
Oesophagus	C15	52	24.4%	60	20	6.5%	62	72	13.8%	60.5
Stomach	C16	9	4.2%	59	11	3.6%	67	20	3.8%	59
Colon, Rectum and Anus	C18-21	10	4.7%	48	18	5.8%	61.5	28	5.4%	58
Liver	C22	6	2.8%	51	12	3.9%	58.5	18	3.4%	52.5
Pancreas	C25	2	0.9%	69	3	1.0%	57	5	1.0%	57
Larynx	C32	7	3.3%	69	1	0.3%	64	8	1.5%	68
Lung	C33-34	12	5.6%	40	11	3.6%	72	23	4.4%	61
Skin	C44	3	1.4%	67	10	3.2%	52	13	2.5%	54
Breast	C50	4	1.9%	55	62	20.1%	48	66	12.6%	48
Cervix uteri	C53				106	34.3%	53	106	20.3%	53
Ovary	C56				9	2.9%	48	9	1.7%	48
Prostate	C61	43	20.2%	71				43	8.2%	71
Kidney	C64-66	2	0.9%	53	3	1.0%	52	5	1.0%	52
Bladder	C67	4	1.9%	53	1	0.3%	75	5	1.0%	56
Brain and Central Nervous System	C70-72	3	1.4%	38	5	1.6%	58	8	1.5%	55.5
Thyroid	C73				2	0.6%	70	2	0.4%	70
Blood	C91-95	14	6.6%	47.5	13	4.2%	56	27	5.2%	50
Other and Unspecified		30	14.1%	50.5	16	5.2%	52	46	8.8%	51
Total		**213**			**309**			**522**		**58**

Appendix 9: Cancer statistics in Kenya (2020)

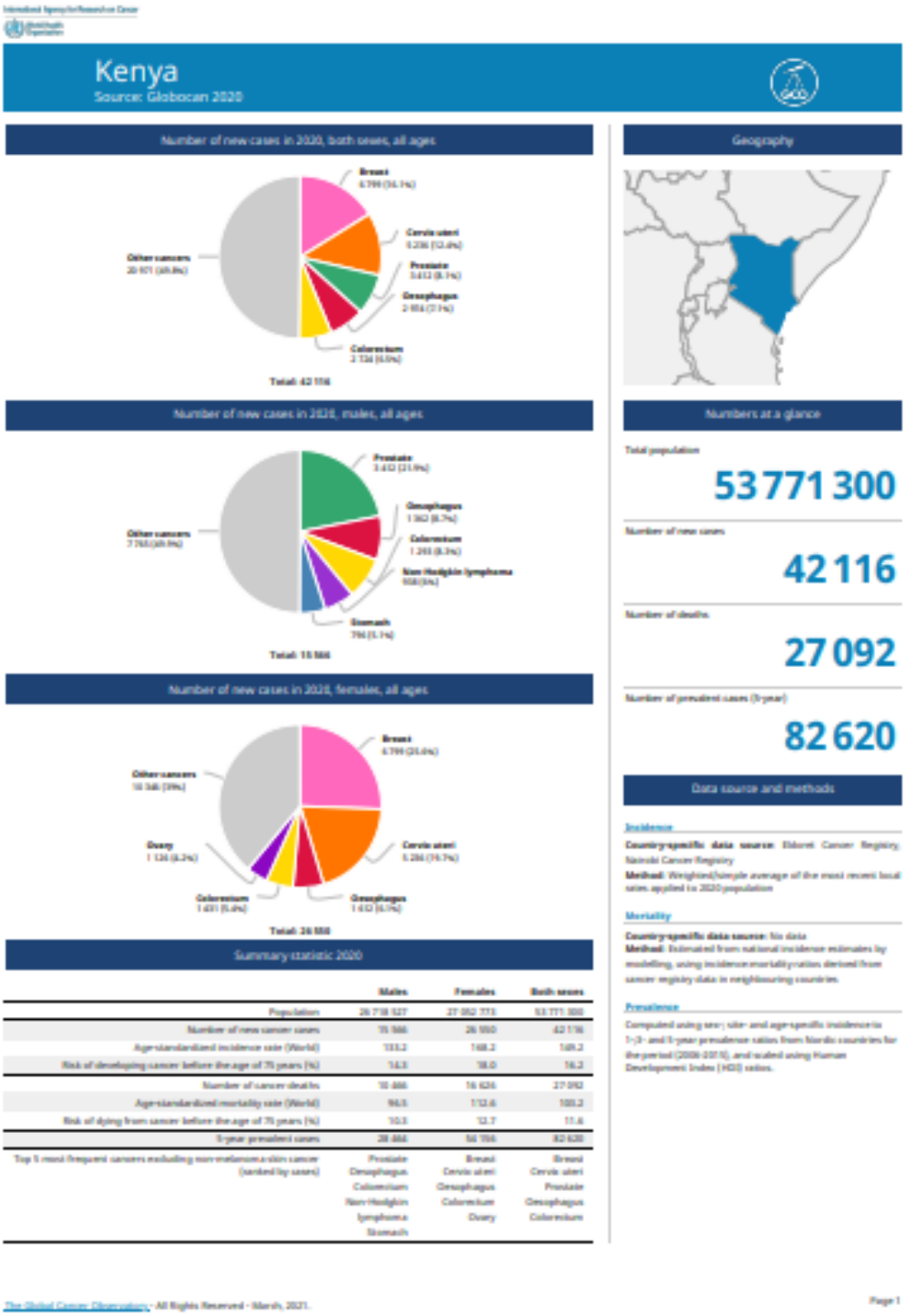

International Agency for Research on Cancer
World Health Organization

Kenya

Source: Globocan 2020

Number of new cases in 2020, both sexes, all ages

Total: 42 116

Number of new cases in 2020, males, all ages

Total: 15 666

Number of new cases in 2020, females, all ages

Total: 26 550

Summary statistic 2020

	Males	Females	Both sexes
Population	26 738 527	27 032 773	53 771 300
Number of new cancer cases	15 666	26 550	42 116
Age-standardized incidence rate (World)	133.2	168.2	149.2
Risk of developing cancer before the age of 75 years (%)	14.3	18.0	16.2
Number of cancer deaths	10 466	16 626	27 092
Age-standardized mortality rate (World)	96.5	112.6	103.2
Risk of dying from cancer before the age of 75 years (%)	10.3	12.7	11.6
5-year prevalent cases	28 464	54 156	82 620
Top 5 most frequent cancers excluding non-melanoma skin cancer (ranked by cases)	Prostate Oesophagus Colorectum Non-Hodgkin lymphoma Stomach	Breast Cervix uteri Oesophagus Colorectum Ovary	Breast Cervix uteri Prostate Oesophagus Colorectum

Geography

Numbers at a glance

Total population
53 771 300

Number of new cases
42 116

Number of deaths
27 092

Number of prevalent cases (5-year)
82 620

Data source and methods

Incidence

Country-specific data source: Eldoret Cancer Registry, Nairobi Cancer Registry

Method: Weighted/simple average of the most recent local rates applied to 2020 population

Mortality

Country-specific data source: No data

Method: Estimated from national incidence estimates by modelling, using incidence-mortality ratios derived from cancer registry data in neighbouring countries

Prevalence

Computed using sex- site- and age-specific incidence in 1-, 3- and 5-year prevalence ratios from Nordic countries for the period (2006-2015), and scaled using Human Development Index (HDI) ratios.

Appendix 10: Research Papers

1. Nyambura C., Hashim N.O., Chege M.W., Tokonami S. and Omonya F.W. (2019). Cancer and non-cancer health risks from carcinogenic heavy metal exposures in underground water from Kilimambogo, Kenya. *Groundwater for Sustainable Development. Elsevier,* **10**: 1-5.https://doi.org/10.1016/j.gsd.2019.100315

2. Nyambura C., Tokonami S., Hashim N.O., Chege M.W., Suzuki T., Kudo H. and Hosoda M. (2019). Annual effective dose assessment due to radon and thoron progenies in dwellings of Kilimambogo, Kenya. *Radiation Protection Dosimetry,***184(3-4):**430-434.https://doi.org/10.1093/rpd/ncz090.

3. Chege M. and Nyambura C., Review of radon and thoron research in Kenya: 1997–2017, *Radiation Protection Dosimetry*, **184(3-4):**479–481. https://doi.org/10.1093/rpd/ncz065

4. Chege M., Hashim N., Nyambura C., Mustapha A., Hosada M. and Tokonami S. (2019). Radon and Thoron; radioactive gases lurking in earthen houses in Rural Kenya. Front. Public Health,**7(113):**1-6.https://doi.org/10.3389/fpubh.2019.00113

5. F O Wanjala, N O Hashim, D Otwoma, C Nyambura, J Kebwaro, A Mauring, J Bartilol, and M Chege (2019). Human exposure to background radiation in Ortum, Kenya, Radiation Protection Dosimetry, ncz264, https://doi.org/10.1093/rpd/ncz264.

6. Wanjala, F. O., Hashim, N. O., Otwoma, D., Nyambura, C., Kebwaro, J., Ndege, M., and Bartilol, S. (2020). Environmental assessment of heavy metal pollutants in soils and water from Ortum, Kenya. Environmental Monitoring and Assessment, 192(2), 118.
7. .Rotich C. K., Hashim N. O., Chege M. W. and Nyambura C. (2020). Measurement of radon activity concentration in underground water of Bureti sub-county of Kericho County Kenya, Radiation Protection Dosimetry, https://doi.org/10.1093/rpd/ncaa193.
8. Rotich C. K., Hashim N. O., Chege M. W. and Nyambura C. (2021). Naturally occurring radionuclides in soil samples of Bureti sub-County oF Kericho County KENYA, Radiation Protection Dosimetry, https://doi.org/10.1093/rpd/ncab006.
9. Odongo W. O. G., Chege M. W., Shinji Tokonami S., Hashim N. O., Kranrod C. and Nyambura C. (2021). Radon and thoron exhalation rates from earthen building materials used in high background radiation areas of Homa and Ruri, Kenya. *Radiation Protection Dosimetry*, 197 (1): 12–18 https://doi.org/10.1093/rpd/ncab156

Appendix 11: Conference presentations

1. C. Nyambura, N. O. Hashim, M. W. Chege, S. Tokonami, 2018, M. Hosoda and F.W. Omonya. Risk Assessment due to Consumption of Natural Radionuclides in Cassava from Kilimambogo, Kenya.The Ninth International Symposium on Naturally Occurring Radioactive Material, on 23-27 September 2019, in Denver, Colorado, USA.

2. C. Nyambura, S. Tokonami, N. O. Hashim, M. W. Chege, T. Suzuki, H. Kudo and M. Hosoda. Annual effective dose assessment due to radon and thoron progenies in dwellings of Kilimambogo, Kenya. Presented at the 9th International Conference on High Level Environmental Radiation Areas (ICHLERA 2018) held from 24th - 27th September, 2018 at Hirosaki University, Aomori, Japan.

3. C. Nyambura, N. O. Hashim, M. W. Chege and S. Tokonami, 2018. *Effective dose equivalent due to radiation exposure from rocks in Kilimambogo, Kenya*. Presented at the 1st International Annual Conference on Attaining Self Reliance Through Research, Innovation and Technology held between 21st and 23rd March 2018 at The Meru National Polytechnic, Kenya.

4. C. Nyambura, N. O. Hashim, M. W. Chege and S. Tokonami, 2018. *Radioactivity and Risk Assessment of Soil Samples from Kilimambogo, Kenya.* Presented at the 10th hope meeting held on 10th to 16th March, 2018 in Yokohama Japan.

Appendix 12: Research Permit (NACOSTI)

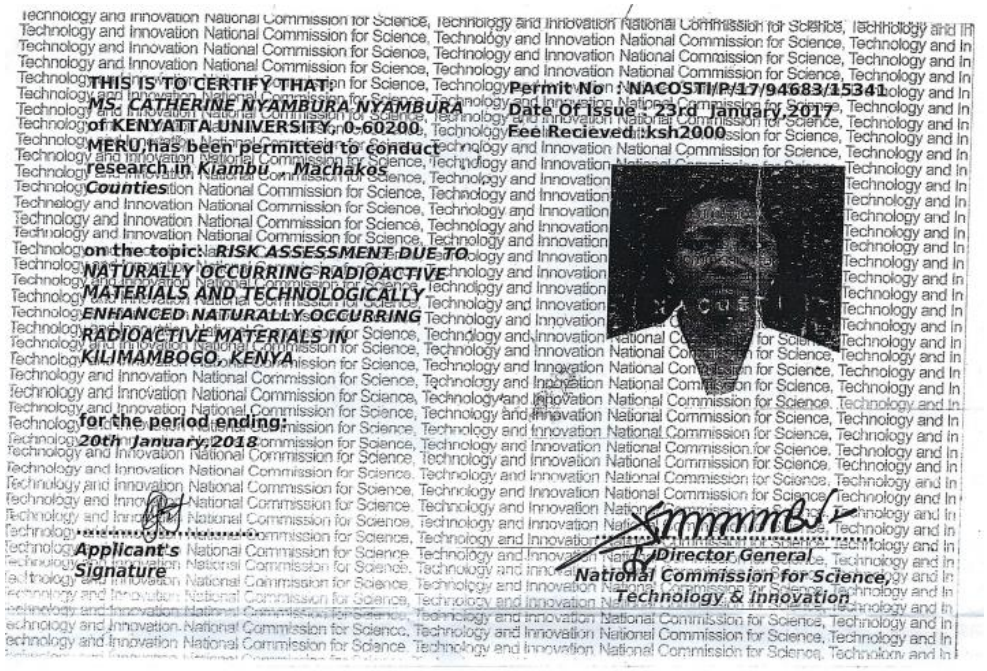

THIS IS TO CERTIFY THAT:
MS. CATHERINE NYAMBURA NYAMBURA
of KENYATTA UNIVERSITY, 0-60200,
MERU has been permitted to conduct
research in Kiambu , Machakos
Counties
on the topic: RISK ASSESSMENT DUE TO
NATURALLY OCCURRING RADIOACTIVE
MATERIALS AND TECHNOLOGICALLY
ENHANCED NATURALLY OCCURRING
RADIOACTIVE MATERIALS IN
KILIMAMBOGO, KENYA
for the period ending:
20th January,2018

Permit No : NACOSTI/P/17/94683/15341
Date Of Issue : 23rd January,2017
Fee Recieved:ksh2000

Applicant's
Signature

Director General
National Commission for Science,
Technology & Innovation

NATIONAL COMMISSION FOR SCIENCE, TECHNOLOGY AND INNOVATION

Telephone:+254-20-2213471,
2241349,3310571,2219420
Fax:+254-20-318245,318249
Email:dg@nacosti.go.ke
Website: www.nacosti.go.ke
When replying please quote

9th Floor, Utalii House
Uhuru Highway
P.O. Box 30623-00100
NAIROBI-KENYA

Ref: No.

Date

NACOSTI/P/17/94683/15341

23rd January, 2017

Catherine Nyambura Nyambura
Kenyatta University
P.O. Box 43844-00100
NAIROBI

RE: RESEARCH AUTHORIZATION

Following your application for authority to carry out research on ***"Risk assessment due to naturally occurring radioactive materials and technologically enhanced naturally occurring radioactive materials in Kilimambogo, Kenya,"*** I am pleased to inform you that you have been authorized to undertake research in **Kiambu and Machakos Counties** for the period ending **20th January, 2018.**

You are advised to report to**the County Commissioners andthe County Directors of Education,Kiambu and Machakos Counties**before embarking on the research project.

On completion of the research, you are expected to submit **two hard copies and one soft copy in pdf** of the research report/thesis to our office.

BONIFACE WANYAMA
FOR: DIRECTOR-GENERAL/CEO

Copy to:

The County Commissioner
Kiambu County.

The County Director of Education
Kiambu County.

Appendix 13: Research authorization (Kiambu county)

OFFICE OF THE PRESIDENT

MINISTRY OF INTERIOR AND CO-ORDINATION OF NATIONAL GOVERNMENT
COUNTY COMMISSIONER, KIAMBU

Telephone: 066-2022709
Fax: 066-2022644
E-mail: countycommkiambu@yahoo.com
When replying please quote

County Commissioner
Kiambu County
P.O. Box 32-00900
KIAMBU

Ref.No: **ED.12/1/VOL.IV/227**

23rd February, 2017

Catherine Nyambura Nyambura
Kenyatta University
P.O. Box 43844-00100
NAIROBI

RE: RESEARCH AUTHORIZATION

Reference is made to National Commission for Science, Technology and Innovation letter Ref No. **NACOSTI/P/17/94603/15341** of **23rd January, 2017.**

You have been authorized to conduct research on ***"Risk assessment due to naturally occurring radioactive materials and technologically enhanced naturally occurring radioactive materials in Kilimambogo, Thika East Sub-County"***. The data collection will be carried out in ***Kiambu County*** *for a period ending* ***20th January, 2018.***

You are requested to share your findings with the County Education Office upon completion of your research.

J. A. RATEMO
FOR: COUNTY COMMISSIONER
KIAMBU COUNTY

Cc County Director of Education
KIAMBU COUNTY

National Commission for Science, Technology and Innovation
P.O. Box 30623-00100
NAIROBI

Deputy County Commissioner
THIKA EAST SUB COUNTY

(For information and record purposes)

"Our Youth our Future. Join us for a Drug and Substance free County".

Appendix 14: Research Authorization (Machakos County)

THE PRESIDENCY

MINISTRY OF INTERIOR AND COORDINATION OF NATIONAL GOVERNMENT

Telephone: 21099 and 21983 - 90100
Email Address:countycommasaku@gmail.com
Fax No. 044-21999

When replying please quote:

OFFICE OF THE
County Commissioner
P.O. Box 1 - 90100
MACHAKOS

REF NO: CC/ST/ADM/5/9/VOL.11/96

DATE: 23rd February, 2017

TO: WHOM IT MAY CONCERN

RE: RRESEARCH AUTHORIZATION – CATHERINE NYAMBURA

The National Commission for Science, Technology and Innovation has authorized the above named student from Kenyatta University to carry out a research on *"Risk assessment due to naturally occurring radioactive materials and technologically enhanced naturally occurring radioactive materials in Kilimambogo, Kenya,"* in Machakos County for the period ending 20th *January*, 2018.

Please be notified and accord her necessary assistance.

COUNTY COMMISSIONER
MACHAKOS
P.O. BOX 1 MACHAKOS

GEORGE OPIYO JUMA
For: COUNTY COMMISSIONER
MACHAKOS